Study for Origins of Homochirality and Life: Investigation for the Cosmic Scenario Using Vacuum Ultraviolet Light and Synchrotron Radiation

泉, 雄大

(Degree)
博士（理学）

(Date of Degree)
2010-03-25

(Date of Publication)
2013-02-26

(Resource Type)
doctoral thesis

(Report Number)
甲4866

(URL)
https://hdl.handle.net/20.500.14094/D1004866

博　士　論　文

Study for Origins of Homochirality and Life: Investigation for the Cosmic Scenario Using Vacuum Ultraviolet Light and Synchrotron Radiation

ホモカイラリティーおよび生命の起源に関する研究：真空紫外光，
シンクロトロン放射を用いた宇宙起源説の検証

平成 21 年 12 月

神戸大学大学院　人間発達環境学研究科

泉　雄大

This thesis was written based on the following papers.

- Y. Izumi, T. Matsui, T. Koketsu and K. Nakagawa, "Preservation of homochirality of aspartic acid films irradiated with 8.5 eV vacuum ultraviolet light", *Radiation Physics and Chemistry* **77**, 1160-1163, 2008.

- Y. Izumi, A. Imazu, A. Mimoto, M. Tanaka, K. Nakagawa, M. Tanaka, A. Agui and T. Muro, "Measurement and comparison of absolute value of soft X-ray natural circular dichroism of serine and alanine", *Journal of Physics*: *Conference Series*, **190**, 012209(1)-012209(4), 2009.

- Y. Izumi and K. Nakagawa, "Quantum efficiency of racemization, decomposition and homo-dimerization of solid L-alanine induced by 7.2 eV vacuum ultraviolet light irradiation: Chiral problem in chemical evolution", *in preparation.*

- Y. Izumi, A. Imazu, A. Mimoto, M. Tanabe, K. Nakagawa, M. Tanaka, A. Agui and T. Muro, "Large soft X-ray natural circular dichroism of aspartic acid: Possibility of asymmetric photolysis induced by circularly polarized soft X-ray", *in preparation.*

Contents

Chapter 1

Introduction

Dominant amino acids, except for glycine (Gly), in proteins and dominant sugars in nucleotides on the earth are L-type and D-type, respectively. This important characteristic of life on the earth is called biomolecular homochirality. It is well known that "chiral defects", random disturbances of homochirality of the primary structure, impede the formation of both the double helix in nucleic acids and α-helixes and β-sheets in proteins (Spach and Brack, 1979; Goldanskii *et al.*, 1986). Therefore, it is important to achieve the homochirality in order to produce biomacromolecules and obtain complex 3D conformation. However it is also well known that both enantiomers are produced in ordinary reaction processes. The ratio of enantiomers is almost 1 (racemic mixture). Thus, it is natural to assume that primitive biomolecules were produced in racemic mixture and L-type amino acids and D-sugars were selected by some sort of abiotic processes.

What is the processes? Since both enantiomers have almost the same physical and chemical properties, ordinary energy sources, for example heat, discharge and so on, cannot effect selective reactions. Therefore asymmetric energy sources or fields, which effect enantiomeric excess, would be necessary.

Asymmetric adsorption surface, for example L-type is easily adsorbed and D-type is not, is proposed as an asymmetric field. An example of asymmetric adsorption surface is Cu (0 0 1) (Zhao *et al.*, 1999; Egawa *et al.*, 2003). Since homochirality is achieved on the surface which absorbed only L-type amino acids, asymmetric adsorption surface is interesting. However story is not so simple. For example, it is reported that the surface covered with only L-type and the surface covered with only D-type are adjacent and the distance is only 6 nm (Egawa *et al.*, 2003). Averaging all molecules on the layer, the ratio of L-type to D-type should be almost 1. In addition, it is not assured that second, third and forth $\cdots$ layers are covered with only L-type since asymmetric adsorption is originated from the interaction between the surface and enantiomers. Thus many steps are remained to achieve homochirality.

Parity-violating weak neutral current interaction (Yamagata, 1966) is an example for asymmetric energy source. The parity-violating weak neutral current interaction mediated by the Z^0 boson discriminates between L-type and D-type, imparting a parity-violating energy shift of $+E_{PV}$ to one enantiomer X and an equal and opposite parity-violating energy shift of $-E_{PV}$ to the other enentiomer Y. Because of the parity-violating energy difference $2E_{PV}$, enantiomer Y is stable than enantiomer X,

and therefore one considers that achievement of homochirality is inevasible result. Recently, MacDermott *et al.* (2009a, b and c) computed that some L-type amino acids in gas phase had nagative parity-violating energy shift $-E_{PV}$, namely those L-type amino acids in gas phase were stable than D-type amino acids. Further works are expected in the case of solid phase and other amino acids.

Circularly polarized light (CPL; Bonner, 1991) is also proposed as one of the asymmetric energy sources. CPL has two degree of freedom. One is left circularly polarized light (LCPL), whose electric vector rotates counterclockwise as seen from a receiver, and another is right circularly polarized light (RCPL). Enantiomers show the difference between absorption cross section for LCPL and for RCPL, namely natural circular dichroism (NCD). If L-type shows negative NCD, D-type shows positive NCD. Modulus of each NCD is the same. Negative and positive NCD mean that RCPL is absorbed rather than LCPL and LCPL is absorbed rather than RCPL, respectively. Therefore, when the racemic mixture is irradiated with LCPL, number of decomposed L-type is less than D-type and L-type excess is detected after LCPL irradiation. Various experimental examinations have already reported (see detail in section 4.1). In addition, following observations are reported.

- CPL, unfortunately infrared region, is observed in the Orion OMC-1 region (Bailey *et al.*, 1998) and the comet C/1999 S4 (LINEAR) (Rosenbush *et al.*, 2007).

- L-type excess was detected from Murchison and Murray meteorites (Cronin and Pizzarello, 1997; Pizzarello and Cronin, 2000; Pizzarello *et al.*, 2003).

Thus, it is expected that the achievement of homochirality was triggered in space by CPL irradiation and was delivered to the primitive earth ("cosmic scenario"). In this thesis, following experiments are reported as the first step to examine the cosmic scenario.

1. Examination for racemization of aspartic acid during photolysis induced by non-polarized 8.5 eV vacuum ultraviolet (VUV) light irradiation

2. Examination for racemization and dimerization of alanine induced by non-polarized 7.2 eV VUV light irradiation

3. Examination for the possibility of asymmetric photolysis induced by circularly polarized soft X-ray

It is noted that those experiments are based on following assumptions.

- Amino acids are abundant.

- All amino acids are monomer.

- All amino acids are solid because of space environment.

Chapter 2

Chiral preservation of aspartic acid films irradiated with 8.5 eV vacuum ultraviolet light

2.1 Introduction

Enrichment of L-type amino acids was detected from Murchison and Murray meteorites (Cronin and Pizzarello, 1997; Pizzarello and Cronin, 2000; Pizzarello *et al.*, 2003). It means that the enrichment of amino acids should been kept during space travel. However there are various racemization factors, which racemize amino acids, in space. For example, proton irradiation (Bonner *et al.*, 1982) and γ-ray irradiation (Bonner and Lemmon, 1978; Bonner *et al.*, 1979; Bonner *et al.*, 1985) were reported to act as racemization factors for amino acid. In addition, we have to pay attention to vacuum ultraviolet (VUV) light which is strongly absorbed by amino acids (Kamohara *et al.*, 2008). For example, it is known that 5.6 eV VUV light decomposes aspartic acid (Asp) and produces alanine (Ala) from Asp (Nakagawa et al., 2000). Does VUV light act as one of racemization factors? Does the chirality preserve during photolysis from large amino acid to small amino acid?

In this chapter, it was examined whether (1) Asp was racemized by 8.5 eV non-polarized VUV light in vacuum and (2) the products had the same chirality as Asp.

2.2 Experimental procedure

2.2.1 Sample preparation

L-Asp (purity $\geq$ 99 %) and D-Asp (purity $\geq$ 98 %) were purchased from Wako Pure Chemical Industries Ltd. and Sigma-Ardrich Inc., respectively. Reagents were used without further purification. All samples were prepared using a vacuum sublimation technique (Nakagawa *et al.*, 2000). Figure 2.1 shows a schematic view of vacuum sublimation chamber. Powder of L- or D-Asp was put on a Kapton sheet and heated up to about 350 K by a nickel-chrome heater. Base pressure of the vacuum sublimation chamber was about 10^{-3} Pa. Two thin films were prepared on a Pyrex glass plate. Thickness of films was estimated to be about 150 nm by using

a quartz crystal oscillator thickness monitor (CRTS-4, CRTM-500, ULVAC Inc.). Diameter of two thin films was 12.0 mm. One of them was used as an irradiation sample and the other was used as a non-irradiation (reference) sample.

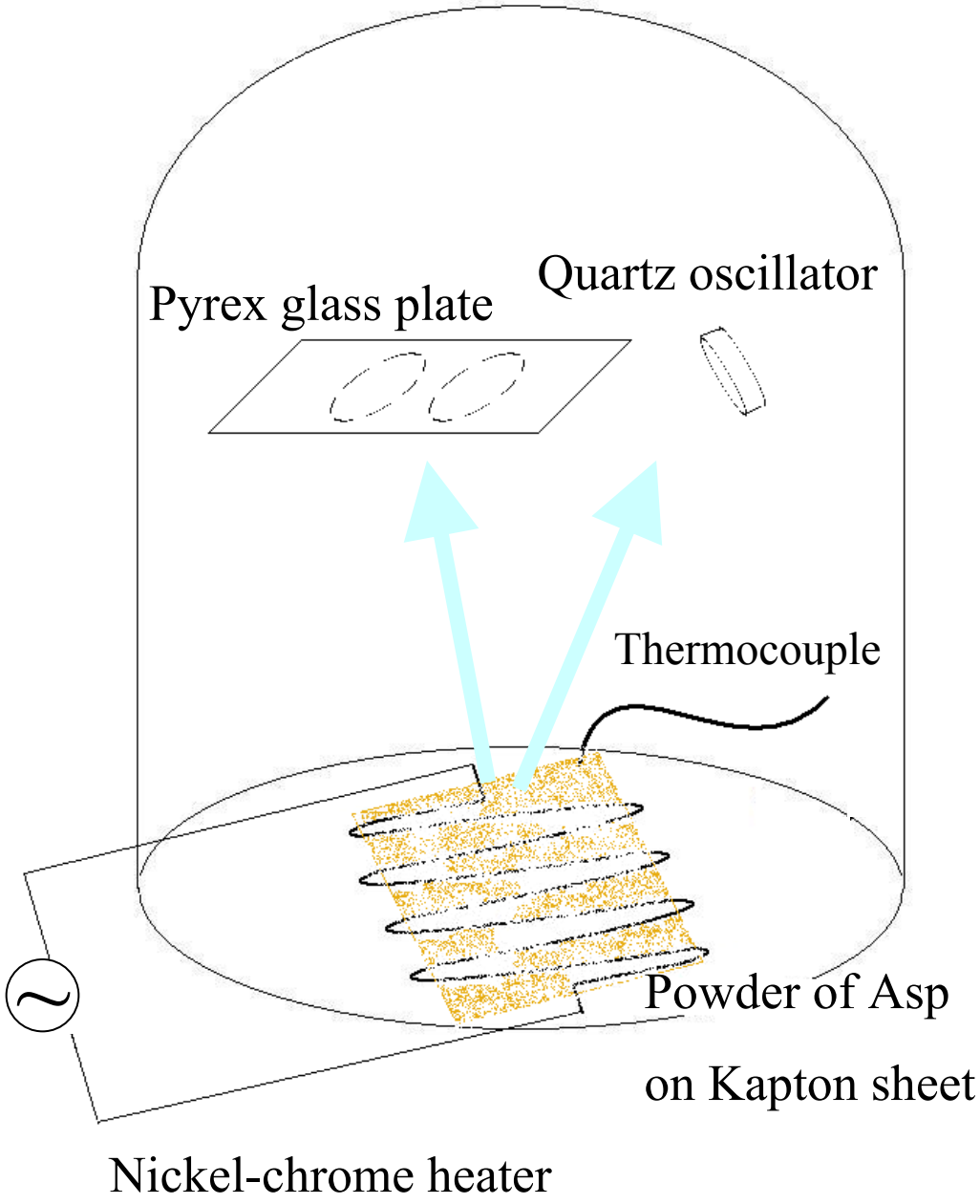

Figure 2.1: Schematic view of vacuum sublimation chamber

2.2.2 VUV irradiation

Figure 2.2 shows a photograph and a schematic view of irradiation chamber. Asp film was irradiated with non-polarized 8.5 eV VUV light by using a Kr_2* excimer lamp UER20H-146 (USHIO Inc.) (Hirose *et al.*, 2000) at 20 °C. Base pressure of

irradiation chamber was lower than 10^{-4} Pa. Irradiation time was set at 2.0, 3.0, 4.0, 6.0 and 10.0 minutes. Light intensity was discussed in section 2.2.5.

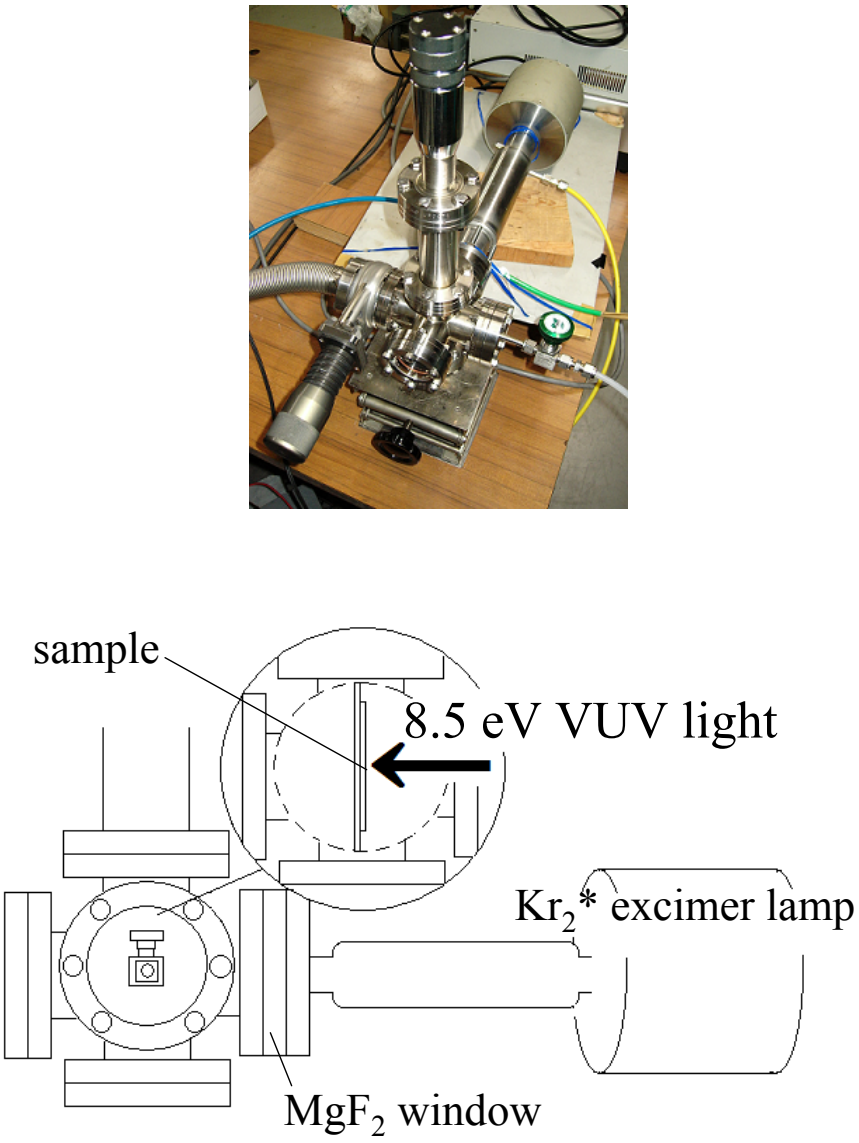

Figure 2.2: Photograph and schematic view of vacuum sublimation chamber

2.2.3 HPLC analyses

Two HPLC systems were used in order to examine racemization and identify products. One of them was HPLC-1 system equipped with an ODS column and the other was HPLC-2 system equipped with a chiral column. Analytical conditions are arranged in Table 2.1 and 2.2, respectively. HPLC-1 system could not discriminate enantiomers and HPLC-2 system could not discriminate D-Asp from other D-type amino acids and Gly from L-Asp. However, all objective amino acids, L-Asp, D-Asp, glycine (Gly), L-Ala, D-Ala and β-Ala, were examined by combined usage of two HPLC systems.

Table 2.1: Analytical conditions of HPLC-1 system

Column	COSMOSIL $5C_{18}$-MS-II Packed Column (Nacalai Tesque Inc.)
HPLC pump	LC-10AD VP (Shimadzu Co. Ltd.)
Mobile phase	50mM KH_2PO_4 and 7.2 mM $CH_3(CH_2)_5SO_2Na$ (pH$\sim$2.5)
Flow rate	0.200 mL/min
UV detector	SPD-10A VP (Shimadzu Co. Ltd.)
Detection wavelength	200 nm
Column temperature	15.0 °C

Table 2.2: Analytical conditions of HPLC-2 system

Column	CrownPak CR(+) (Daisel Chemical Co.)
HPLC pump	LC-10AD (Shimadzu Co. Ltd.)
Mobile phase	$HClO_4$ aq. (0.3 v/v%, pH$\sim$1)
Flow rate	0.200 mL/min
UV detector	SPD-10A (Shimadzu Co. Ltd.)
Detection wavelength	200 nm
Column temperature	15.0 °C

Actual procedure was as follows. In order to determine the retention time of objective amino acids, aqueous solution of objective amino acids (standard sample) was analyzed by using both HPLC systems. Irradiated Asp films were dissolved with 50 μL distilled water. 10 μL aqueous solutions of each film were analyzed by using HPLC-1 system. Compared with the retention time of standard sample, production of Gly, Ala and β-Ala was examined. Another 10 μL aqueous solutions were analyzed by using HPLC-2 system and examined racemization comparing with the retention time of standard sample. Non-irradiated Asp films were also analyzed in a similar way and examined thermal decomposition and thermal racemization during sample preparation. The absolute amount of each amino acid was determined using calibration curves (See detail in section 2.2.6).

2.2.4 Mass spectrum measurement of desorbed species

Chemical species desorbed during VUV irradiation were analyzed since desorbed chemical species and residuals of photochemical reactions which analyzed by using HPLC should be consistent with each other.

Base pressure of the irradiation chamber was lower than 10^{-6} Pa. A Pyrex glass plate or L-Ala film was irradiated at 20 °C with non-polarized 8.5 eV VUV light from the Kr_2* excimer lamp. Desorbed chemical species were analyzed by using a quadrupole mass spectrometer (QMS) (Microvision, Spectra International Inc.). Detection limit of QMS was about 10^{-12} Pa for neutral chemical species such as CO_2 and NH_3.

2.2.5 Calibration of light intensity

Light intensity of Kr_2* excimer lamp was determined in order to discuss quantitatively. Figure 2.3 shows a schematic view of light intensity measurement procedures.

Sodium salicylate (Wako Pure Chemical Industries Ltd., purity $\geq$ 99.5 %) ,which can convert the wavelength from 35-300 nm into 420 nm and the quantum efficiency of which is constant in this wavelength region (Samson, 1967), was dissolved with 99.5 % ethyl alcohol (Wako Pure Chemical Industries Ltd.). The solution was sprayed onto a SiO_2 plate (Suprasil P-20 fused silica; Ohyo Koken Kogyo Co. Ltd.) (SS on SiO_2). Calibrated photodiode (PD; S1337-1010BQ, Hamamatsu Photonics K. K.) and "SS on SiO_2" were set in the irradiation chamber. An aperture, diameter of which was 6 mm, was set between PD and "SS on SiO_2".

"SS on SiO_2" was irradiated with 8.5 eV VUV light in vacuum (pressure $\leq 1 \times 10^{-4}$ Pa) at room temperature. Converted visible light through the SiO_2 plate and the aperture illuminated PD. Output current from PD was measured by using a picoammeter (Model 617 Programable Electrometer, Keithley Instruments Inc.) (Measurement 1). Light irradiated from Kr_2* excimer lamp includes visible light. Therefore light intensity $I_1^{excimer}$ measured in "Measurement 1" is summation of VUV component and visible component. In order to cancel out visible component, similar measurement was carried out in atmospheric pressure (Measurement 2). Since VUV is absorbed by atmospheric molecules, light intensity $I_2^{excimer}$ measured in "Measurement 2" should be only visible component. Therefore it was concluded that the difference between $I_1^{excimer}$ and $I_2^{excimer}$ was true 8.5 eV VUV light intensity $I_3^{excimer}$, namely $I_3^{excimer} = I_1^{excimer} - I_2^{excimer}$. In order to calibrate the sensitivity of the SS + PD system to converted light, similar measurements were carried out using monochromatic light. The light emitted by 150 W deuterium lamp (L1835, Hamamatsu Photonics K. K.) was monochromated by a vacuum monochromator (VM504, Acton Research Co.). Wavelength of monochromatic light was 210 nm. Converted light intensity through the the SiO_2 plate and the aperture illuminated PD and measured (Measurement 3). After changing "SS on SiO_2" plate into SiO_2 plate, similar measurement was carried out (Measurement 4).

2.2.6 HPLC calibration curves

Calibration curves were prepared in order to obtain absolute amount of amino acids. 1.0×10^{-2} M aqueous solution of L-Asp and 1.0×10^{-3} M aqueous solution of Gly, of L-Ala and of β-Ala were prepared. 5.0, 10.0 and 12.5 μL solutions were analyzed using HPLC-1 system (See section 2.2.3). Since HPLC-1 system could not discriminate enantiomers, D-Asp and D-Ala were not analyzed. Peak area of chromatogram was plotted as a function of amount of analyzed molecules. Calibration curves were obtained fitting the plots with linear function. Analytical conditions are arranged in Table 2.1 and 2.2.

2.2.7 Estimation of sample preparation error

Absorbed light intensity is dependent on sample thickness according to Lambert-Beer's law. Therefore, estimation of sample thickness before irradiation is important.

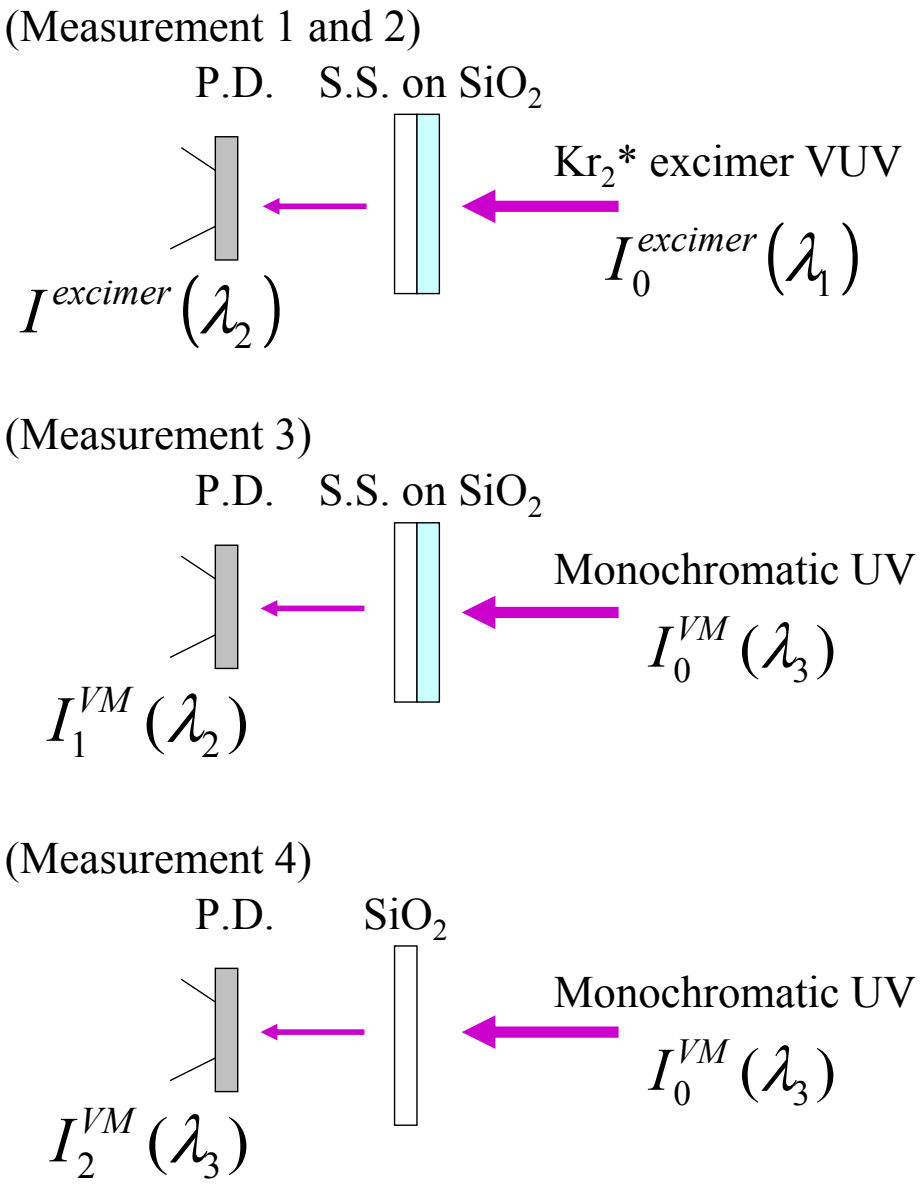

Figure 2.3: Schematic view of light intensity measurement procedures. Central wavelength of incident light λ_1, λ_2 and λ_3 was 146 nm, 420 nm and 210 nm, respectively.

As mentioned above (see detail in section 2.2.1), two thin films were prepared on each Pyrex glass plate and one of them was used as reference sample in order to estimate sample thickness before irradiation. In ideal case, thickness of both films is the same. But it was difficult to make same thickness samples using our sublimation system. Thus, it was necessary to determine the thickness of each film[1].

Two sublimation films of L-Asp were prepared on each Pyrex glass plate by vacuum sublimation technique. Both films were dissolved with 50 μL distilled water. Each 10 μL of solution was analyzed using HPLC. Comparing peak areas, difference of amount of L-Asp, which was proportional to thickness difference, between two films was determined. Analytical condition is arranged in Table 2.1. This experiment was carried out 4 times changing thickness of samples.

2.3 Results and Discussion

2.3.1 Calibration curves

Functions of calibration curves as a function of number of objective molecules are arranged in Table 2.3. Figure 2.4-2.7 show obtained calibration curves. The amount included in the 10 μl solutions of non-irradiation and irradiation samples was within the range of calibration curve. For example, number of L-Asp included in 10 μl solution of non-irradiation sample and of irradiation sample were about 2×10^{16} molecules and about 0.4-1$\times 10^{16}$ molecules, respectively (See detail in Table 2.5 and 2.6).

Table 2.3: Functions of calibration curves

L-Asp	$(PeakArea/10^6) = 0.34 \times (molecules/10^{16}) - 9.1 \times 10^{-4}$
L-Ala	$(PeakArea/10^5) = 0.20 \times (molecules/10^{15}) - 7.1 \times 10^{-3}$
Gly	$(PeakArea/10^5) = 0.16 \times (molecules/10^{15}) - 1.3 \times 10^{-3}$
β-Ala	$(PeakArea/10^6) = 0.11 \times (molecules/10^{15}) - 1.4 \times 10^{-2}$

2.3.2 Light intensity

Output current of "Measurement 1" $I_1^{excimer}(\lambda_2)$ and of "Measurement 2" $I_2^{excimer}(\lambda_2)$ were 12.88 $\pm$ 0.03 μA and 9.73 $\pm$ 0.04 μA, respectively. Dark current I^{dark} was 2.5 pA. Therefore, output current of true 8.5 eV VUV component $I_3^{excimer}(\lambda_2)$ was determined as below.

$$I_3^{excimer}(\lambda_2) = I_1^{excimer}(\lambda_2) - I_2^{excimer}(\lambda_2) - I^{dark} = 3.15 \pm 0.05\ \mu\text{A} \qquad (2.1)$$

[1]Since absorption coefficient of L-Asp has been reported (Nakagawa *et al.*, 2000), it is possible to determine the sample thickness T without destruction using optical density (OD) and absorption coefficienct μ, namely $T = \text{OD}/(\mu \log_{10} e)$. However, in this work, it was unable to determine thickness in this way since the samples were too thick to measure OD.

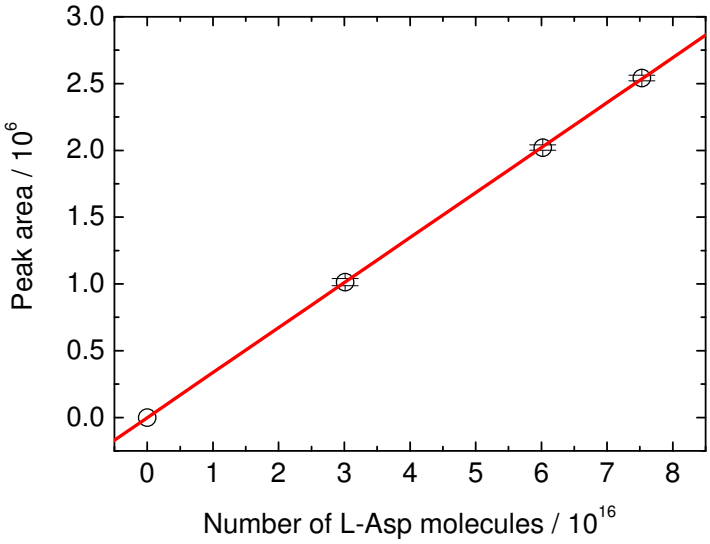

Figure 2.4: Calibration curve of L-Asp

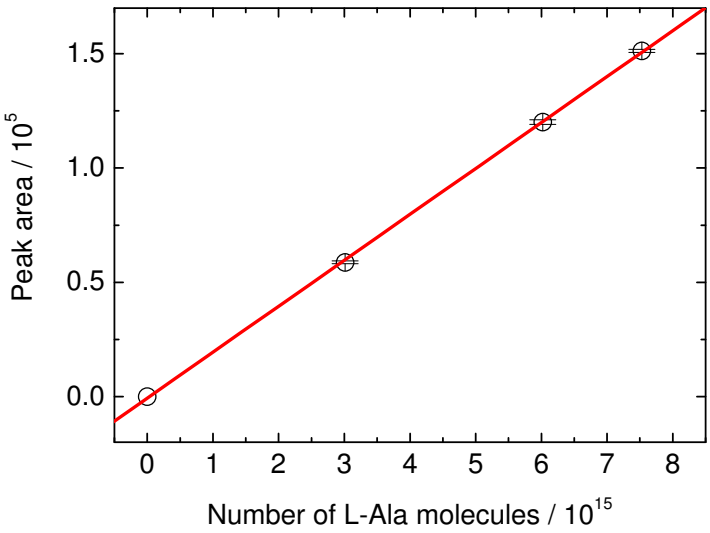

Figure 2.5: Calibration curve of L-Ala

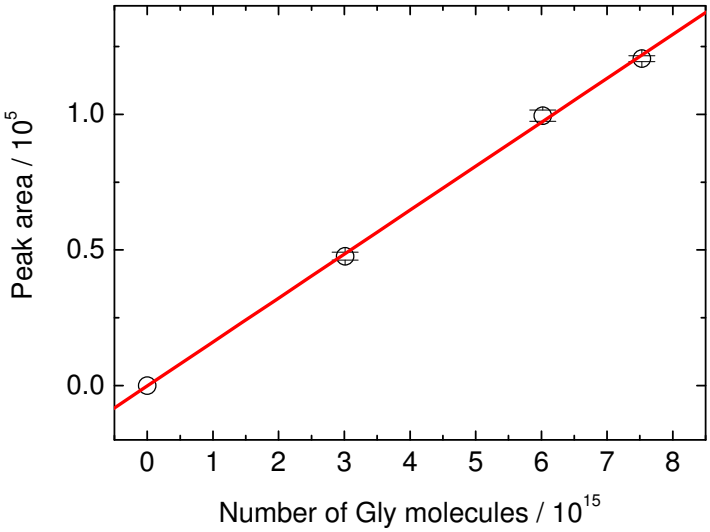

Figure 2.6: Calibration curve of Gly

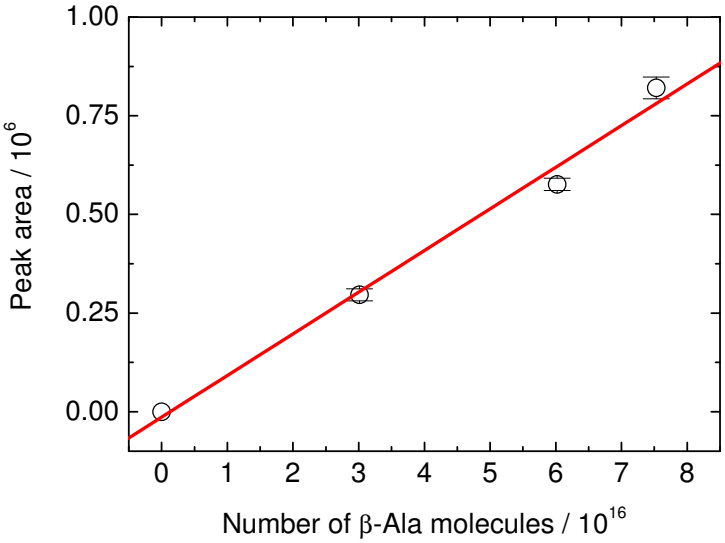

Figure 2.7: Calibration curve of β-Ala

Output current of "Measurement 3" $I_1^{VM}(\lambda_2)$ and of "Measurement 4" $I_2^{VM}(\lambda_3)$ were 143.6 ± 0.4 pA and 1.19 ± 0.03 nA, respectively.

Output current $I_3^{excimer}(\lambda_2)$, $I_1^{VM}(\lambda_2)$ and $I_2^{VM}(\lambda_3)$ are described as follows.

$$\begin{aligned} I_3^{excimer}(\lambda_2) &= I_0^{excimer}(\lambda_1)\cdot\delta\cdot T(\lambda_2)\cdot S(\lambda_2), && (2.2)\\ I_1^{VM}(\lambda_2) &= I_0^{VM}(\lambda_3)\cdot\delta\cdot T(\lambda_2)\cdot S(\lambda_2), \text{ and} && (2.3)\\ I_2^{VM}(\lambda_3) &= I_0^{VM}(\lambda_3)\cdot T(\lambda_3)\cdot S(\lambda_3), && (2.4) \end{aligned}$$

where $I_0^{excimer}(\lambda_1)$ is 8.5 eV VUV light intensity at the sample surface without visible component, δ is light conversion quantum efficiency of sodium salicylate, T is transmittance of SiO_2 plate, S is response function of PD and $I_0^{VM}(\lambda_3)$ is monochromatic light intensity. From equation (2.3) and (2.4),

$$\delta\cdot T(\lambda_2)\cdot S(\lambda_2) = \frac{I_1^{VM}(\lambda_2)}{I_0^{VM}(\lambda_3)} \quad (2.5)$$

and

$$I_0^{VM}(\lambda_3) = \frac{I_2^{VM}(\lambda_3)}{T(\lambda_3)\cdot S(\lambda_3)} \quad (2.6)$$

are obtained. Using equation (2.5) and (2.6),

$$\delta\cdot T(\lambda_2)\cdot S(\lambda_2) = \frac{I_1^{VM}(\lambda_2)\cdot T(\lambda_3)\cdot S(\lambda_3)}{I_2^{VM}(\lambda_3)} \quad (2.7)$$

is obtained. Substituting equation (2.7) into equation (2.2),

$$\begin{aligned} I_3^{excimer}(\lambda_2) &= \frac{I_0^{excimer}(\lambda_1)\cdot I_1^{VM}(\lambda_2)\cdot T(\lambda_3)\cdot S(\lambda_3)}{I_2^{VM}(\lambda_3)}\\ \Leftrightarrow I_0^{excimer}(\lambda_1) &= \frac{I_3^{excimer}(\lambda_2)\cdot I_2^{VM}(\lambda_3)}{I_1^{VM}(\lambda_2)\cdot T(\lambda_3)\cdot S(\lambda_3)} && (2.8) \end{aligned}$$

is obtained. Thus, taking in mind area of aperture 0.283 cm^2, 8.5 eV VUV light intensity emitted from Kr_2* excimer lamp $I_0^{excimer}(\lambda_1)$ was determined to be

$$\begin{aligned} I_0^{excimer}(\lambda_1) &= \frac{3.15(\pm0.05)\,\mu\text{A}\cdot 1.19(\pm0.03)\,\text{nA}}{143.6(\pm0.04)\,\text{pA}\cdot 0.9\cdot 0.1763\,\text{A/W}}\cdot\frac{1}{0.283\,\text{cm}^2}\\ &\fallingdotseq 5.84(\pm0.05)\times10^{-4}\,\text{W/cm}^2\,. && (2.9) \end{aligned}$$

Since wavelength of converted light was 420 nm, photon flux N_0 of 8.5 eV VUV light emitted was

$$\begin{aligned} N_0 &= I_0^{excimer}(\lambda_1)\cdot\frac{420\cdot\text{nm}}{6.63\times10^{-34}\,\text{J}\cdot\text{s}\ \cdot\ 3.0\times10^{8}\text{m/s}}\\ &\fallingdotseq 1.24(\pm0.01)\times10^{15}\,\text{photons}\cdot\text{cm}^{-2}\cdot\text{s}^{-1}. && (2.10) \end{aligned}$$

2.3.3 Sample preparation error

Each peak area obtained by 4 times of experiments are arranged in Table 2.4. When the thickness was thinner than 100 nm, difference of thickness between two films was about 1 %. In the case of about 150 nm, difference of thickness between two films was about 15 %. In the other case, the difference was more than 40 %. Thus, it was difficult to make similar thickness samples thicker than 100 nm. It is necessary to establish sublimation technique to make similar thickness samples. In the irradiation experiments, error of ± 15 % was given as thickness of irradiation film, namely (thickness of irradiation film) = (thickness of reference film) ± 15 %, since thickness of films used in irradiation experiments were about 150 nm.

Table 2.4: Peak area and calculated thickness

	Peak area of thin film 1 (Thickness / nm)	Peak area of thin film 2 (Thickness / nm)
1	198927.5 ± 4248.5 (34.6 ± 0.9)	201437 ± 1782 (35.0 ± 0.5)
2	359139 ± 5768 (62.4 ± 1.2)	362644 ± 9137 (63.0 ± 1.7)
3	884715.5 ± 6044.5 (153.4 ± 1.2)	1015112 ± 991 (176.0 ± 0.3)
4	1175985.5 ± 6241.5 (203.8 ± 1.2)	1668288.5 ± 36254.5 (289.1 ± 6.4)

2.3.4 Product analyses of irradiated Asp films

In order to identify the products, HPLC-1 system, which was unable to distinguish D-type from L-type, was used. Figure 2.8 shows some chromatograms of L-Asp films obtained with HPLC-1 system. The largest peak found around 12.5 minutes was originated from the contamination by used gloves. The chromatograms in the case of 2 minutes irradiation were shown in figure 2.9. Before irradiation, large peak found around 18.7 minutes was identified to be Asp. Slight peaks were found around 22.5 and 24.4 minutes. Those peaks were ascribed to be pyrolytic products during sample preparation. Since the peaks of pyrolytic products were much smaller than the peak of Asp, it was concluded that pure Asp films were obtained. After irradiation, decrease of Asp peak and increase of Ala and β-Ala peak were observed. However, the peak of Gly was not observed. In other cases, similar results were observed except for 10 minutes irradiation (see detail in section 2.3.7). Therefore it was concluded that L-Asp was decomposed into Ala, β-Ala and other achiral molecules (CO_2, NH_3 and so on) using HPLC-1 system. In the case of D-Asp, similar chromatograms were obtained.

In order to examine the chirality of Asp and Ala after irradiation, HPLC-2 system was used. Figure 2.10 shows the chromatograms obtained with HPLC-2 system. The largest peak found around 6.2 minutes was originated from the contamination by used gloves. The chromatograms in the case of 2, 4 and 10 minutes irradiation were shown in figure 2.11. As seen from the figure 2.11, the peak of L-Asp decreased with the increase of irradiation time. It means that t L-Asp was decomposed. However the peak of D-type amino acids, this HPLC system was unable to discriminate between each of D-type amino acid as mentioned above, was not observed. Therefore it

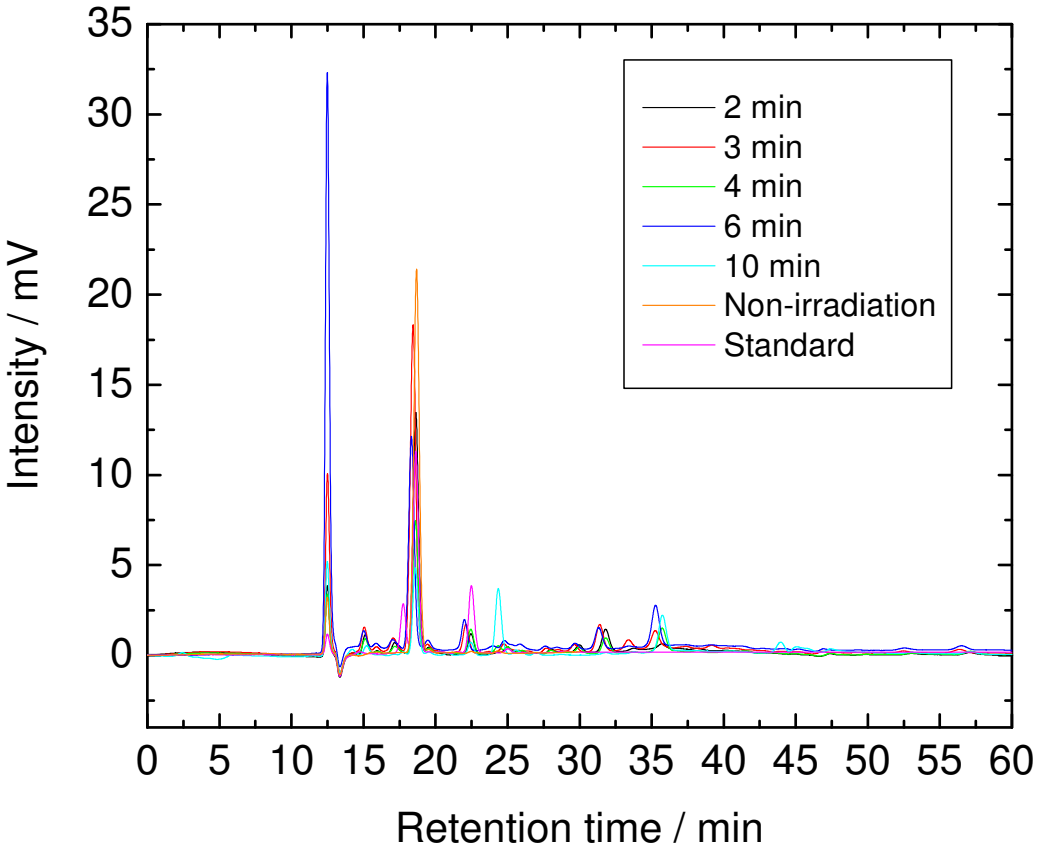

Figure 2.8: HPLC chromatograms of L-Asp films obtained with HPLC-1 system.

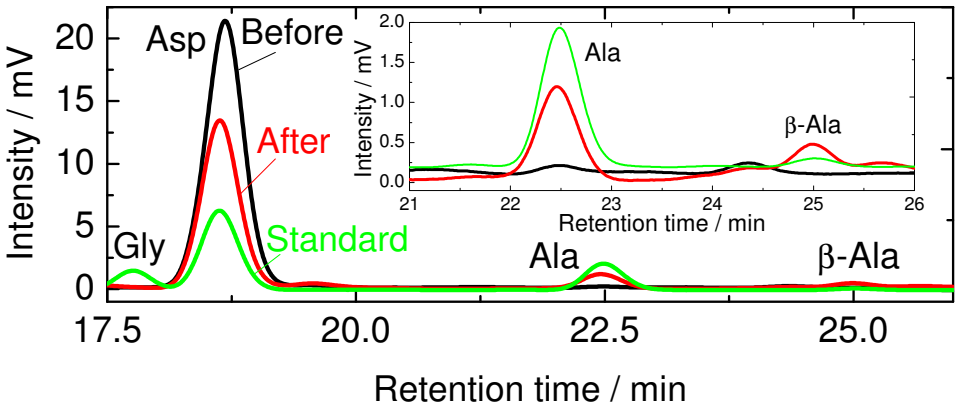

Figure 2.9: HPLC chromatograms of L-Asp films obtained with HPLC-1 system. Black: reference film (before irradiation); red: after 2 minutes irradiation; green: standard sample. The magnification is the chromatograms around 21-26 minutes.

was concluded that D-type amino acids were not produced. In the case of D-Asp irradiation, the peak of L-Asp and of L-Ala were not observed.

Thus it was concluded that "L-Asp + $h\nu$ → L-Ala + β-Ala (+ other achiral molecules)" and "D-Asp + $h\nu$ → D-Ala + β-Ala (+ other achiral molecules)" occurred, *i.e.* Asp was not racemized by 8.5 eV non-polarized VUV light in vacuum and the products, Ala, had same chirality as Asp.

2.3.5 Mass spectrum of desorbed chemical species

Figure 2.12 shows a mass spectrum of desorbed chemical species from L-Asp film surface irradiated with 8.5 eV VUV light. The insertion is the molecular structure of Asp. Largest signal was observed at $m/Z = 44$. It was identified to be CO_2^+ originated from carboxyl group. Therefore it was concluded that decarboxylation was main reactions induced by 8.5 eV VUV light. Since 8.5 eV VUV light excites carboxyl group (Inagaki, 1973), detection of decarboxylation is consistent. Decarboxylation of Asp induced by VUV irradiation was also reported in the Perseus-Exobiology experiment (Boillot *et al.*, 2002). As seen from the molecular structure of L-Asp, desorption of CO_2 was consistent with the productions of Ala and β-Ala. Some of other signals were also identified to be NH_2^+ ($m/Z = 16$), NH_3^+ ($m/Z = 17$). Deamination means that the photon energy absorbed by carboxyl group spread throughout the molecule. Signal of H_2O^+ ($m/Z = 18$) was also observed. It is noted that these intensities are not absolute value since other species would be included. Since no signal of $m/Z = 59$ was observed, it was concluded that the side chain of Asp (-CH_2COOH) was hardly desorbed by 8.5 eV photons irradiation. This result was consistent with the absence of Gly.

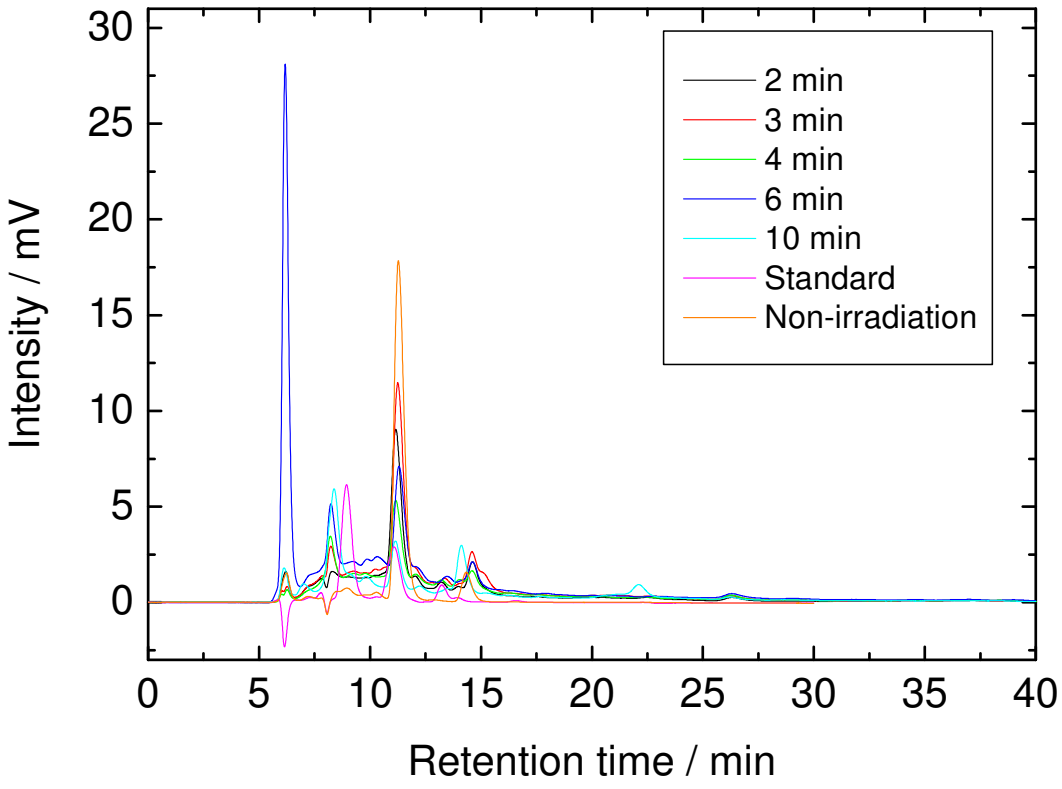

Figure 2.10: HPLC chromatograms of L-Asp films obtained with HPLC-2 system.

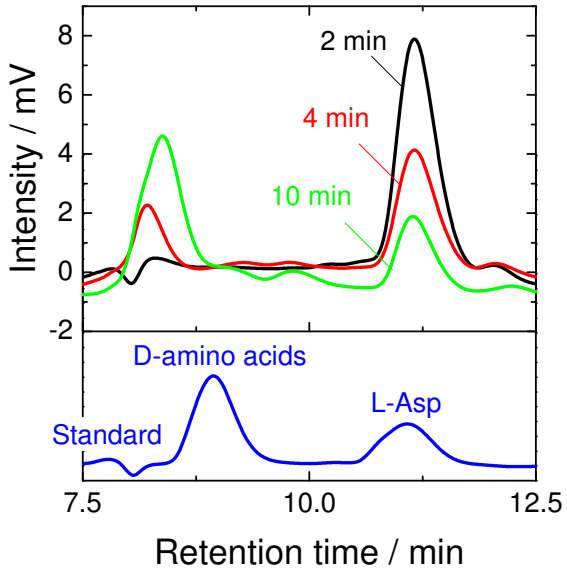

Figure 2.11: HPLC chromatograms of L-Asp films obtained with HPLC-2 system. Black: 2 minutes irradiation; red: 4 minutes irradiation; green: 10 minutes irradiation; blue: standard sample.

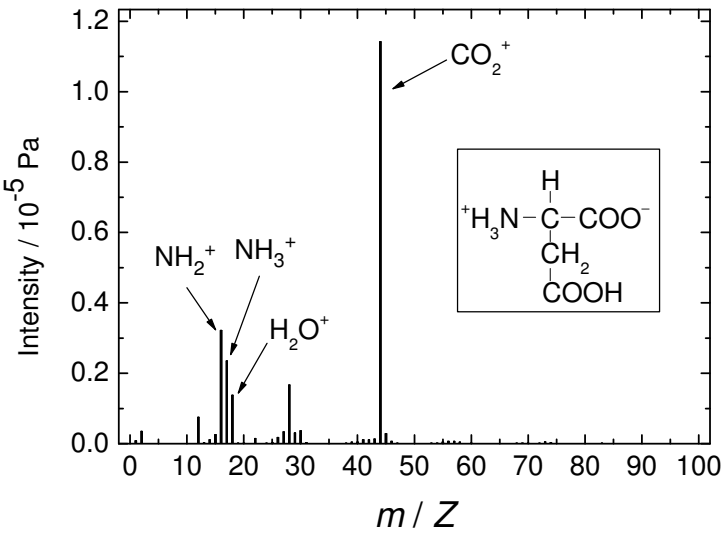

Figure 2.12: Mass spectrum of desorbed chemical species from L-Asp film surface irradiated with 8.5 eV VUV light

2.3.6 No racemization of Asp in solid films

Racemization processes of amino acid were already reported (*e.g.* Neuberger, 1948; Smith and Sivakua, 1983) although those were not photo-racemization but pyrolytic-racemization (figure 2.13). According to those reports, alternative recombination (*i.e.* from the upper side of framework or under side) of chemical species (in their reports, H) with α-carbon atom is responsible for the racemization. In this work, strong desorption of CO_2 and NH_3 was observed, but desorption of H ($m/Z = 1$) or H_2 ($m/Z = 2$) was very weak. This may means that decarboxylation and deamination reactions are advantageous to preserve the chirality of solid amino acids in vacuum environment against non-polarized VUV radiation since CO_2 and NH_3 are stable and hardly recombine.

2.3.7 Optical quantum efficiency

In order to discuss in quantitative way, optical quantum efficiency η was defined to be $M = \eta N$, where M is the number of molecules decomposed or produced, and N is the number of photons absorbed by Asp, in a similar way reported Tanaka *et al.* (2008) and Nakagawa *et al.* (2009).

Values of N depends on both thickness l and absorption coefficient μ of samples (Lambert-Beer's law): namely, $N = N_0 S t \left(1 - e^{-\mu l}\right)$, where N_0 is irradiation photon flux, S is irradiation area and l is thickness of film. Because $\mu = 4.55 \times 10^5$ cm^{-1} at 8.5 eV (146 nm) (Nakagawa *et al.*, 2000), about 99 % photons irradiated were absorbed by 150 nm Asp film. However, in this experiment, thickness of films continuously decreased during VUV irradiation due to photolysis of Asp. Therefore thickness l was defined as irradiation time dependent function decided by chemical kinetics to be $l(t) = l_0 e^{-kN_0 St}$. Values of l_0 and $l(t)$ were the thickness of before irradiation (reference film) and that of film after irradiation time t, respectively. A rate constant k was defined experimentally to satisfy this equation. Therefore, the number of absorbed photons N was determined as below.

$$N = \int_0^t N_0 S \left(1 - e^{-\mu l(t)}\right) \mathrm{d}t = \int_0^t N_0 S \left(1 - e^{-\mu l_0 \exp(-kN_0 St)}\right) \mathrm{d}t. \tag{2.11}$$

In this work, N_0 was about 1.24×10^{15} photons cm^{-2} s^{-1} at 146 nm, S was about 1.1 cm^2. Value of k was determined, for example, to be 2×10^{-18} photons^{-1} for the case of Asp decomposition in this work.

The number of molecules M decomposed or produced was defined as the modulus of the difference between number of molecules M_R in reference film and number of molecules M_I in irradiated film, namely $M = |M_R - M_I|$. Total amount of amino acids was determined by using HPLC-1 system since no racemization was observed. Since total amount of aqueous solutions of non-irradiation and irradiation samples were 50 μl and 10 μl solutions were analyzed, total amount was determined to be the analyzed results multiplied by 5. Values of M_R and M_I are arranged in Table 2.5 and 2.6

Linear function ($M = \eta N$) was applied to the experimental results and obtained the best fit value using the least squares method. Obtained results of L-Asp irradiation are shown in figure 2.14-2.16 as a function of absorbed photon number N.

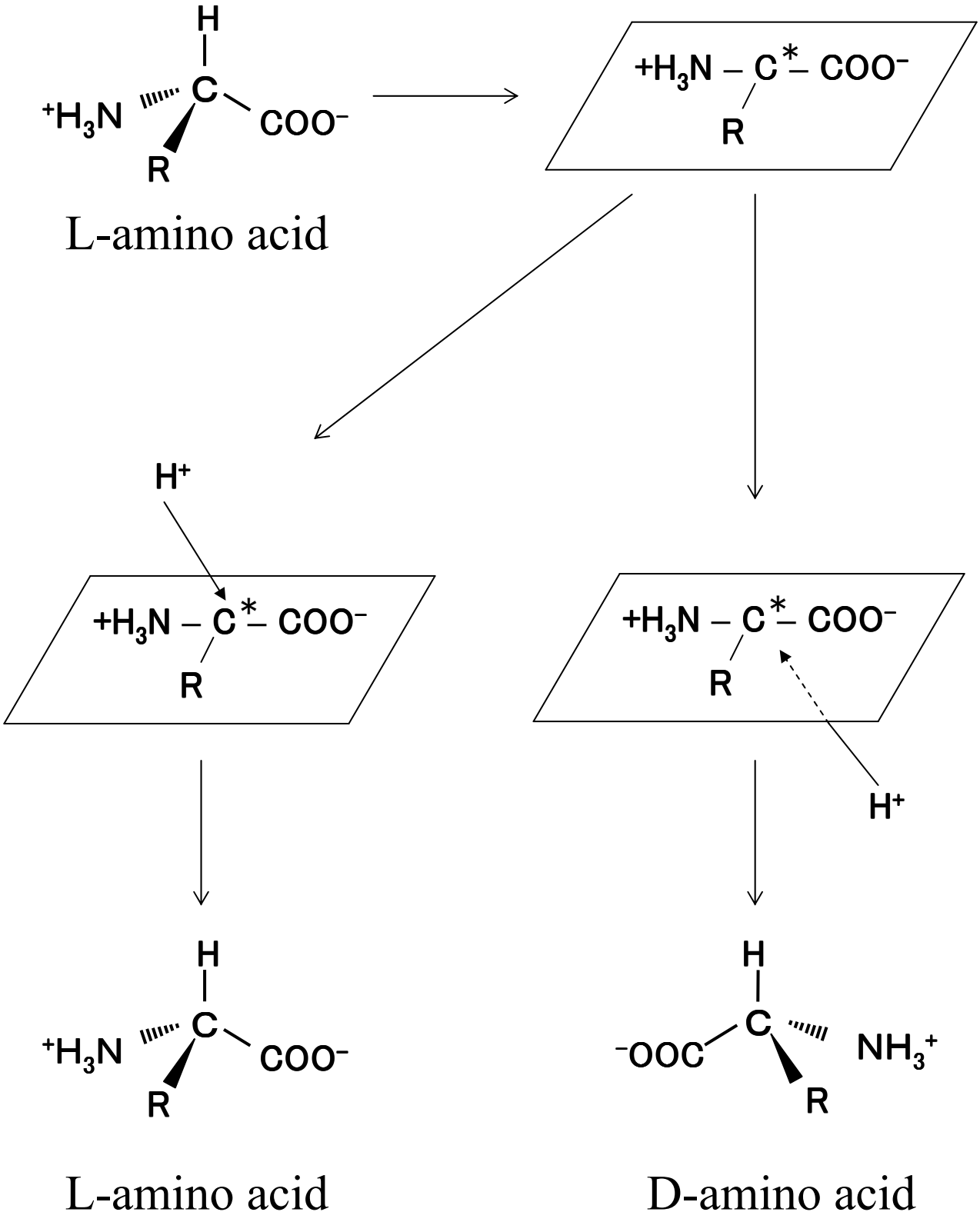

Figure 2.13: Racemization processes of amino acid

Table 2.5: Number of L-Asp molecules before irradiation and after irradiation

Irradiation time / minutes	Before irradiation M_R / 10^{17}	After irradiation M_I / 10^{17}
2	0.873 ± 0.173	0.555 ± 0.011
3	1.315 ± 0.261	0.783 ± 0.005
4	0.922 ± 0.183	0.295 ± 0.007
6	1.403 ± 0.278	0.525 ± 0.001
10	1.327 ± 0.263	0.201 ± 0.005

Table 2.6: Number of L-Ala and β-Ala produced from L-Asp molecules after irradiation

Irradiation time / minutes	L-Ala after irradiation M_I / 10^{16}	β-Ala after irradiation M_I / 10^{16}
2	0.762 ± 0.025	0.547 ± 0.123
3	1.003 ± 0.040	0.627 ± 0.023
4	0.854 ± 0.033	0.563 ± 0.034
6	1.240 ± 0.013	1.088 ± 0.146
10	0.207 ± 0.062	0

The data at $N \sim 7.4 \times 10^{17}$ photons was removed from this analysis because the photo-products were decomposed under this severe irradiation.

The best fit values of decomposition quantum efficiencies of L-Asp and D-Asp were determined to be 0.18 ± 0.04 and 0.23 ± 0.04, respectively. This means that with probability about 80 %, solid Asp itself was preserved for VUV irradiation. It is reported that in the case of aqueous solutions irradiated with 222 nm UV light (Nakagawa *et al.*, 2000), the decomposition quantum efficiency was 0.48 ± 0.02. Although the irradiation energy was smaller than this work, Asp in water was easily decomposed. These results suggest that solid Asp was much stable than aqueous.

Production quantum efficiency of L-Ala and β-Ala from L-Asp was 0.035 ± 0.004 and 0.023 ± 0.004, respectively. Production quantum efficiency of D-Ala and β-Ala from D-Asp was 0.046 ± 0.006 and 0.022 ± 0.004, respectively. Thus, it was concluded that the quantum efficiencies between L- and D-amino acids were equal within experimental error.

2.4 Conclusion

Reactions expressed as "L-Asp + $h\nu \rightarrow$ L-Ala + β-Ala (+ other achiral molecules)" and "D-Asp + $h\nu \rightarrow$ D-Ala + β-Ala (+ other achiral molecules)" occurred for L- or D-Asp films irradiated with non-polarized VUV light (8.5 eV) in vacuum (pressure $\leq 10^{-4}$ Pa) at about 20 °C. It is concluded that chirality was preserved for photolysis of Asp to Ala. Decomposition quantum efficiency of solid Asp was smaller than that of aqueous solution. This result suggests that solid Asp is much stable than

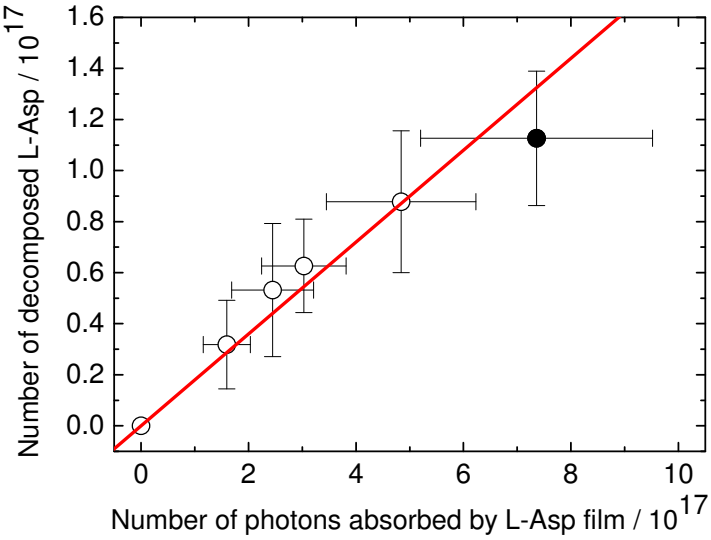

Figure 2.14: Number of decomposed L-Asp molecules as a function of the absorbed 8.5 eV photons. From the slope of strait line decomposition quantum efficiency of L-Asp was determined. The data represented as filled circle (•) was removed from fitting.

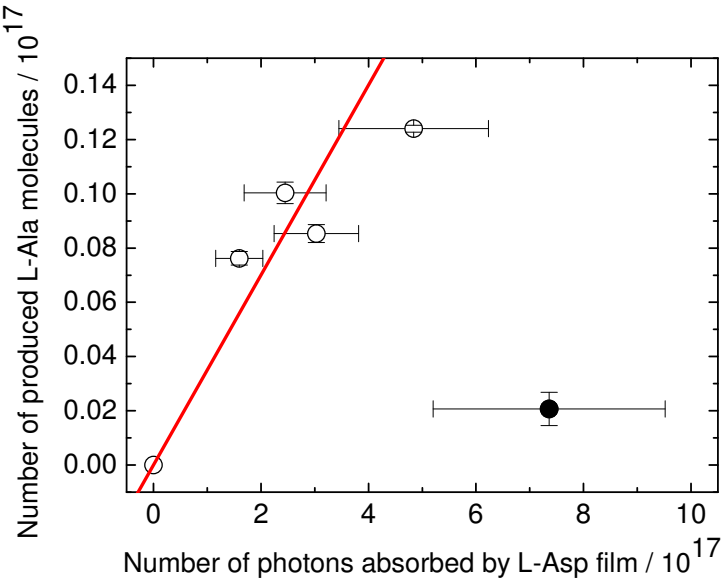

Figure 2.15: Number of produced L-Ala molecules from L-Asp as a function of the absorbed 8.5 eV photons. From the slope of line and broken line, values of production quantum efficiencies of L-Ala was determined. The data represented as filled circle (•) was removed from fitting.

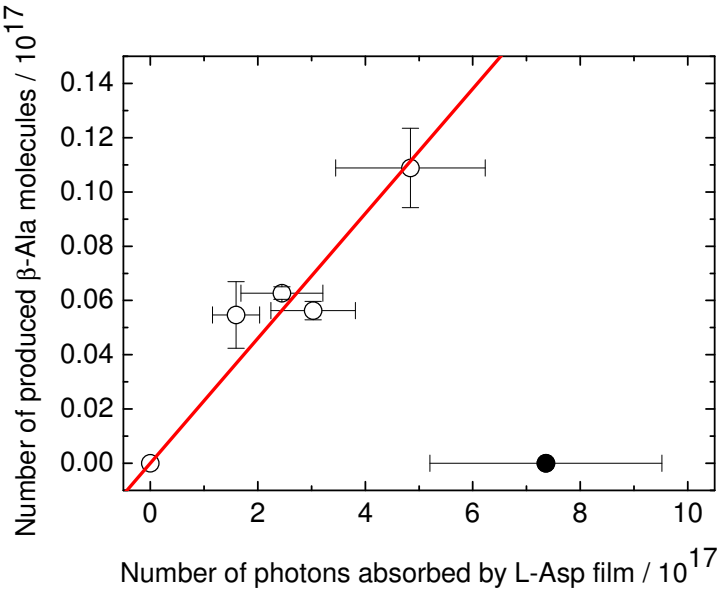

Figure 2.16: Number of produced β-Ala molecules from L-Asp as a function of the absorbed 8.5 eV photons. From the slope of line and broken line, values of production quantum efficiencies of β-Ala was determined. The data represented as filled circle (•) was removed from fitting.

aqueous solution and supports cosmic scenario. It is interesting to carry out the similar experiments using high energy particles and/or γ-ray irradiation.

Chapter 3

Quantum efficiency of decomposition, racemization and dimerization of solid L-alanine induced by 7.2 eV vacuum ultraviolet light irradiation: Chiral problem in chemical evolution

3.1 Introduction

Before the origin of life on the earth, biomolecules, and finally biomacromolecules such as protein, DNA, RNA and so on, should have been created from simple inorganic molecules. This process is called "chemical evolution". Chemical evolution from inorganic molecules to amino acids (*e.g.* Miller, 1953; Harada and Fox, 1964; Kobayashi *et al.*, 2001) has been studied well. However nobody can know how large oligomers are produced since those products were identified after hydrolysis. In order to compensate potential weakness, many examinations of the process of chemical evolution from amino acids to oligomers in various environments have been reported.

On the primitive earth, hydrothermal vents on the sea floor (Corliss *et al.*, 1979; Edmond *et al.*, 1982; Yanagawa and Kojima, 1985; Russell *et al.*, 1988), environments of which are high temperature and high pressure, are attractive environment for chemical evolution. Molecules were heated in hot vents and new bonds were formed. The products passing through the hot environment were rapidly cooled in the surrounding water. In the cold water, the products are more stable. The products circulated in the hot and cool environments over and over again and would be polymerized. In the stage of chemical evolution from amino acids to oligomers, it was reported that glycine (Gly) (Imai *et al.*, 1999; Alargov *et al.*, 2002; Islam *et al.*, 2003; Furuichi *et al.*, 2005; Goto *et al.*, 2005) or alanine (Ala) (Ogata *et al.*, 2000; Kawamura *et al.*, 2005) was oligomerized at a simulated hydrothermal vent system. In the case of Gly, decamer was detected (Goto *et al.*, 2005).

Another attractive environment is space. It is reasonable to assume that ra-

diation in space environment played an important role in chemical evolution. It is reported that oligomerization of solid tyrosine (Tyr) (Khoroshilova *et al.*, 1991), Gly (Kaneko *et al.*, 2005; Nakagawa *et al.*, 2009) or Ala (Tanaka *et al.*, 2008) induced by vacuum ultraviolet (VUV) light or soft X-ray and production of glycyl-tryptophan and glycyl-tyrosine induced by VUV light or γ-ray irradiation (Simakov *et al.*, 1996). If biomolecules were produced in space, those should be delivered to the primitive earth. Since biomolecules are easily pyrolyzed, one may think the delivery was impossible. However, amino acids have been detected from many meteorites after hydrolysis (*e.g.* Shimoyama *et al.*, 1979; Cronin and Pizzarello, 1997; Pizzarello and Cronin, 2000; Pizzarello *et al.*, 2003). In addition, the earth is constantly showered by a lot of space dusts (2.0-6.0 $\times$ 10^7 kg/year, the particle size is about 100 μm) even now (Love and Brownlee, 1993). Since those are much smaller than meteorites, they can escape from heat during atmospheric entry and have an advantage over in delivering biomolecules (Chyba and Sagan, 1997).

Thus, hydrothermal vent and space are interesting environments in view of chemical evolution from amino acid to oligomer. However problem is still remained. Amino acids have enantiomers, but L-type amino acids are dominant, called homochirality, in protein of life on the earth. It is well known that "chiral defects", random disturbances of the homochirality of the primary structure, impedes the formation of both α-helixes and β-sheets in proteins (Spach and Brack, 1979; Goldanskii *et al.*, 1986). On the other hand, it was also reported that racemization of Ala itself at the simulated hydrothermal vent system (Kawamura and Yukioka, 2001; Nemoto *et al.*, 2005) and of leucine itself irradiated with proton (Bonner, *et al.*, 1982) or γ-ray (Bonner and Lemmon, 1978). Thus, amino acids must polymerize against racemization. In view of origin of life, it is important to examine the ratio of racemization rate to homo-oligomerization rate, namely production rate of oligomers composed only L-type or only D-type molecules.

In this work, the decomposition, racemization and dimerization rate of solid L-Ala induced by 7.2 eV VUV light were determined in vacuum at room temperature as the first step to examine the racemization and dimerization rate of solid amino acids on the space dust surface in space.

3.2 Experimental procedure

3.2.1 VUV irradiation procedure

L-Ala (purity $\geq$ 99 %) was purchased from Wako Pure Chemical Industries Ltd. and used without further purification. All irradiation samples were prepared in a similar way as section 2.2.1. Three films were prepared on each SiO_2 plate (Suprasil P-20 fused silica plate; Ohyo Koken Kogyo Co., Ltd.). Thickness of films was estimated to be about 150 nm. Diameter of films was 12.0 mm. Middle film was used as non-irradiated reference (reference film). The others were used as the sample for irradiation (irradiation film). Thickness difference among three films on each plate was about $\pm$10 %.

VUV irradiation was carried out in a similar way as section 2.2.2. L-Ala film was irradiated with non-polarized 7.2 eV (172 nm) VUV light by using a Xe_2* excimer

lamp (UER20H-172A, USHIO Inc.) at 20 °C in vacuum (pressure $\leq 10^{-4}$ Pa). Irradiation flux was determined to be 5.4×10^{15} photons cm^{-2} s^{-1} (see detail in section 2.2.5 and 2.3.2). Irradiation time was set at 20, 30, 60, 240 and 600 seconds.

All samples were dissolved with 50 μL distilled water. A 10 μL of aqueous solution was analyzed using a HPLC system. Analytical conditions are arranged in Table 3.1. In order to determine the retention time of Gly, D-Ala, L-Ala and Ala dimer, namely L-alanyl-L-alanine (LL), L-alanyl-D-alanine (LD), D-alanyl-L-alanine (DL) and D-alanyl-D-alanine (DD), aqueous solutions of each objective amino acids and peptides (standard sample) was also analyzed using the HPLC system. The absolute amount of each amino acids was determined using calibration curves (See detail in section 3.2.4)

Table 3.1: Analytical conditions of HPLC system

Column	CrownPak CR(+) (Daisel Chemical Co.)
HPLC pump	LC-10AD (Shimadzu Co. Ltd.)
Mobile phase	$HClO_4$ aq. (0.3 v/v%, pH$\sim$1)
Flow rate	0.100 mL/min
UV detector	SPD-10A (Shimadzu Co. Ltd.)
Detection wavelength	200 nm
Column temperature	20.0 °C

3.2.2 Absorption spectroscopy of LL

In order to determine the quantum efficiency (see detail in section 3.3.6), optical absorption cross section $\sigma_{LL}(\lambda)$ of LL was determined. Thin films of LL was prepared on the Suprasil P-20 fused silica plate in a similar way as section 3.2.1. The reagent of LL was purchased from Sigma-Ardrich Inc. and used without further purification. Thickness of films was estimated to be about 30 nm. Diameter of films was 11.0 mm.

Base pressure of the measurement chamber was lower than 10^{-3} Pa. Measurement of optical density was measured within the wavelength range from 160 nm to 240 nm. The light emitted by a 150 W deuterium lamp (L1835, Hamamatsu Photonics K. K.) was monochromated by a vacuum monochromator (VM-504, Acton Research Co.), dispersion of which was 2.1 nm/mm. Both entrance and exit slit width were set at 1 mm. Transmitted monochromatic light through the sample was converted into 420 nm visible light using sodium salicylate. The intensity of converted light was measured by using a photomultiplier tube (PMT; R1166, Hamamatsu Photonics K. K.) applied -800 V. Signal current from the PMT was measured using a picoammeter (Model 617 Programable Electrometer, Keithley Instruments Inc.). Signal current without any samples at the wavelength of 162 nm was about -800 nA. Dark current was about -2 nA. First, transmitted light intensity through the Suprasil P-20 fused silica plate $I_0(\lambda)$ was measured. After that, transmitted light intensity through the each LL film sublimated on the Suprasil P-20 fused silica

plate $I(\lambda)$ was measured. Minimum signal current at the wavelength of 162 nm was about -250 nA. Thus, OD(λ) of LL, $\log_{10}(I_0(\lambda)/I(\lambda))$, was determined.

After OD measurements, LL films were dissolved with distilled water. 10 μL of each solution was analyzed by using HPLC system and absolute amount of LL N_{LL} was determined using the peak area and the calibration curve. The analytical condition was above mentioned. According to Lambert-Beer's law, absorption cross section σ_{LL} of LL is described as below.

$$\sigma_{\mathrm{LL}}(\lambda) = \frac{\mathrm{OD}(\lambda)}{(N_{\mathrm{LL}}/S)\log_{10} e}\,, \tag{3.1}$$

where S is area of films. Thus, absorption cross section $\sigma_{\mathrm{LL}}(\lambda)$ of LL was determined within wavelength range from 160 nm to 240 nm.

A semiempirical molecular orbital calculation was carried out in order to assign some transitions. Geometry optimization and oscillator strength calculation of LL were carried out using PM3 method (Stewart, 1989a, b) and INDO/S method (Ridley and Zerner, 1973) in the WinMOPAC3.0 package (MOPAC, 2000).

3.2.3 Mass spectrum measurement of desorbed molecules

L-Ala film (26 mm $\times$ 76 mm) was prepared on Pyrex glass plate in a similar way as 3.2.1. Thickness of film was estimated to be about 300 nm.

Base pressure of the irradiation chamber was about 1×10^{-5} Pa. L-Ala film was irradiated at 14 °C with non-polarized 7.2 eV VUV light from the Xe_2* excimer lamp. Desorbed chemical species were ionized by electron collision. The ions were analyzed with a quadrupole mass spectrometer (QMS; Microvision, Spectra International Inc.). Detection limit of QMS was about 10^{-12} Pa.

3.2.4 Calibration curves

Calibration curves were prepared in order to obtain absolute amount of amino acids. 5.0×10^{-3} M aqueous solution of L-Ala and of D-Ala and 5.0×10^{-5} M aqueous solution of each dimer were prepared. 5.0, 10.0 and 12.5 μL solutions were analyzed using HPLC system. 1.0×10^{-2} M aqueous solution of L-Ala was also prepared and 5.0 and 10.0 μL solutions was also analyzed. Peak area of chromatograms was plotted as a function of amount of analyzed molecules. Calibration curves were obtained fitting the plots with linear function. Analytical conditions are arranged in Table 3.1.

3.3 Results and Discussion

3.3.1 Calibration curves

Functions of calibration curves are arranged in Table 3.2. Figure 3.1-3.6 show obtained calibration curves. The amount included in the 10 μl solutions of non-irradiation and irradiation samples was within the range of calibration curve. For example, number of L-Ala included in 10 μl solution of non-irradiation sample and of

irradiation sample were about 2×10^{16} molecules and about 0.3-1$\times 10^{16}$ molecules, respectively (See detail in Table 3.3 and 3.4).

Table 3.2: Functions of calibration curves

L-Ala	$(PeakArea/10^5) = 2.51 \times (molecules/10^{16}) - 1.24 \times 10^{-1}$
D-Ala	$(PeakArea/10^5) = 2.46 \times (molecules/10^{16}) - 1.75 \times 10^{-2}$
LL	$(PeakArea/10^5) = 0.163 \times (molecules/10^{13}) - 1.75 \times 10^{-2}$
LD	$(PeakArea/10^5) = 0.120 \times (molecules/10^{13}) - 1.21 \times 10^{-2}$
DL	$(PeakArea/10^5) = 0.149 \times (molecules/10^{13}) - 2.93 \times 10^{-2}$
DD	$(PeakArea/10^5) = 0.163 \times (molecules/10^{13}) - 7.34 \times 10^{-3}$

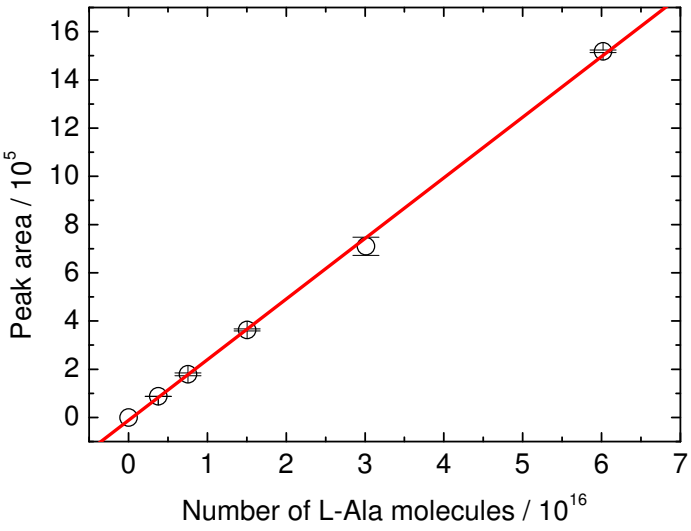

Figure 3.1: Calibration curve of L-Ala

3.3.2 Absorption spectrum of LL

Figure 3.7 shows absorption spectra of LL and L-Ala. The spectrum of L-Ala was reproduced from Kamohara *et al.* (2008). The determination accuracy of absorption cross section of L-L was grater than 90 %. For example, absorption cross section of L-Ala was about 2.1×10^{-17} cm^2 and of LL was about 4.2×10^{-17} cm^2 at 7.2 eV (172 nm).

Figure 3.8 shows absorption spectrum of LL and calculated oscillator strength. Large oscillator strength was predicted at 185.6 nm. It was assigned to be oxygen of COO^- n (lone pair) $\rightarrow$ COO^- π^* transition (figure 3.9). Small oscillator strengths were predicted at 203.8 and 237.3 nm. Those were assigned to be oxygen of peptide

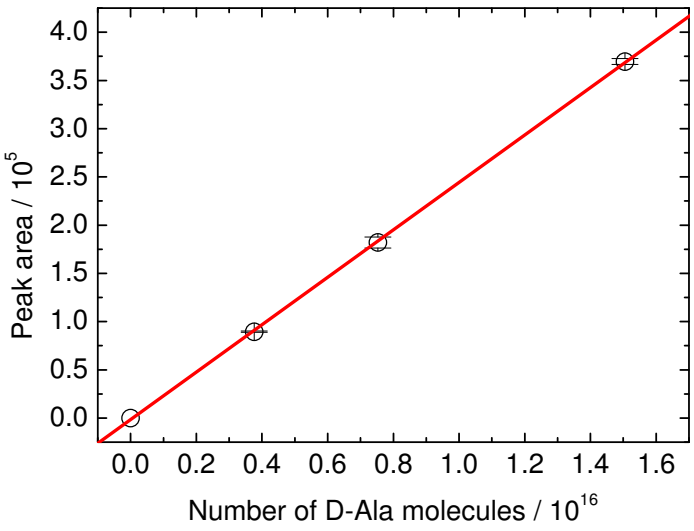

Figure 3.2: Calibration curve of D-Ala

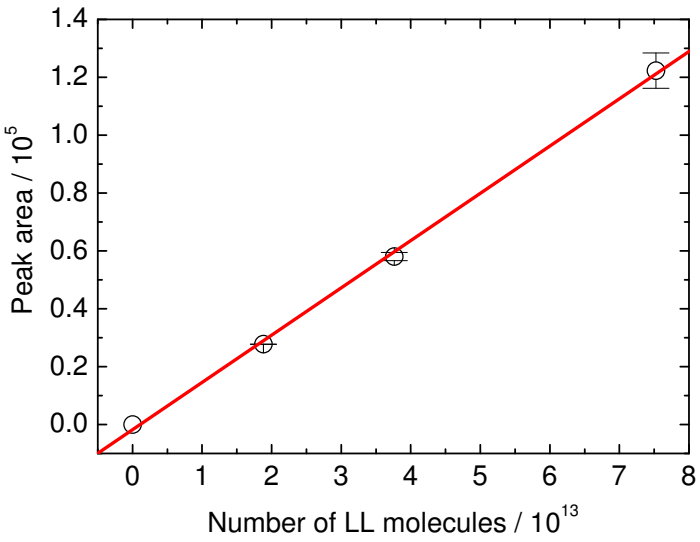

Figure 3.3: Calibration curve of LL

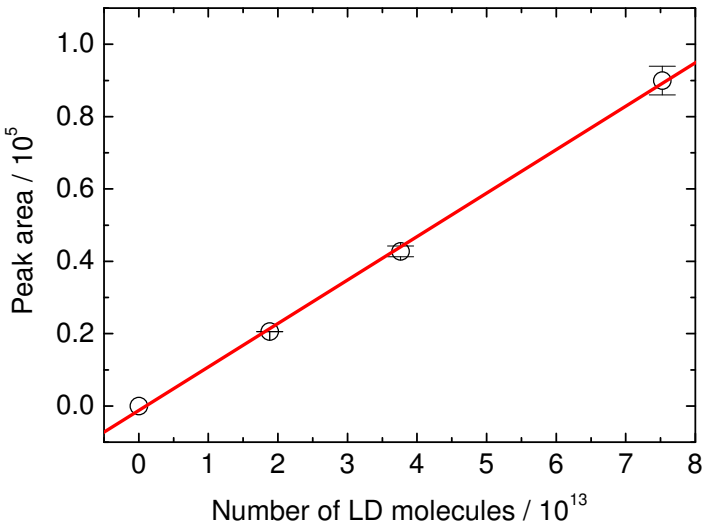

Figure 3.4: Calibration curve of LD

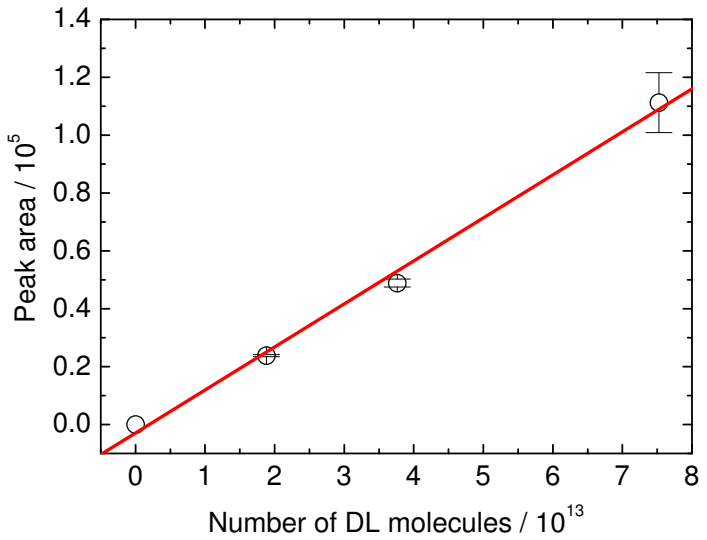

Figure 3.5: Calibration curve of DL

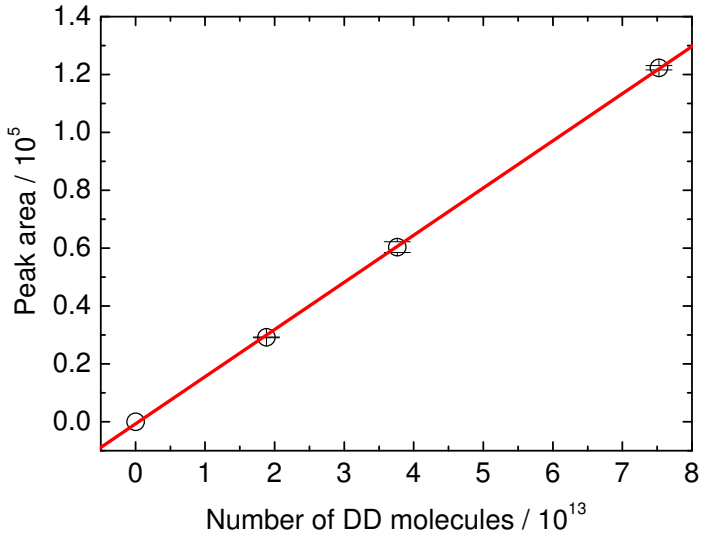

Figure 3.6: Calibration curve of DD

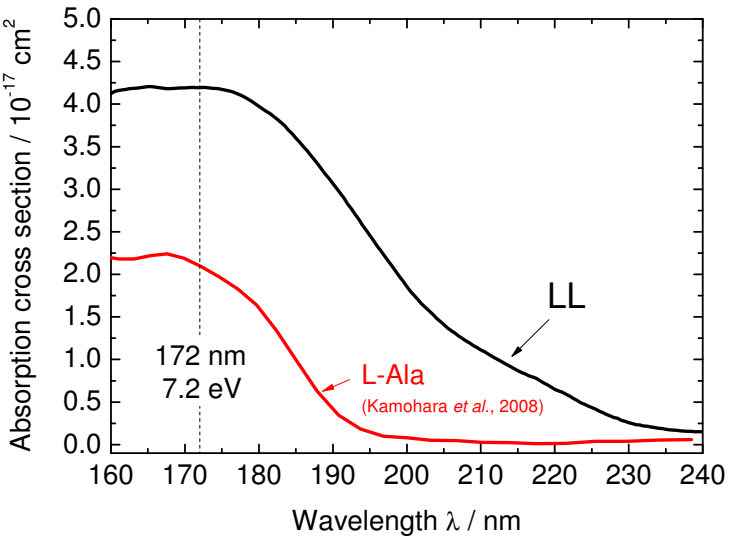

Figure 3.7: Absorption spectra of LL (black) and L-Ala (red; Kamohara *et al.*, 2008)

bond $n \rightarrow$ C=O π^* transition (figure 3.10) and oxygen of COO^- $n \rightarrow COO^-$ π^* transition (figure 3.11), respectively.

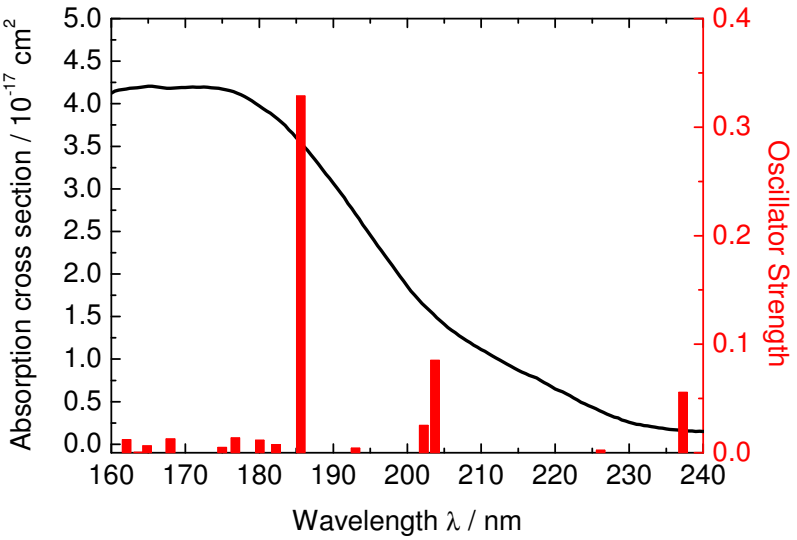

Figure 3.8: Absorption spectra of LL (black, left axis) and calculated oscillator strength (red, right axis)

3.3.3 Products analyses of irradiated thin films

Figure 3.12 shows some chromatograms. Figure 3.13 shows the magnification of figure 3.12 in the case of non-irradiation and 60 and 600 seconds irradiation. By analyzing standard sample, the retention time of D-Ala, DD, Gly, L-Ala, DL, LL and LD were determined to be 17.3, 19.8, 20.6, 23.5, 25.1, 38.0 and 40.3 minutes, respectively (figure 3.13 below). In the case of reference film, large peak of L-Ala was observed. Amount of L-Ala was $(8.2 \pm 1.4) \times 10^{16}$ molecules. Since other large peaks were not observed, it was concluded that no dimerization and racemization occurred during sample preparation. After 60 seconds irradiation, decrease of L-Ala was observed. Since total amount of aqueous solutions of non-irradiation and irradiation samples were 50 μl and 10 μl solutions were analyzed, total amount was determined to be the analyzed results multiplied by 5. Decomposed L-Ala was $(3.3 \pm 1.4) \times 10^{16}$ molecules. The peak of D-Ala, DL, LL and LD were also observed. Number of produced molecules after 60 seconds irradiation was $(7.7 \pm 0.3) \times 10^{14}$, $(1.8 \pm 1.0) \times 10^{13}$, $(1.5 \pm 0.1) \times 10^{14}$ and $(2.1 \pm 0.8) \times 10^{13}$ molecules, respectively. However, in the case of 600 s irradiation, slight peak of L-Ala was only observed. Some peaks found around 16, 19 and 28-32 minutes were not identified. Those peaks would be derived from achiral molecules since those were not living amino acids and their enantiomers. Detail amount of objective amino acids and dimers are arranged in Table 3.3 and 3.4. Since the peak of DL was close to the large peak of L-Ala

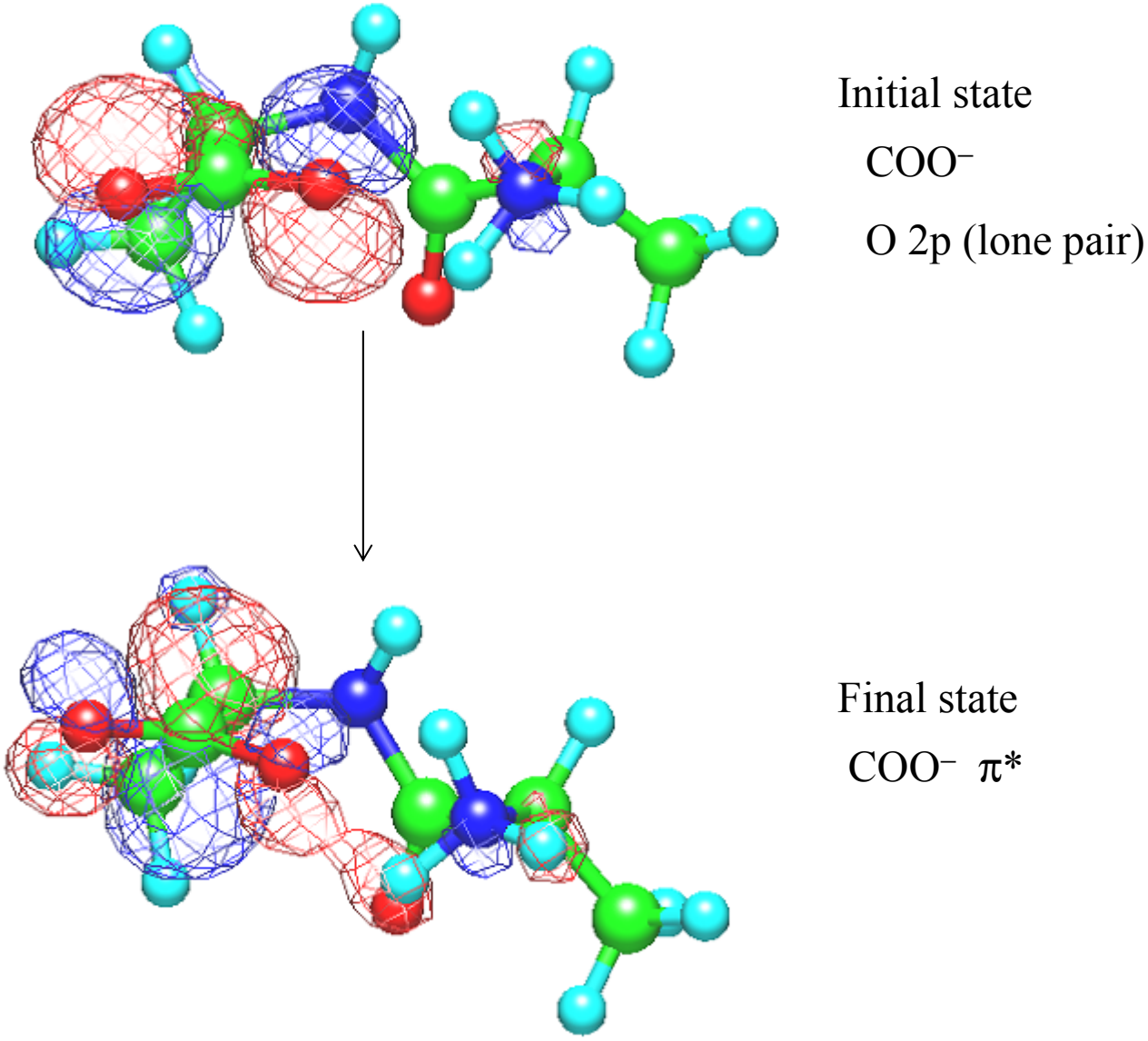

Figure 3.9: Molecular structure of LL and isosurface levels of the wavefunctions assigned to be COO^- $n \rightarrow \pi^*$ transition. Red wireframe: positive isosurface of wavefunction; blue wireframe: negative isosurface of wavefunction

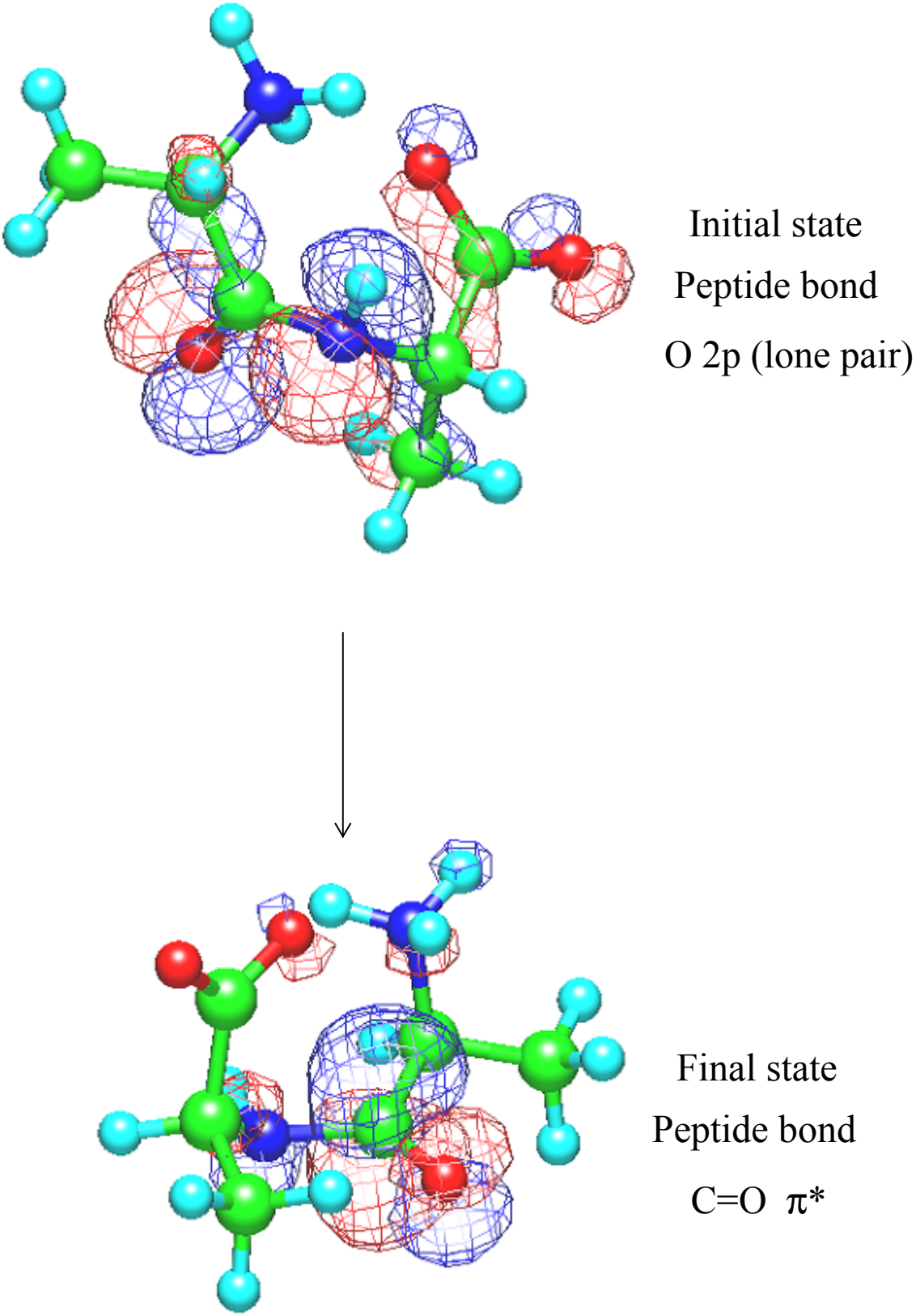

Figure 3.10: Molecular structure of LL and isosurface levels of the wavefunctions assigned to be oxygen of peptide bond $n \rightarrow$ C=O π^* transition. Red wireframe: positive isosurface of wavefunction; blue wireframe: negative isosurface of wavefunction

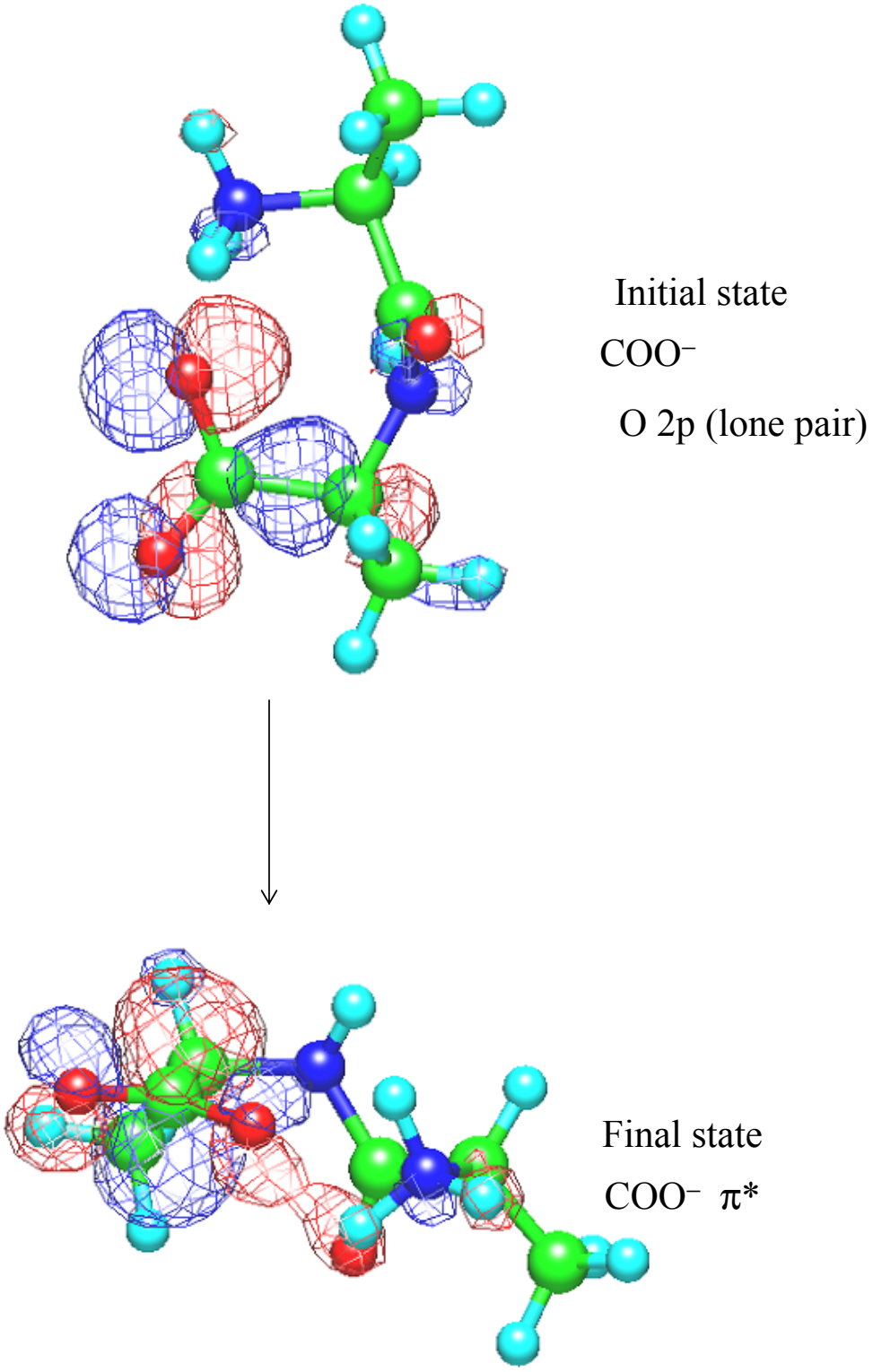

Figure 3.11: Molecular structure of LL and isosurface levels of the wavefunctions assigned to be oxygen of COO^- $n \rightarrow \pi^*$ transition. Red wireframe: positive isosurface of wavefunction; blue wireframe: negative isosurface of wavefunction

(figure 3.13), it was difficult to divide the peak of DL from the peak of L-Ala and determine the absolute amount of DL except 60 seconds irradiation sample.

Thus, it was concluded that the reactions expressed as "L-Ala + $h\nu \rightarrow$ LL + DL + LD + D-Ala (+ other achiral molecules)" occurred, namely racemization, homo-dimerization and hetero-dimerization were observed.

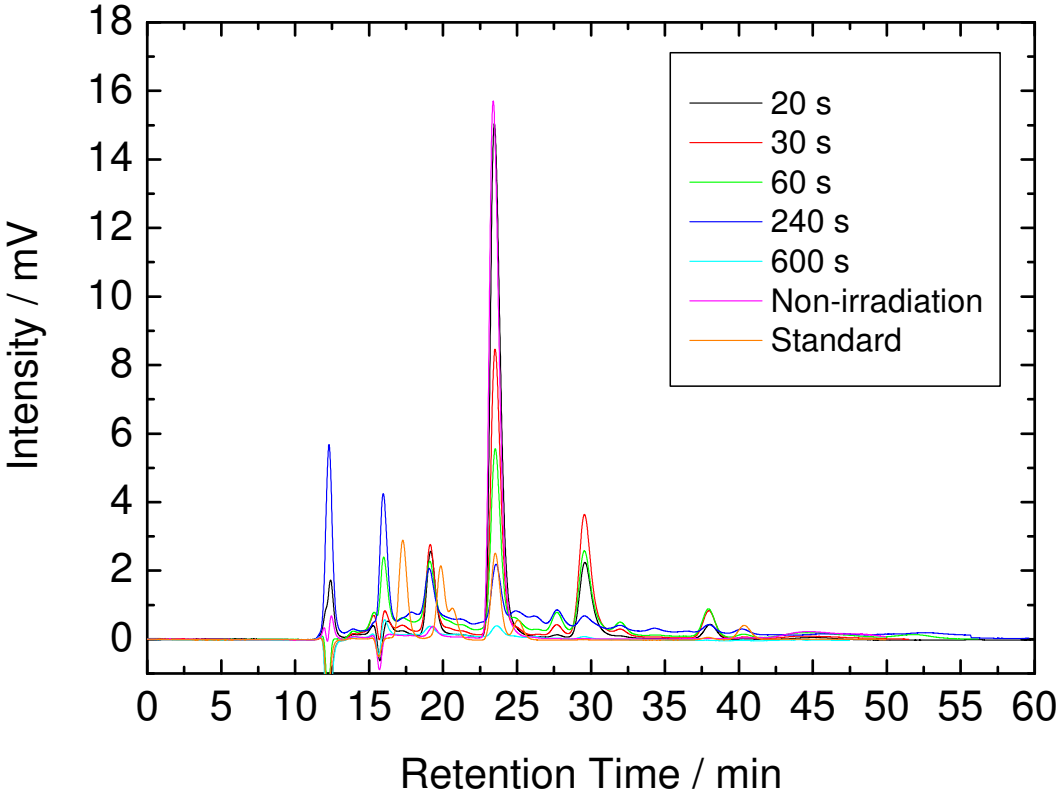

Figure 3.12: HPLC chromatograms of L-Ala films.

3.3.4 Mass spectrum of desorbed chemical species

Figure 3.14 shows a mass spectrum of desorbed chemical species from L-Ala film surface after 60 seconds 7.2 eV VUV light irradiation. The insertion is the molecular structure of Ala. The largest signal was observed at $m/Z = 44$. It was identified to be CO_2^+ originated from carboxyl group. The QMS detects CO_2 molecules as $m/Z = 44$, 28 (CO^+), 16 (O^+) and 12 (C^+). The intensity ratio is $CO_2{}^+$: CO^+ : O^+ : C^+ = 10 : 1.1 : 0.9 : 0.6. Thus the partial pressure of detected CO_2 was determined to be about 1.9×10^{-4} Pa. Assuming ideal gas, number of desorbed CO_2 was calculated to be about 4.4×10^{13} molecules since the volume of irradiation chamber was 9.2×10^{-4} m^3 and temperature was 287 K. The signal observed at

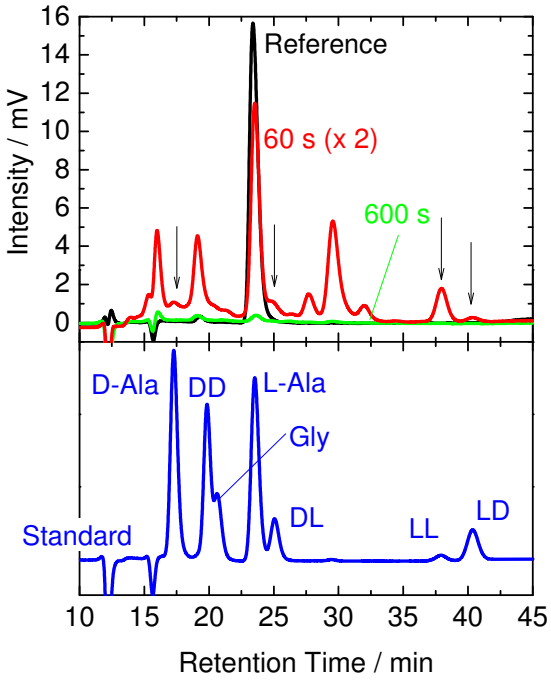

Figure 3.13: HPLC chromatograms of L-Ala films. Black: reference film (before irradiation); red: 60 seconds irradiation multiplied by 2; green: 600 seconds irradiation; blue: standard sample. The arrows (↓) shows the peaks of observed objective amino acids and peptides.

Table 3.3: Number of L-Ala molecules before irradiation and after irradiation

Irradiation time / s	Before irradiation / 10^{17}	After irradiation / 10^{17}
20	0.980 ± 0.160	0.887 ± 0.038
30	0.816 ± 0.137	0.759 ± 0.033
60	0.816 ± 0.137	0.483 ± 0.036
240	1.58 ± 0.246	0.157 ± 0.029
600	1.09 ± 0.176	0.0536 ± 0.0260

Table 3.4: Number of D-Ala, LL, DL, LD molecules after irradiation

Irradiation time / s	D-Ala / 10^{14}	LL / 10^{14}	DL / 10^{13}	LD / 10^{13}
20	4.40 ± 0.22	1.43 ± 0.08	-	1.13 ± 0.78
30	8.41 ± 0.16	1.46 ± 0.08	-	1.02± 0.77
60	7.74 ± 0.31	1.51 ± 0.12	1.80 ± 1.00	2.09± 0.83
240	-	0.362 ± 0.080	-	3.14± 0.79
600	0	0	0	0

$m/Z = 17$ was identified to be NH_3^+ originated from amino group. NH_3 molecules are detected as $m/Z = 17$, 16 (NH_2^+), 15 (NH^+) and 14 (N^+). The intensity ratio is $NH_3^+ : NH_2^+ : NH^+ : N^+ = 5 : 4 : 0.4 : 0.1$. Thus the partial pressure of detected NH_3 was determined to be about 1.6×10^{-4} Pa. Assuming ideal gas, number of desorbed NH_3 was calculated to be about 3.7×10^{13} molecules. Other signal was much smaller than the signal originated from CO_2 and NH_3. Therefore it was concluded that decarboxylation and deamination were main reactions induced by 7.2 eV VUV light.

Small signal of $m/Z = 18$ was also observed. It was identified to be H_2O^+. The QMS detected H_2O molecule as $m/Z = 18$, 17 (OH^+) and 16 (O^+). The intensity ratio was $H_2O^+ : OH^+ : O^+ = 3.757 : 1 : 0.075$. The intensity of H_2O^+ was 4.29×10^{-5} Pa. Thus the partial pressure of detected H_2O was determined to be about 5.5×10^{-5} Pa. Assuming ideal gas, number of desorbed H_2O was calculated to be about 1.3×10^{13} molecules. Number of desorved H2O was about 10 % of number of produced LL molecules detected by using HPLC.

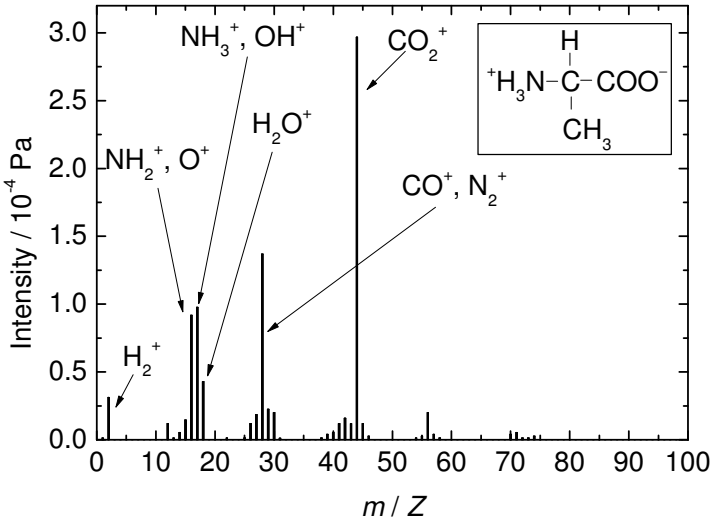

Figure 3.14: Mass spectrum of desorbed chemical species from L-Ala film surface irradiated with 7.2 eV VUV light

3.3.5 Racemization process of L-Ala

As mentioned in section 2.3.6, alternative recombination of chemical species with α-carbon atom is responsible for the racemization. Therefore, stable radical including α-carbon is necessary. In the case of L-Ala, it is well known that a radical $CH_3\dot{C}HCO_2^-$ formed by deamination is stable (Kuroda and Miyagawa, 1982). Since desorption of NH_3 from L-Ala film was observed (figure 3.14), it was concluded

that the racemization of L-Ala was occurred due to recombination of the radical $CH_3\dot{C}HCO_2^-$ and desorbed NH_3 (figure 3.15).

In contrast, no Asp was racemized induced by 8.5 eV VUV irradiation although irradiation photon energy and absorption coefficient (Nakagawa *et al.*, 2000) were larger than this work (see detail in chapter 2). In addition, no racemization of Asp, glutamic acid (Glu), Tyr and leucine (Leu) was not observed after space flight (Barbier *et al.*, 2002; Boillot *et al.*, 2002). These results suggest that amino acids are divided into two groups. One is a low "chiral stability", namely racemization easily occurred, group like Ala, and the other is a high "chiral stability" group like Asp. High "chiral stability" amino acids would play important roles to preserve enantiomeric excess in meteorite, comet or space dust. Racemization is a critical problem in production of biomacromolecules and origin of homochirality. Therefore it is necessary to carry out the similar experiments using other amino acids, other environments and other energy sources in order to examine the "chiral stability" of amino acids and so on.

3.3.6 Quantum efficiency

Photolysis of L-Ala

The rate of photolysis of L-Ala is described as below ignoring L-Ala production from LL decomposition since production rate is much smaller than L-Ala decomposition rate.

$$-\frac{\mathrm{d}\,[\mathrm{L}]}{\mathrm{d}t} = \phi_1 \sigma_\mathrm{L} p\,[\mathrm{L}]\,, \tag{3.2}$$

where [L] is column density of L-Ala (molecules/cm^2) at irradiation time t, ϕ_1 is a quantum efficiency of L-Ala decomposition and p is the photon flux at the surface of L-Ala film, 5.4×10^{15} photons cm^{-1} s^{-1}, and σ_L is the absorption cross section of L-Ala at 7.2 eV, 2.1×10^{-17} cm^2. Solving this differential equation, the ratio of [L] divided by initial column density of L-Ala $[\mathrm{L}]_0$ was obtained to be equation (3.3).

$$\frac{[\mathrm{L}]}{[\mathrm{L}]_0} = \exp\left(-\phi_1 \sigma_\mathrm{L} p t\right). \tag{3.3}$$

The equation (3.3) was applied to experimental result. Figure 3.16 shows experimental results and the best fit curve. Using the best-fit value, the rate constant ϕ_1 was determined to be $(8.2 \pm 0.7) \times 10^{-2}$.

Production and decomposition of LL

Production and decomposition processes of LL are described as follows ignoring L-Ala production.

$$\begin{aligned} \text{L-Ala} + h\nu &\rightarrow \mathrm{L}^* + \mathrm{X}^*, \\ \mathrm{L}^* + \text{L-Ala} &\rightarrow \mathrm{LL} + \mathrm{H_2O}, \text{ and} \\ \mathrm{LL} + h\nu &\rightarrow \mathrm{Y_1} + \mathrm{Y_2} + \cdots, \end{aligned}$$

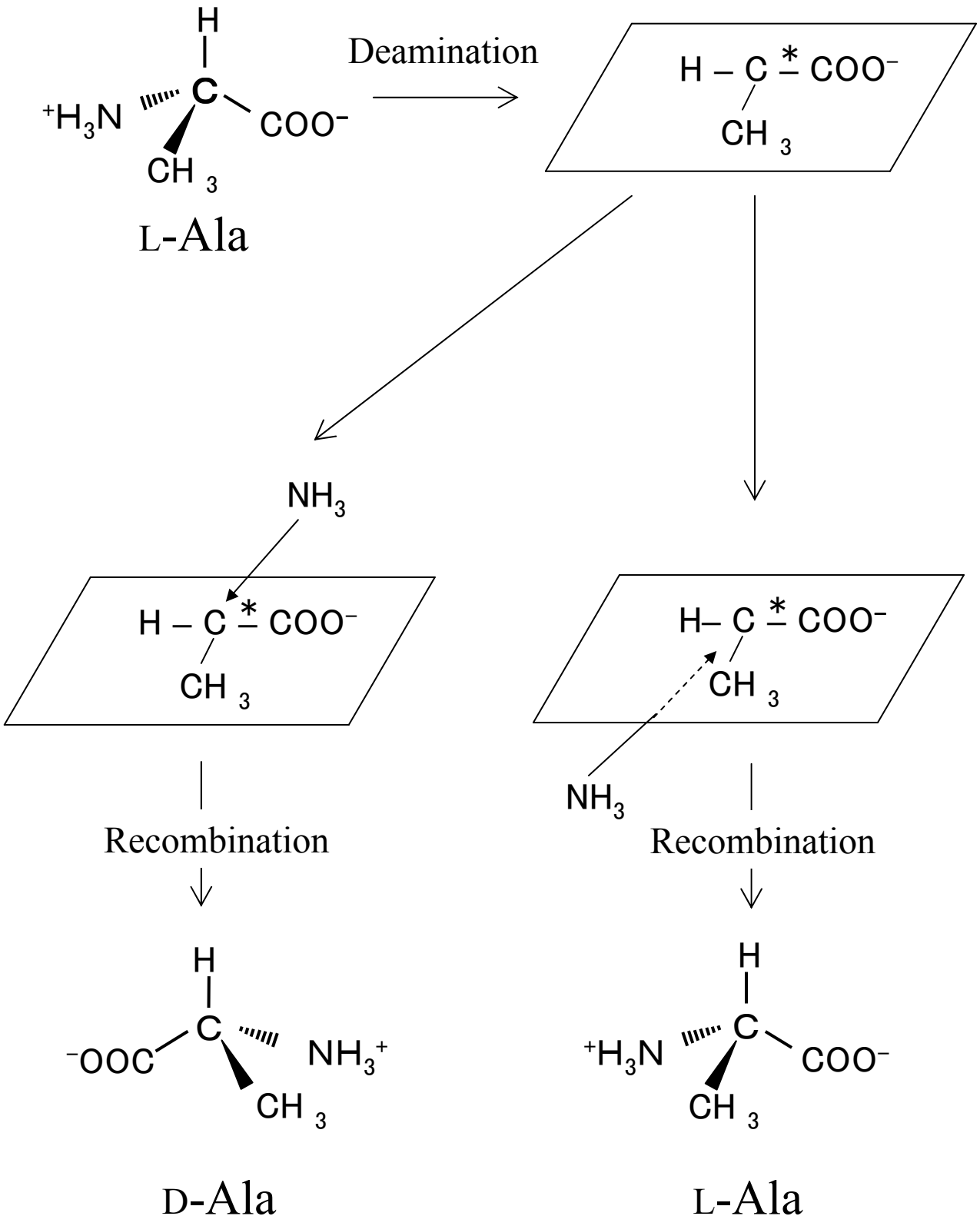

Figure 3.15: Assumed racemization processes of L-Ala

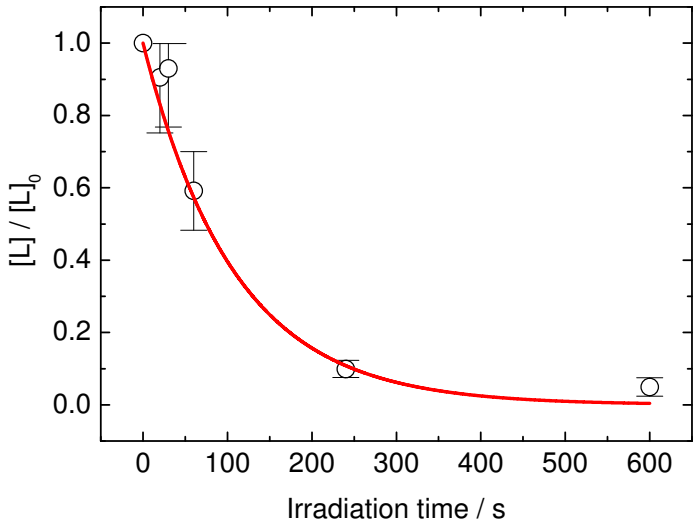

Figure 3.16: The ratio of column density of L-Ala after irradiation divided by before irradiation as a function of irradiation time. Symbol; experimental data, solid line; the best fit curve based on chemical kinetics.

where L* and X* are a radical including α-carbon and not including α-carbon originated from L-Ala, respectively, and Y_n is decomposition product of LL. In these cases, following differential equations are obtained.

$$\frac{\mathrm{d}\,[\mathrm{L}]}{\mathrm{d}t} = -\phi_2\sigma_\mathrm{L}p\,[\mathrm{L}] - k\,[\mathrm{L}^*]\,[\mathrm{L}]\,, \tag{3.4}$$

$$\frac{\mathrm{d}\,[\mathrm{L}^*]}{\mathrm{d}t} = \phi_2\sigma_\mathrm{L}p\,[\mathrm{L}] - k\,[\mathrm{L}^*]\,[\mathrm{L}]\,, \text{ and} \tag{3.5}$$

$$\frac{\mathrm{d}\,[\mathrm{LL}]}{\mathrm{d}t} = k\,[\mathrm{L}^*]\,[\mathrm{L}] - \phi_3\sigma_\mathrm{LL}p\,[\mathrm{LL}]\,, \tag{3.6}$$

where k is the rate constant of production of LL, ϕ_2 and ϕ_3 are quantum efficiency of L-Ala decomposition and LL decomposition, respectively, and σ_LL is absorption cross section of LL at 7.2 eV, 4.2×10^{-17} cm^2.

By applying the steady state approximation to equation (3.5), namely $\frac{\mathrm{d}[\mathrm{L}^*]}{\mathrm{d}t} = 0$, and solving these differential equations,

$$\frac{[\mathrm{L}]}{[\mathrm{L}]_0} = \exp\left(-2\phi_2\sigma_\mathrm{L}pt\right) \tag{3.7}$$

and

$$\frac{[\mathrm{LL}]}{[\mathrm{L}]_0} = \frac{\phi_2\sigma_\mathrm{L}}{\phi_3\sigma_\mathrm{LL} - 2\phi_2\sigma_\mathrm{L}}\left[\exp\left(-2\phi_2\sigma_\mathrm{L}pt\right) - \exp\left(-\phi_3\sigma_\mathrm{LL}pt\right)\right] \tag{3.8}$$

are obtained.

The equation (3.8) was applied to experimental results. Figure 3.17 shows experimental results and best fit curve. By using best fit value, the L-Ala decomposition quantum efficiency ϕ_2 and the LL decomposition quantum efficiency ϕ_3 were determined to be $(9.2 \pm 0.3) \times 10^{-2}$ and $(8.3 \pm 0.2) \times 10^{-2}$, respectively. Values of ϕ_1 and ϕ_2 represent the same reaction, namely L-Ala decomposition and the value of ϕ_1 should be equal to the value of ϕ_2. Since these values were equal within experimental error, it was concluded that the reaction described precisely. Since we could not detect the L* in this work, we could not determine the LL production rate constant k. Further works are necessary to determine the value of rate constant of LL production k.

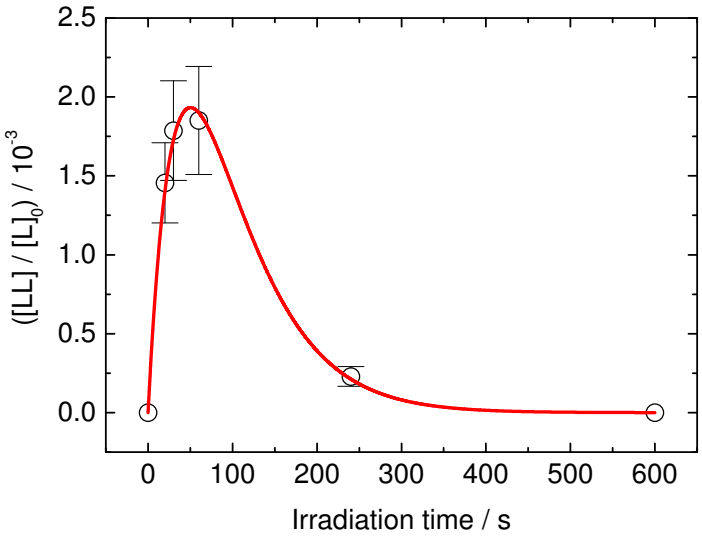

Figure 3.17: The ratio of column density of LL after irradiation divided by column density of L-Ala before irradiation as a function of irradiation time. Symbol; experimental data, solid line; the best fit curve based on chemical kinetics.

Production of D-Ala

The peak of D-Ala was close to large unidentified peaks (figure 3.13), and it was difficult to judge whether the peak of D-Ala was found or not in the case of 240 seconds irradiation. Therefore we could not obtain the time-dependent plot precisely (figure 3.18) and determine the quantum efficiency in a similar way above mentioned. Further experiments are necessary. Thus, we determined the production quantum efficiency using a similar way reported by Tanaka *et al.* (2008) in the case of D-Ala.

The production quantum efficiency η was defined as $N = \eta P$, where N was number of produced D-Ala molecules at irradiation time t and P was total number of photons absorbed by L-Ala during irradiation time t. It should be noted that number of absorbed photons decreases with increase of irradiation time due to photolysis of

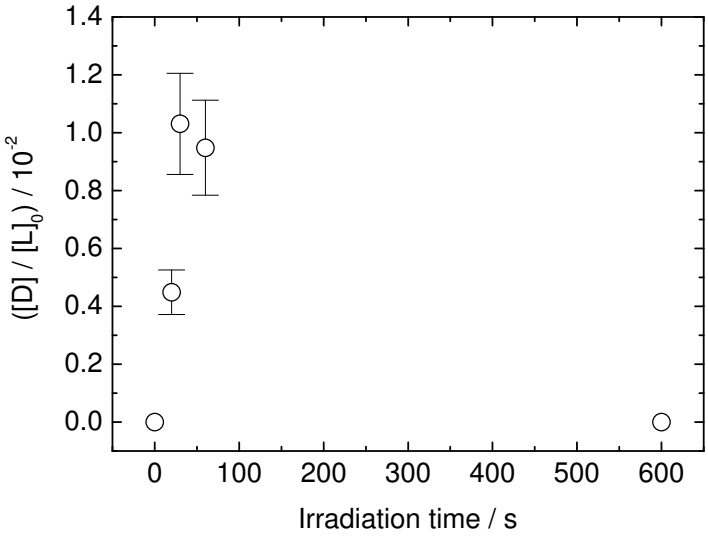

Figure 3.18: The ratio of column density of D-Ala after irradiation divided by column density of L-Ala before irradiation as a function of irradiation time.

L-Ala. Using Lambert-Beer's law, P was defined as below.

$$P = \int_0^t pS\left[1 - \exp\left(-\sigma_{\mathrm{L}}[\mathrm{L}]\right)\right] \mathrm{d}t, \tag{3.9}$$

where p was the photon flux, 5.4×10^{15} photons cm^2 s^{-1}, S was the area of films, 1.1 cm^2, σ_{L} was absorption cross section at 7.2 eV, 2.1×10^{-17} cm^2 (Kamohara *et al.*, 2008) and [L] was described as equation (3.3). N was defined as the difference between number of molecules in irradiation film and of reference film. Linear function was applied to the experimental result and obtained the best fit value using the least squares method. Obtained results are shown in figure 3.19. The data represented as filled circle (•) in figure 3.19 were ignored by fitting. Using the best fit value, D-Ala production quantum efficiency η_{D} was determined to be $(5.2 \pm 0.6) \times 10^{-3}$.

Production of LD and DL

Figure 3.20 shows the ratio of column density of LD after irradiation divided by column density of L-Ala before irradiation as a function of irradiation time. LD production processes would be described to be (1) "L-Ala + D-Ala + $h\nu \rightarrow$ LD", namely hetero-dimerization after racemization of L-Ala, and/or (2) "LL + $h\nu \rightarrow$ LD", namely racemization of LL after homo-dimerization. However we could not determine the quantum efficiencies of LD precisely since quantum efficiencies of D-Ala decomposition was not determined.

By assuming one-photon process, tentative LD production quantum efficiency was determined in a similar way as D-Ala production. Figure 3.21 shows obtained results. The data represented as filled circle (•) in figure 3.21 were ignored by fitting.

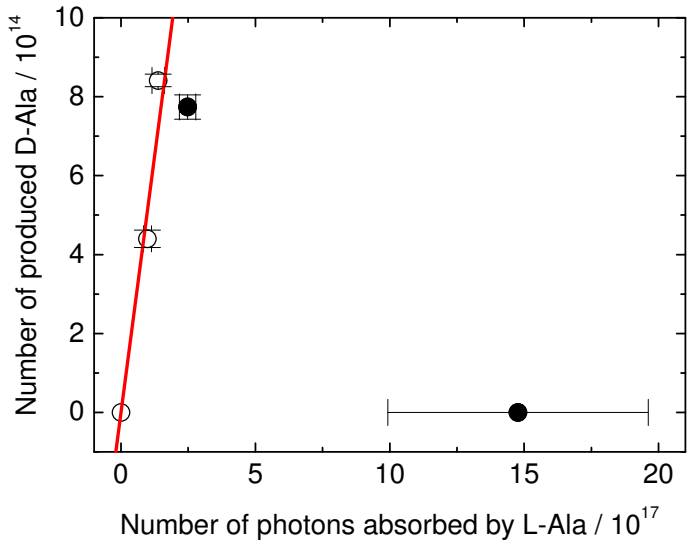

Figure 3.19: Number of produced D-Ala molecules as a function of number of photons absorbed L-Ala. From the slope of straight line, production quantum efficiency was determined. The data represented as filled circle (•) was ignored by fitting.

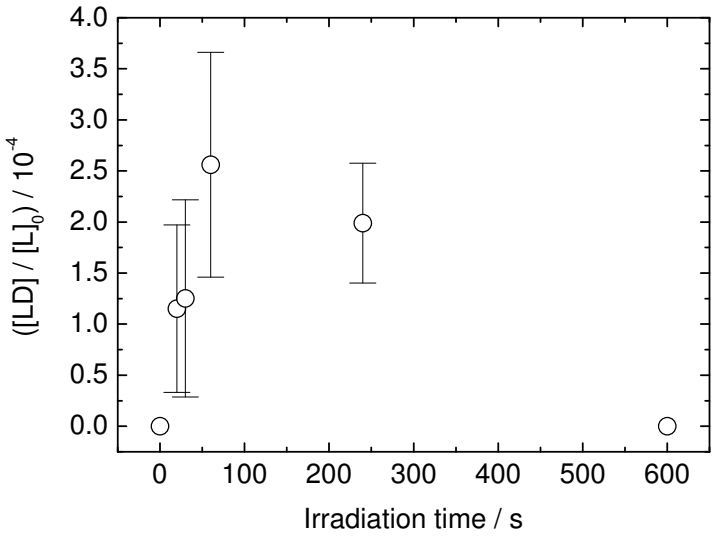

Figure 3.20: The ratio of column density of LD after irradiation divided by column density of L-Ala before irradiation as a function of irradiation time.

Using the best fit value, LD production quantum efficiency η_{LD} was determined to be $(8.5 \pm 2.8) \times 10^{-5}$.

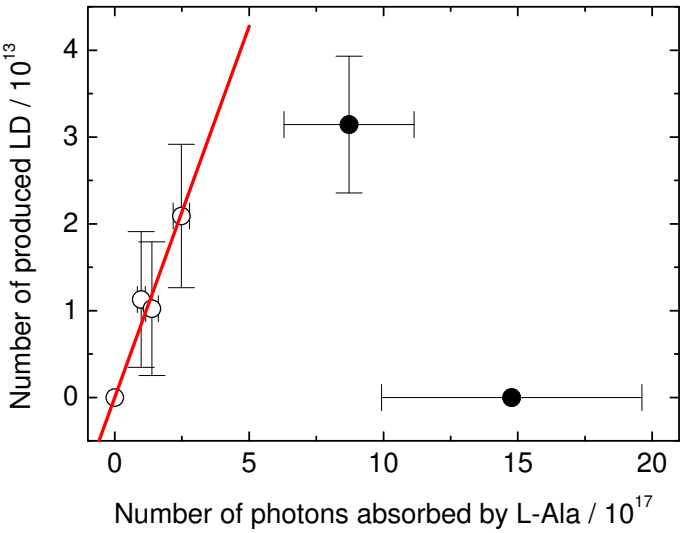

Figure 3.21: Number of produced LD molecules as a function of number of photons absorbed L-Ala. From the slope of straight line, production quantum efficiency was determined. The data represented as filled circle (•) was ignored by fitting.

As above mentioned, it was difficult to divide the peak of DL from the peak of L-Ala and determine the absolute amount of DL except 60 seconds irradiation sample. However, since the reaction process of DL should be the same as the reaction process of LD, it was concluded that DL production quantum efficiency η_{DL} was also $(8.5 \pm 2.8) \times 10^{-5}$, assuming one-photon process.

Comparison of quantum efficiency

In order to compare the quantum efficiency of L-Ala decomposition and of LL production with the quantum efficiencies of D-Ala production directly, decomposition quantum efficiency of L-Ala and production quantum efficiency of LL were determined in a similar way as D-Ala production. The decomposition quantum efficiency of L-Ala η_{L} and the production quantum efficiency of LL η_{LL} were determined to be 0.11 ± 0.05 (figure 3.22) and $(1.3 \pm 0.1) \times 10^{-3}$ (figure 3.23), respectively.

The magnitude of η_{L} means that L-Ala was decomposed with the probability of 11 ($\pm$5) % by 7.2 eV absorbed photon, in other words, L-Ala is stable with the probability of 89 ($\pm$5) % by 7.2 eV absorbed photon. The detail of 11 % was; 0.52 % racemization, namely production D-Ala, 0.13 % homo-dimerization, namely production of LL and 10.35 % the other production of other achiral molecules.

Although the probability of racemization was only 0.52 %, the magnitude of η_{D} was 4 times as large as the magnitude of η_{LL}, namely racemization is more dominant

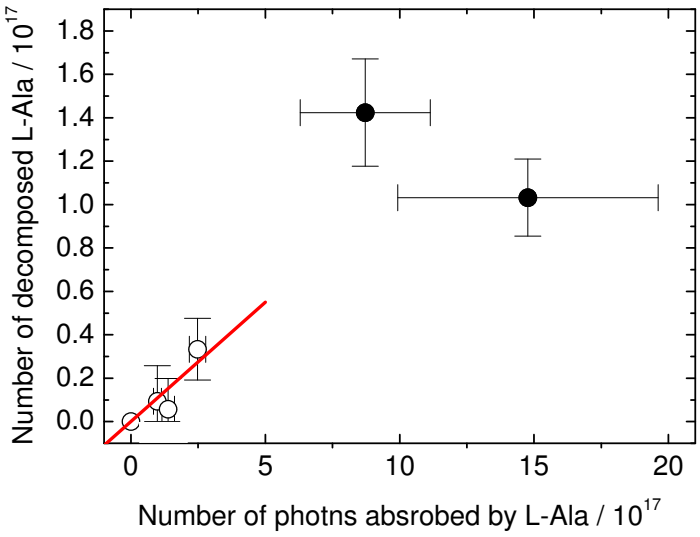

Figure 3.22: Number of decomposed L-Ala molecules as a function of number of photons absorbed L-Ala. From the slope of straight line, production quantum efficiency was determined. The data represented as filled circle (•) was ignored by fitting.

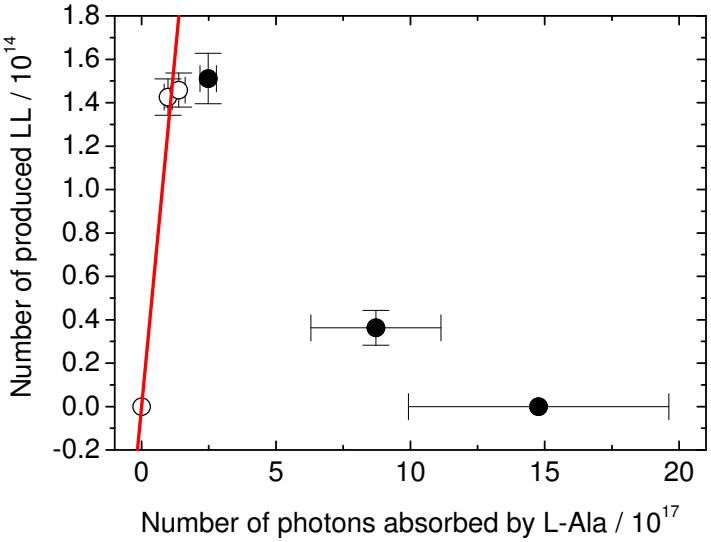

Figure 3.23: Number of produced LL molecules as a function of number of photons absorbed L-Ala. From the slope of straight line, production quantum efficiency was determined. The data represented as filled circle (•) was ignored by fitting.

than homo-dimerization in our experimental conditions. In view of chemical evolution in space and achievement of homochirality, this result may be critical problem. Therefore it is necessary to carry out similar experiments at low temperature.

3.4 Conclusion

The decomposition, racemization and dimerization rate of solid L-Ala induced by 7.2 eV VUV light in vacuum at room temperature were determined as the first step to examine the decomposition, racemization and dimerization rate of solid amino acids on the space dust surface in space. L-Ala was stable with the probability of 11 % per 7.2 eV absorbed photon. The detail of 11 % was; 0.52 % racemization, namely production D-Ala, 0.13 % homo-dimerization, namely production of LL and 10.35 % the other production of other achiral molecules. The rate of racemization was 4 times as large as the rate of homo-dimerization. In view of chemical evolution in space and achievement of homochirality, this result may be critical problem. Therefore it is necessary to carry out similar experiments at low temperature. It is also interesting to examine the ratio of racemization rate to homo-oligomerization rate in hydrothermal vent environment.

Chapter 4

Soft X-ray natural circular dichroism spectroscopy: Possibility of asymmetric photolysis of amino acids induced by circularly polarized soft X-ray

4.1 Introduction

Racemic mixture (L/D $\fallingdotseq$ 1) of amino acids or sugars are produced in typical chemical syntheses, but L-type amino acids and D-type sugars are dominant on earth. One of the leading hypotheses is that homochiral amino acids and sugars were originated from asymmetric production and/or decomposition induced by chiral energy sources in space (Bonner, 1991). Circularly polarized light (CPL) is proposed as an effective chiral energy source. CPL is produced from Mie scattering by dust clouds in star formation region (Bailey *et al.*, 1998; Fukue *et al.*, 2009) or comet (Rosenbush *et al.*, 2007) and synchrotron radiation (SR) from charged particles captured by strong magnetic field around neutron stars or white dwarfs in supernova remnant area (Greenberg, 1994).

Some examinations of asymmetric reactions of amino acids by using circularly polarized ultraviolet (UV) have been reported. Flores *et al.* (1977) reported asymmetric photolysis of aqueous solution of racemic leucine. Nishino *et al.* (2001, 2002) reported its pH dependence. Takano *et al.* (2007) reported that enantiomeric excess in alanine was detected after circularly polarized ultraviolet irradiation to amino acids precursor and hydrolysis. In solid phase, Meierhenrich *et al.* (2005) reported asymmetric photolysis of leucine and Takahashi *et al.* (2009) also reported asymmetric photolysis of solid phenylalanine, alanine and isovaline. Thus asymmetric reaction of amino acids induced by circularly polarized ultraviolet is well known reactions. However the effect of circularly polarized X-ray has never examined although SR from supernova remnant area includes not only UV but also X-ray (*e.g.* Atoyan and Aharonian, 1996). It is well known that X-ray, especially soft X-ray which includes absorption edges of biomolecules, has higher reactivity than UV.

Does circularly polarized soft X-ray also act as a chiral energy source?

Buchardt (1974) reported the conditions which was need for asymmetric reaction induced by CPL. According to the report, first condition is that the light must be absorbed. Secondly, it is necessary to irradiate with light of such a wavelength (an energy) that the natural circular dichroism (NCD), which is defined to be a difference in the magnitude of absorption cross section for left circularly polarized light (LCPL) and right circularly polarized light (RCPL), is different from zero, or the integral of the NCD over all wavelengths (energies) used must be different from zero if broad band light is used. Therefore, one can judge whether asymmetric reactions by measuring in soft X-ray region.

In this chapter, NCD spectra of amino acids, aspartic acid (Asp), serine (Ser) and alanine (Ala), were measured in the energy region of oxygen K-edge. Comparing those spectra, possibility of asymmetric photolysis induced by circularly polarized soft X-ray was examined and enantiomeric excess of those amino acids induced by circularly polarized soft X-ray were estimated.

4.2 Experimental procedures

4.2.1 Sample preparation

L-Ser (purity $\geq$ 98 %), D-Ser (purity $\geq$ 98 %), L-Ala (purity $\geq$ 98 %) and D-Ala (purity $\geq$ 98 %) were purchased from Sigma-Aldrich Corporation and L-Asp (purity $\geq$ 99 %) and D-Asp (purity $\geq$ 98 %) were purchased from Wako Pure Chemical Industries, Ltd. All samples were prepared in a similar way as section 2.2.1.Those amino acids were used without further purification. A thin film of Ser or Ala was prepared on a SiN membrane (3 mm $\times$ 3mm, thickness 100 nm; ATN/MEM-N03001/7.5M, NTT Advanced Technology Corporation). Thickness of film was estimated to be about 300 nm by using a quartz crystal oscillator thickness monitor. In the case of Asp, other SiN membranes (5 mm $\times$ 5 mm, thickness 100 nm; Silson Ltd.) were used and thickness of film was estimated to be about 500 nm.

4.2.2 Measurement of XANES and NCD

Measurement of X-ray absorption near edge structure (XANES) and NCD was carried out at the SPring-8 BL25SU, Japan (Muro *et al.*, 2007). SPring-8 was operated in 203 bunches mode with electron energy of 8 GeV and in top-up injection mode which keeps the storage ring current 100 mA. LCPL and RCPL were switched with 1 Hz using the twin helical undulators (Shirasawa *et al.*, 2004) composed of two tandem helical undulators and five kicker magnets. In this work, the CPL whose electric vector rotated counterclockwise as seen from an observer was defined as LCPL.

Figure 4.1 and 4.2 show a photograph of the experimental chamber and a schematic view of the measurement system. Incident light intensity (I_0) and transmitted light intensity (I) were obtained by measuring the drain current from a SiC membrane positioned at the upstream side of samples and from a gold film evaporated onto stainless steel plate positioned at the downstream side of samples, respectively. Drain

current was converted into pulse signals by a current amplifier (Model428 current amplifier, Keithley Instruments Inc.; "A/V" in figure 4.2), the current gain of which was set at 10^{10}, and a voltage to frequency converter (DS-VFC2, SEIKO EG&G Co., Ltd.; "V/F" in figure 4.2), the conversion gain of which was set at 10^5, and recorded (Muro *et al.*, 2004). For the NCD detection, photon energy of LCPL and of RCPL must be same since artificial NCD is observed. Since the energy difference depends on the position of the front-end slit (Muro *et al.*, 2007), the position was carefully adjusted to produce minimum energy difference using samples which shows no NCD, such as oxygen gas and nickel oxide (II) powder.

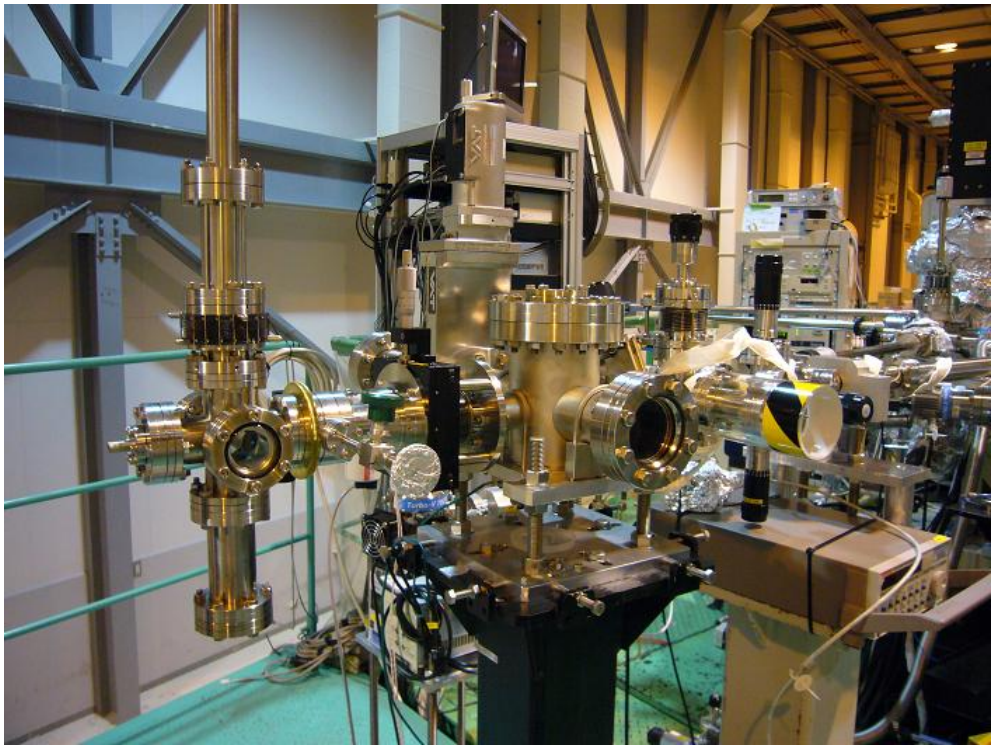

Figure 4.1: A photo of the experimental chamber

For each measurement, two series of XANES spectra in both cases of LCPL and RCPL were measured in the photon energy region of $520 < E < 560$ eV at room temperature. Optical density ($\mathrm{OD} = \log(I_0/I)$) for LCPL ($\mathrm{OD}^{\mathrm{LCPL}}$) and OD for RCPL ($\mathrm{OD}^{\mathrm{RCPL}}$) were determined. It was assumed that the experimental absorption cross section $\sigma(E)$ at the pre-edge and the post-edge region should be equal to the summation of atomic absorption cross section σ_{atom} of its component atoms (Henke *et al.*, 1993), and determined the constant α which satisfied equation (4.1) at pre-edge and post-edge region since precise thickness of each film was not determined.

$$\sigma_{\mathrm{atom}}(E) = \alpha\,\mathrm{OD}(E) = \sigma(E). \tag{4.1}$$

Thus, absorption cross section for LCPL (σ^{LCPL}) and for RCPL (σ^{RCPL}) were determined. Subtracting σ^{RCPL} from σ^{LCPL}, difference of absorption cross section $\Delta\sigma$ was obtained.

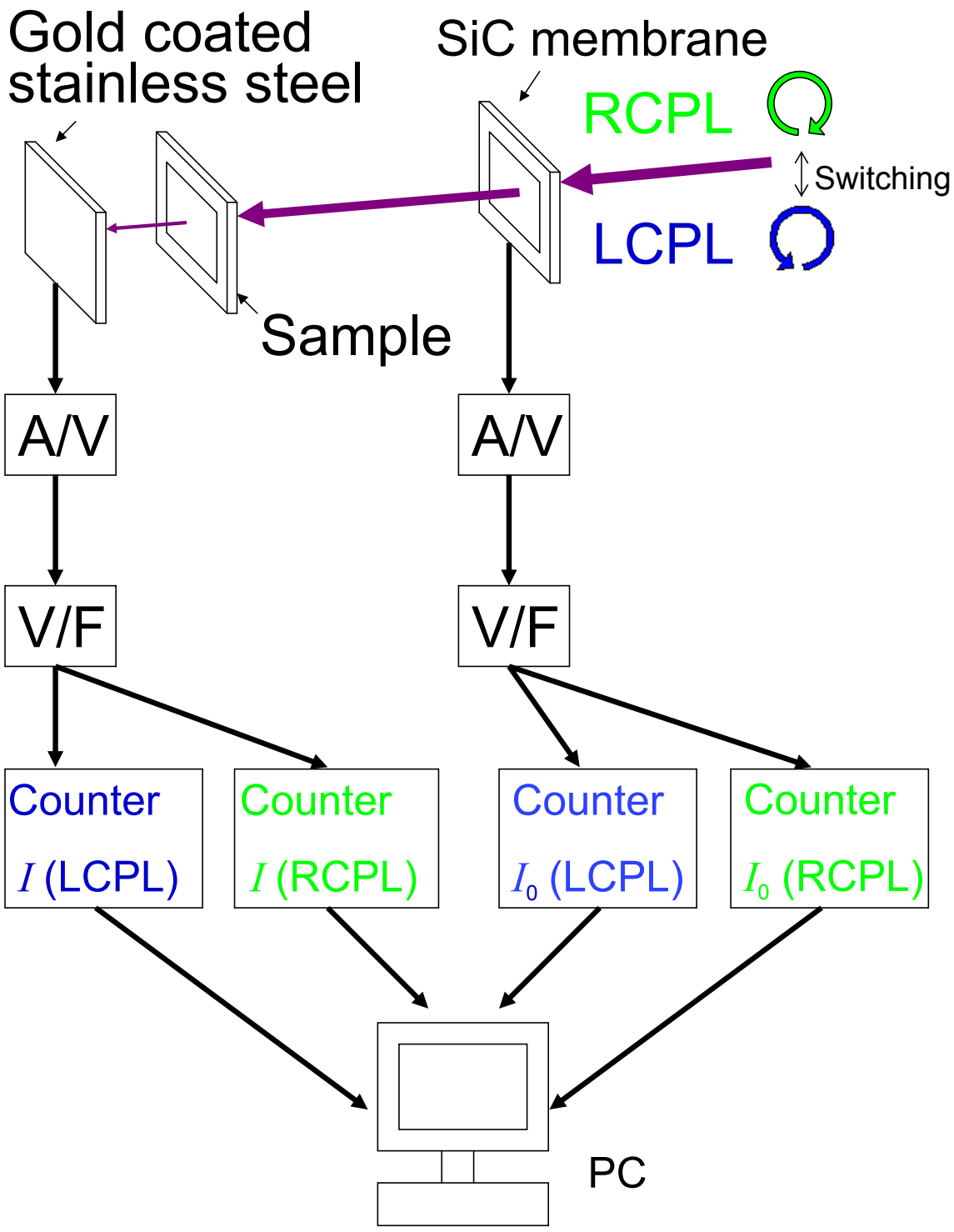

Figure 4.2: A schematic view of the measurement system

$\Delta\sigma$ is equal to NCD in ideal case. However $\Delta\sigma$ of solid samples ordinary include the effect of linear anisotropy, namely linear dichroism (LD) and linear birefringence (LB). Since LD and LB are much larger than NCD, one cannot conclude that $\Delta\sigma$ measured only once reflects true NCD immediately. However Shindo *et al.* (1990) and Kuroda *et al.* (2001) have developed a universal method to extract true NCD signals from observed signals includes LD and LB. According to their reports, LD and LB depend on sample rotation angles θ and ϕ, where θ and ϕ are rotation angles around parallel axis and perpendicular axis to the direction of incident light, respectively (figure 4.3), and observed $\Delta\sigma$ is described as below.

$$\Delta\sigma\left(E,\theta,\phi=0^\circ\right)=\mathrm{CD}+\left(\mathrm{LD}'\mathrm{LB}-\mathrm{LDLB}'\right)/2+\left(\mathrm{LD}'\sin 2\theta-\mathrm{LD}\cos 2\theta\right)\beta, \quad (4.2)$$

and

$$\Delta\sigma\left(E,\theta,\phi=180^\circ\right)=\mathrm{CD}-\left(\mathrm{LD}'\mathrm{LB}-\mathrm{LDLB}'\right)/2+\left(-\mathrm{LD}'\sin 2\theta-\mathrm{LD}\cos 2\theta\right)\beta, \quad (4.3)$$

where CD is true NCD signals, LD and LD′ are LD in 0°-90° direction and LD in 45°-135° direction, respectively, LB and LB′ are LB in 0°-90° direction and LB in 45°-135° direction, respectively and β is the component originated from optical system. For each sample, two series of spectra at $\phi = 0^\circ$ and 180° were measured as a function of θ in order to obtained linear anisotropy free signals. By averaging the $\Delta\sigma\left(E,\theta,\phi\right)$ for $\theta = 0^\circ$, $\pm 45^\circ$ and 90° at $\phi = 0^\circ$ and 180°, NCD component $\Delta\sigma_{\mathrm{av}}(E)$ was extracted from observed $\Delta\sigma$ spectra.

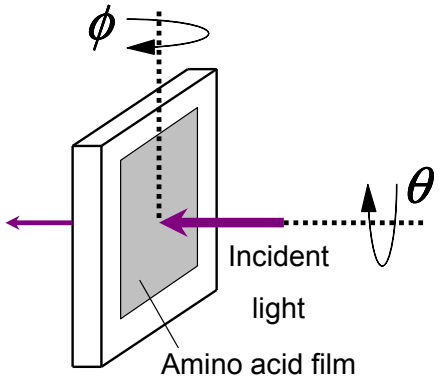

Figure 4.3: A schematic view of the rotation angles

4.3 Results and Discussion

4.3.1 XANES and NCD spectra of Asp

Figure 4.4 shows XANES spectrum of L-Asp $\sigma(E)$ and of its component atoms $\sigma_{\mathrm{atom}}(E)$. Experimental error was less than 5 %. Four peaks were found at 532.60, 534.43, 540.55 and 542.98 eV. The magnitude of absorption cross section of L-Asp

was 5.37×10^{-18} cm^2, 2.87×10^{-18} cm^2, 5.22×10^{-18} cm^2 and 5.31×10^{-18} cm^2, respectively. The peaks found at 532.60 and 534.43 eV were assigned to be oxygen of COO^- 1s $\rightarrow \pi^*$ transition and oxygen of COOH 1s $\rightarrow \pi^*$ transition, respectively (Clark *et al.*, 1976; Tanaka *et al.*, 2001; Zubavichus *et al.*, 2005). The peaks found at 540.55 eV and 542.98 eV were assigned to both oxygen COO and COOH 1s $\rightarrow$ σ^* transitions (Clark *et al.*, 1976; Tanaka *et al.*, 2001; Zubavichus *et al.*, 2005).

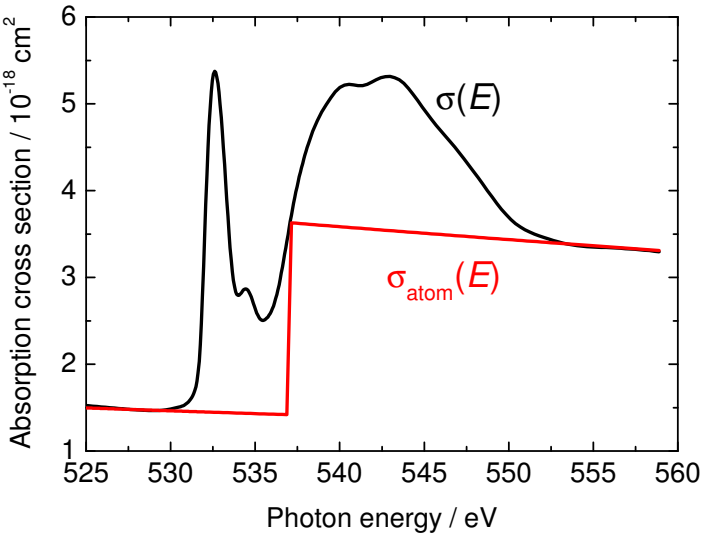

Figure 4.4: XANES spectrum of L-Asp $\sigma(E)$ (black) and of component atoms $\sigma_{\mathrm{atom}}(E)$ (red)

Figure 4.5 shows $\Delta\sigma$ spectra of L-Asp as a function of θ and ϕ. In the case of $\phi = 0°$, positive $\Delta\sigma$ was observed independently θ around 543 eV (figure 4.5-(a)). In contrast, negative $\Delta\sigma$ was observed independently θ around 543 eV in the case of $\phi = 180°$. In figure 4.5-(b), θ and/or ϕ dependence was also observed around 531-535 eV. Similar results were observed in the case of D-Asp. Therefore it was concluded that linear anisotropy component which depends on θ and ϕ was included in $\Delta\sigma$ spectra.

Figure 4.6 shows NCD component spectra $\Delta\sigma_{\mathrm{av}}(E)$ of L- and D-Asp extracted from $\Delta\sigma$ spectra. L- and D-Asp had opposite peaks each other around 530-535 eV. Peak gap between $\Delta\sigma_{\mathrm{av}}$ spectrum of L-Asp and of D-Asp was also observed around 540-545 eV. These differences were originated from NCD. However, it is established that NCD of enantiomers, in soft X-ray region, should have the same modulus and opposite sign each other (Alagna *et al.*, 1998; Stewart *et al.*, 1999; Turchini *et al.*, 2004). Therefore it was concluded that background component BG(E) was still included. Since the background component was independent from sample rotation angles θ and ϕ, it would be originated from the optical system or the detector.

Similar way reported by Turchini *et al.* (2004) was used in order to cancel out the background component BG(E). True NCD signal of L-Asp $\mathrm{CD^L}(E)$ and of D-Asp

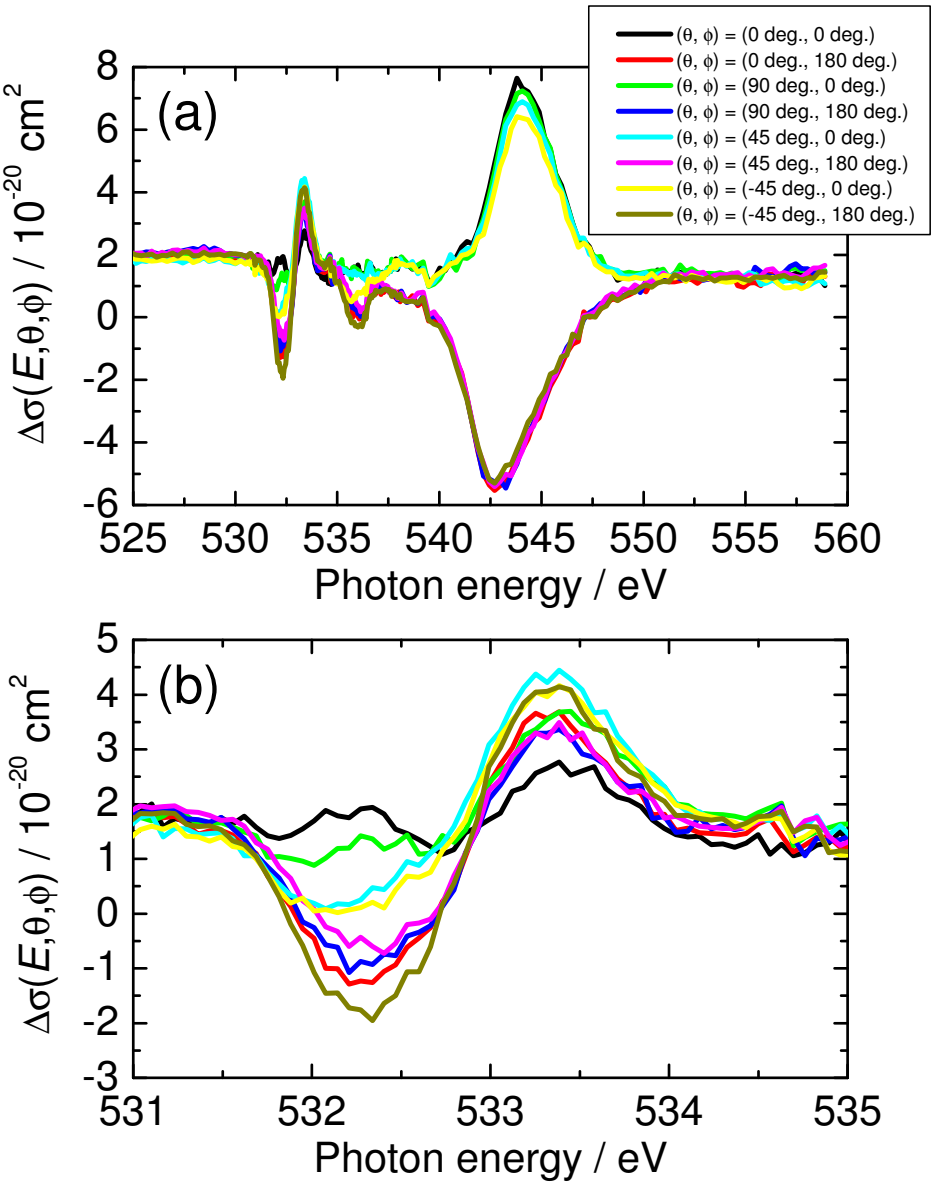

Figure 4.5: (a) $\Delta\sigma$ spectra of L-Asp as a function of θ and ϕ. (b) Magnification of figure 4.5-(a) around 531-535 eV

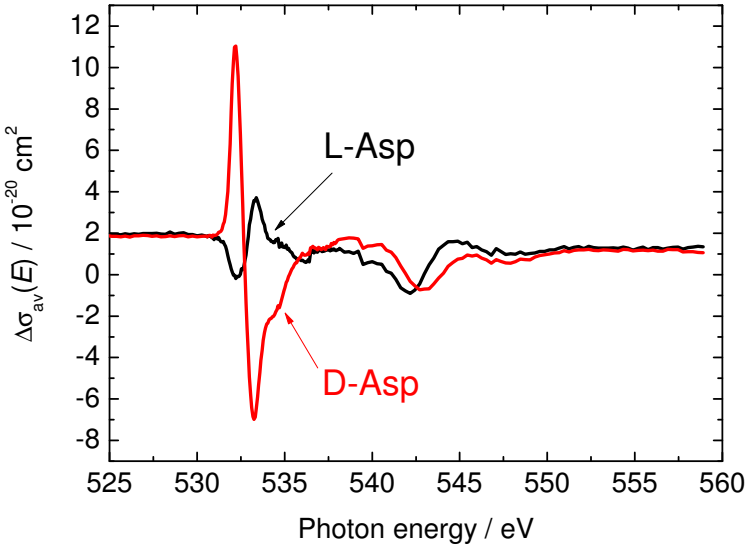

Figure 4.6: NCD component spectra $\Delta\sigma_{\mathrm{av}}(E)$ of L- and D-Asp extracted from $\Delta\sigma$ spectra

$\mathrm{CD}^{\mathrm{D}}(E)$ was described as below using $\Delta\sigma_{\mathrm{av}}(E)$ and $\mathrm{BG}(E)$.

$$\mathrm{CD}^{\mathrm{L}}(E) = \Delta\sigma^{\mathrm{L}}_{\mathrm{av}}(E) - \mathrm{BG}(E) \tag{4.4}$$

and

$$\mathrm{CD}^{\mathrm{D}}(E) = \Delta\sigma^{\mathrm{D}}_{\mathrm{av}}(E) - \mathrm{BG}(E). \tag{4.5}$$

Equation (4.6) was obtained subtracting equation (4.5) from equation (4.4) since $\mathrm{BG}(E)$ was not dependent on samples.

$$\mathrm{CD}^{\mathrm{L}}(E) - \mathrm{CD}^{\mathrm{D}}(E) = \Delta\sigma^{\mathrm{L}}_{\mathrm{av}}(E) - \Delta\sigma^{\mathrm{D}}_{\mathrm{av}}(E). \tag{4.6}$$

Since $\mathrm{CD}^{\mathrm{L}}(E)$ and $\mathrm{CD}^{\mathrm{D}}(E)$ have the same modulus and opposite sign each other, namely $\mathrm{CD}^{\mathrm{L}}(E) = -\mathrm{CD}^{\mathrm{D}}(E)$. Thus, true NCD signal of L-Asp $\mathrm{CD}^{\mathrm{L}}(E)$ was described as below.

$$2\mathrm{CD}^{\mathrm{L}}(E) = \Delta\sigma^{\mathrm{L}}_{\mathrm{av}}(E) - \Delta\sigma^{\mathrm{D}}_{\mathrm{av}}(E) \tag{4.7}$$

$$\Leftrightarrow \mathrm{CD}^{\mathrm{L}}(E) = \frac{\Delta\sigma^{\mathrm{L}}_{\mathrm{av}}(E) - \Delta\sigma^{\mathrm{D}}_{\mathrm{av}}(E)}{2}. \tag{4.8}$$

True NCD signal of D-Asp $\mathrm{CD}^{\mathrm{D}}(E)$ was obtained to be $\left(-\Delta\sigma^{\mathrm{L}}_{\mathrm{av}}(E) + \Delta\sigma^{\mathrm{D}}_{\mathrm{av}}(E)\right)/2$.

Figure 4.7 shows true NCD spectrum of L-Asp. Large negative and positive peaks were observed at 532.21 and 533.25 eV, respectively. The magnitude of NCD was -5.61×10^{-20} cm^2 and 5.29×10^{-20} cm^2, respectively. Both peaks would be assigned to be oxygen of COO^- 1s $\rightarrow \pi^*$ transition. The shoulder observed around 534.43 eV (1.74×10^{-20} cm^2) would be assigned to be oxygen of COOH 1s

$\rightarrow \pi^*$ transition. Small negative and positive peaks were also observed at 541.63 (-0.53×10^{-20} cm^2) and 543.79 eV (0.70×10^{-20} cm^2), respectively. Those peaks would be assigned to both oxygen COO^- and COOH 1s $\rightarrow \sigma^*$ transitions. It is noted that NCD peak assignment was carried out by analogy from the XANES peak assignment. Therefore precise theoretical analyses may be necessary. Theoretical corroboration is expected.

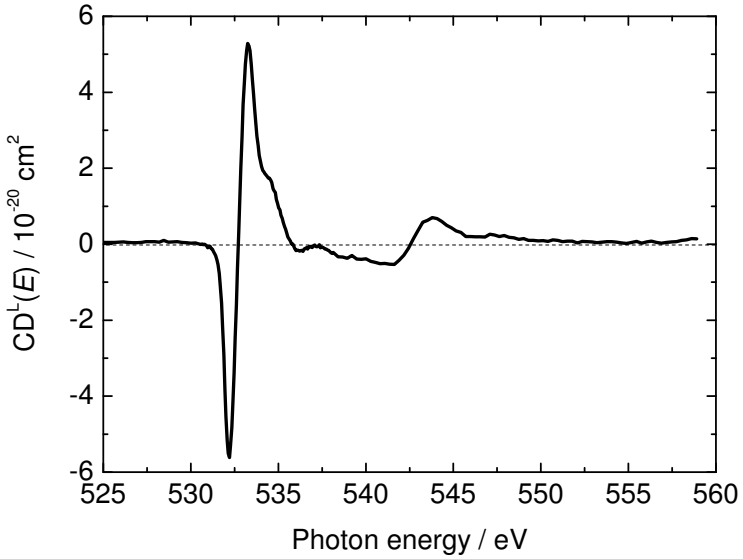

Figure 4.7: True NCD spectrum of L-Asp $CD^L(E)$

4.3.2 XANES and NCD spectra of Ser

Figure 4.8 shows XANES spectrum of L-Ser $\sigma(E)$ and theoretical XANES spectrum of L-Ser reported by Plashkevych *et al.* (1998). Experimental error was less than 5 %. Photon energy of theoretical spectrum was shifted by about 1.5 eV to lower energy side in order to compare with our experimental data around 532.1 eV. In the experimental spectrum, two peaks were observed around 532.1 and 538.2 eV and two shoulders were observed around 535.0 and 545.6 eV. The magnitude was 3.5×10^{-18} cm^2, 4.5×10^{-18} cm^2, 2.6×10^{-18} cm^2 and 3.5×10^{-18} cm^2, respectively. The peak found around 532.1 eV was assigned to be oxygen of COO^- 1s $\rightarrow \pi^*$ transition (Plashkevych *et al.*, 1998; Tanaka *et al.*, 2001; Zubavichus *et al.*, 2005). The shoulder found around 535.0 eV and part of the peak found around 538.2 eV were assigned to be oxygen of OH 1s $\rightarrow \sigma^*$ transition (Plashkevych *et al.*, 1998; Tanaka *et al.*, 2001; Zubavichus *et al.*, 2005). The shoulder found around 545.6 eV and part of the peak found around 538.2 eV were assigned to be oxygen of COO^- 1s $\rightarrow \sigma^*$ transition (Tanaka *et al.*, 2001; Zubavichus *et al.*, 2005). In the theoretical spectrum, three peaks which correspond with the experimental peaks were predicted

around 532.1, 534.8 and 537.4 eV. Another peak was predicted around 533.6 eV, but no peak was observed experimentally. In addition, no peak was predicted around 545.6 eV although the shoulder was observed around 545.6 eV.

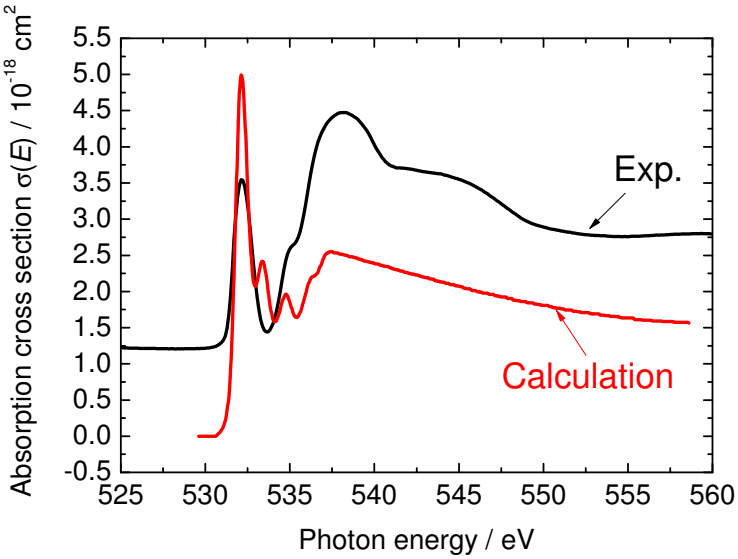

Figure 4.8: XANES spectrum of L-Ser $\sigma(E)$ (black) and theoretical calculation (red; Plashkevych *et al.*, 1998)

Figure 4.9 shows NCD component spectra $\Delta\sigma_{\mathrm{av}}(E)$ of L- and D-Ser. In the case of Ser films, rotation angle dependence were not observed. However it was concluded that background component was included since the spectra did not have same modulus and opposite sign each other. In order to cancel out the background component, similar way mentioned in section 4.3.1 was used. Figure 4.10 shows true NCD spectrum of L-Ser $\mathrm{CD^L}(E)$. Negative NCD peaks were observed around 532.5, 538.5 and 542-548 eV.The magnitude was -0.17×10^{-20} cm^2, -0.47×10^{-20} cm^2 and about -0.2×10^{-20} cm^2, respectively. Those peaks would be assigned to be oxygen of $\mathrm{COO^-}$ 1s $\rightarrow \pi^*$ transition, oxygen of OH 1s $\rightarrow \sigma^*$ transition and oxygen of $\mathrm{COO^-}$ 1s $\rightarrow \sigma^*$ transition, respectively. Positive NCD signal was observed around 541.4 eV and the magnitude was 0.27×10^{-20} cm^2. This peak may also be assigned to be oxygen of $\mathrm{COO^-}$ 1s $\rightarrow \sigma^*$ transition. It was concluded that positive signal found around 552.7 eV was not NCD signal since absorption peak was not observed around 552.7 eV.

NCD spectrum was compared with theoretical calculation based on the electric-dipole-magnetic-dipole interaction mechanism (E1M1 mechanism) in length gauge (Plashkevych *et al.*, 1998). Figure 4.11-(a) shows experimental and theoretical XANES spectra of L-Ser and figure 4.11-(b) shows true NCD spectrum of L-Ser $\mathrm{CD^L}(E)$ and theoretical rotatory strengths of L-Ser. Figure 4.12 shows the magnification of figure 4.11 around 530-535 eV. The relation between rotatory strength R

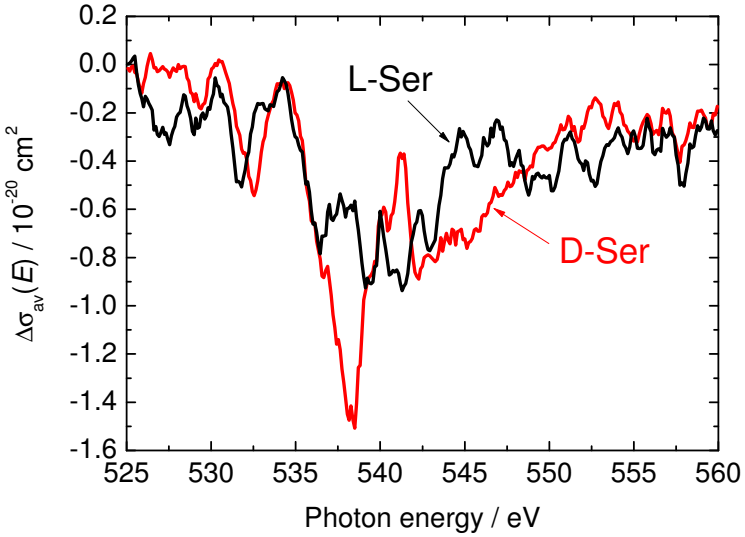

Figure 4.9: NCD component spectra $\Delta\sigma_{\mathrm{av}}(E)$ of L- and D-Ser

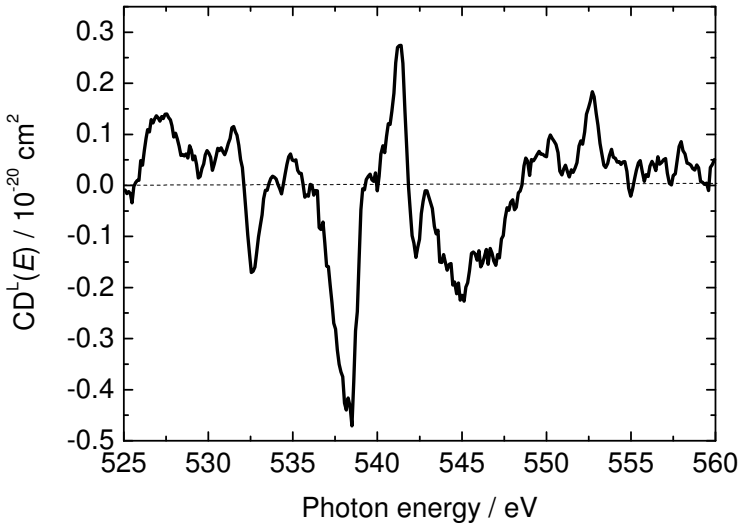

Figure 4.10: True NCD spectrum of L-Ser $\mathrm{CD}^{\mathrm{L}}(E)$

[esu^2 cm^2] and NCD spectrum CD [cm^2] is given by the following equation.

$$R = \frac{3hc}{32\pi^3} \int_{E_1}^{E_2} \frac{\mathrm{CD}}{E} \mathrm{d}E, \tag{4.9}$$

where h is Planck constant and c is light speed. In figure 4.11, positive rotatory strengths were predicted at 537.0 ($R = 1.0 \times 10^{-43}$ esu^2 cm^2) and 537.3 eV ($R = 1.2 \times 10^{-43}$ esu^2 cm^2). However, no positive NCD peak was observed around 537 eV. Summation of these rotatory strengths may correspond to positive NCD peak found around 541.4 eV. In figure 4.12, nagative peak observed around 532.5 eV would be correspond to the summation of two nagative rotatory strengths predicted at 532.05 ($R = -1.8 \times 10^{-43}$ esu^2 cm^2) and 532.15 eV ($R = -1.5 \times 10^{-43}$ esu^2 cm^2). In order to compare the experimental NCD with theoretical rotatory strength, experimental NCD was converted into rotatory strength using equation (4.9). The experimental rotatory strength was -1.4×10^{-42} esu^2 cm^2 and about four times as large as summation of theoretical rotatory strengths. A positive rotatory strength predicted at 532.02 eV may correspond to the positive NCD signals found around 531.5 eV whose S/N ratio was bad. Although another positive rotatory strength was predicted at 533.39 eV, no NCD peak was observed around this energy. It would be correspond that no XANES peak was observed around this energy.

Thus, NCD peak assigned to be oxygen of COO^- 1s $\rightarrow \pi^*$ transition was reproduced by the theoretical calculation based on E1M1 mechanism qualitatively. However, other NCD peaks were not reproduced. Further experimental and theoretical studies are necessary.

4.3.3 XANES and NCD spectra of Ala

Figure 4.13 shows XANES spectrum of L-Ala $\sigma(E)$. Experimental error was less than 5 %. Large peak was observed around 532.9 eV and this peak was assigned to be oxygen of COO^- 1s $\rightarrow \pi^*$ transition (Tanaka *et al.*, 2001; Zubavichus *et al.*, 2005; Jiemchooroj *et al.*, 2007). The magnitude of absorption cross section was 4.1×10^{-18} cm^2. Both peaks observed around 539.7 and 544.0 eV were assigned to be oxygen of COO^- 1s $\rightarrow \sigma^*$ transition (Tanaka *et al.*, 2001; Zubavichus *et al.*, 2005; Jiemchooroj *et al.*, 2007). The magnitude of both peaks was 2.8×10^{-18} cm^2.

Figure 4.14 shows NCD component spectra $\Delta\sigma_{\mathrm{av}}(E)$ of L- and D-Ala. In the case of Ala films, rotation angle dependence were not observed. Since evaporated film of Ala is an aggregate of randomly oriented microcrystallites (Tanaka *et al.*, 2009), the effect of linear anisotropy factor may be avoided. However it was concluded that background component was included since the spectra did not have same modulus and opposite sign each other. In order to cancel out the background component, similar way mentioned in section 4.3.1 was used. Figure 4.15 shows true NCD spectrum of L-Ala $\mathrm{CD^L}(E)$.

Negative NCD peak was observed around 532.9 eV and the magnitude was -1.4×10^{-20} cm^2. This peak was assigned to be oxygen of COO^- 1s $\rightarrow \pi^*$ transition (Jiemchooroj *et al.*, 2007). It was unable to judge whether negative signals observed around 536.8 and 540-550 eV were true NCD signals or not since S/N ratio was bad. Further works were necessary.

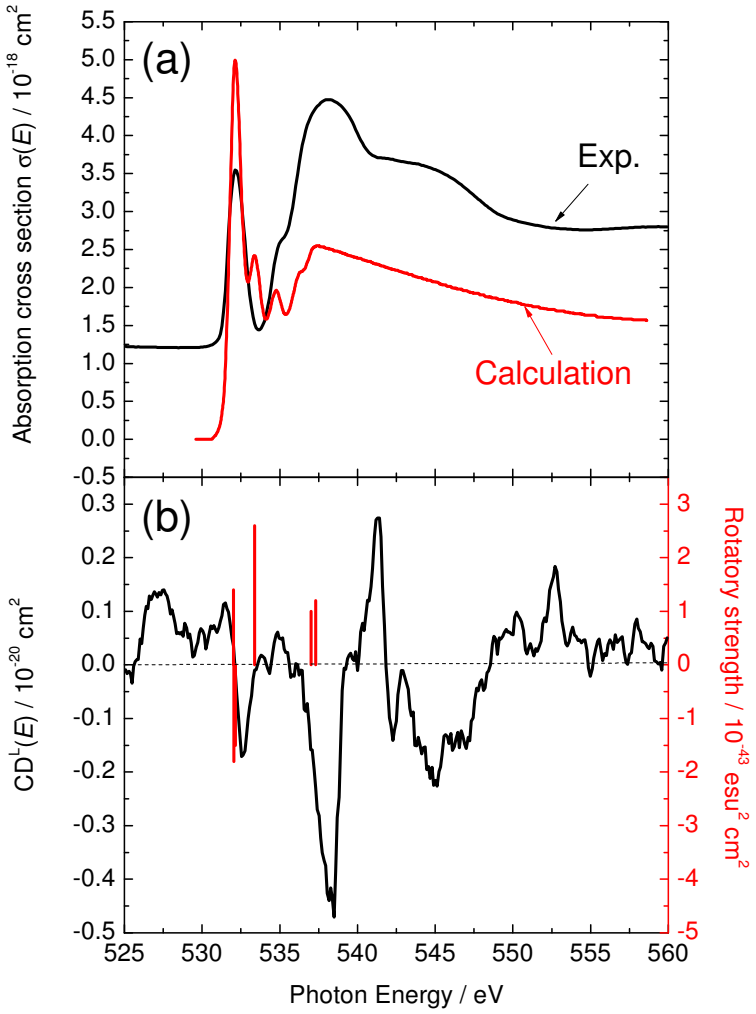

Figure 4.11: (a) Experimental XANES spectrum of L-Ser $\sigma(E)$ (black) and theoretical XANES spectrum of L-Ser (red; Plashkevych *et al.*, 1998) (b) True NCD spectrum of L-Ser $CD^{L}(E)$ and calculated rotatory strengths of L-Ser (Plashkevych *et al.*, 1998)

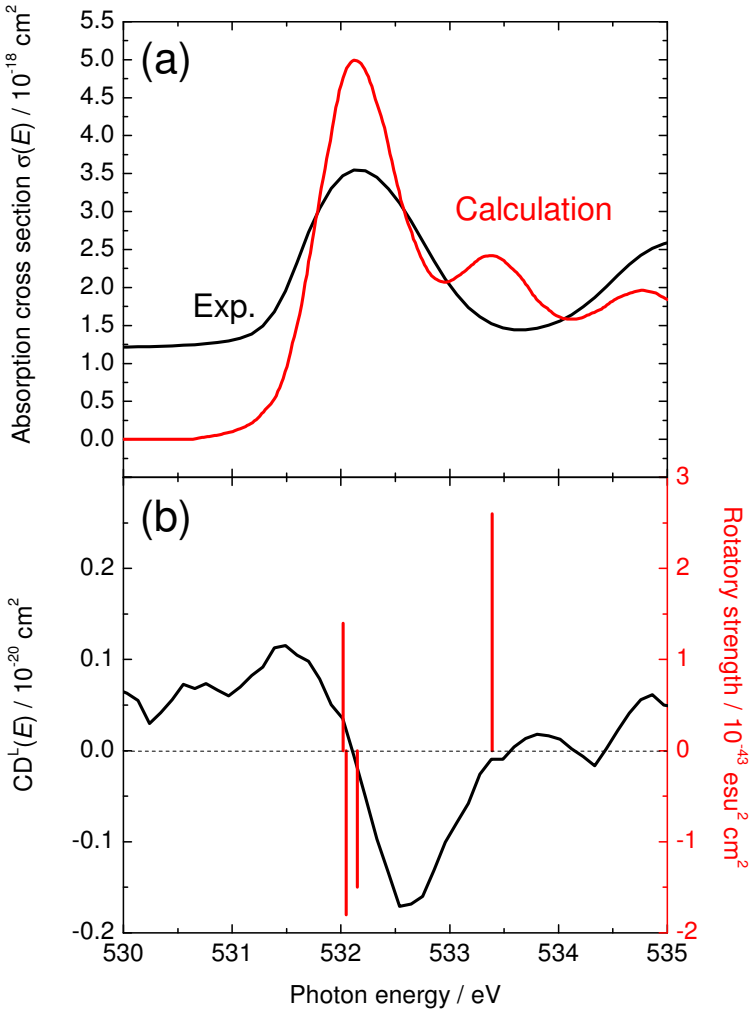

Figure 4.12: Magnification of figure 4.11. (a) experimental XANES spectrum of L-Ser $\sigma(E)$ (black) and theoretical XANES spectrum of L-Ser (red; Plashkevych *et al.*, 1998) (b) True NCD spectrum of L-Ser $CD^{L}(E)$ and calculated rotatory strengths of L-Ser (Plashkevych *et al.*, 1998)

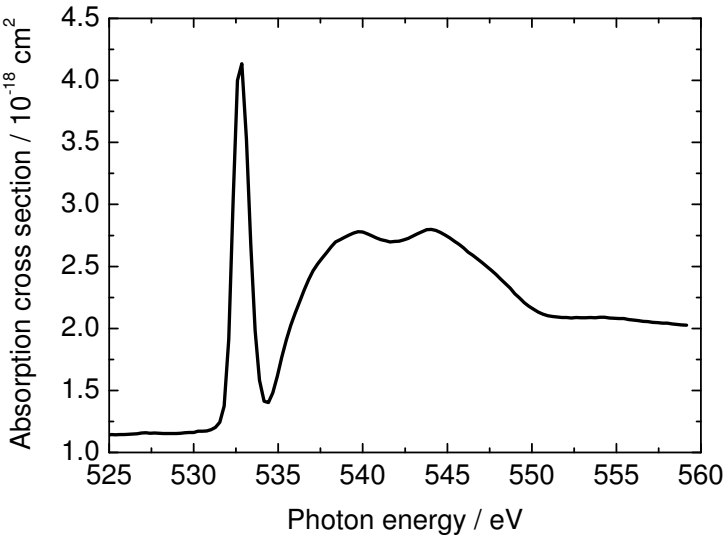

Figure 4.13: XANES spectrum of L-Ala $\sigma(E)$

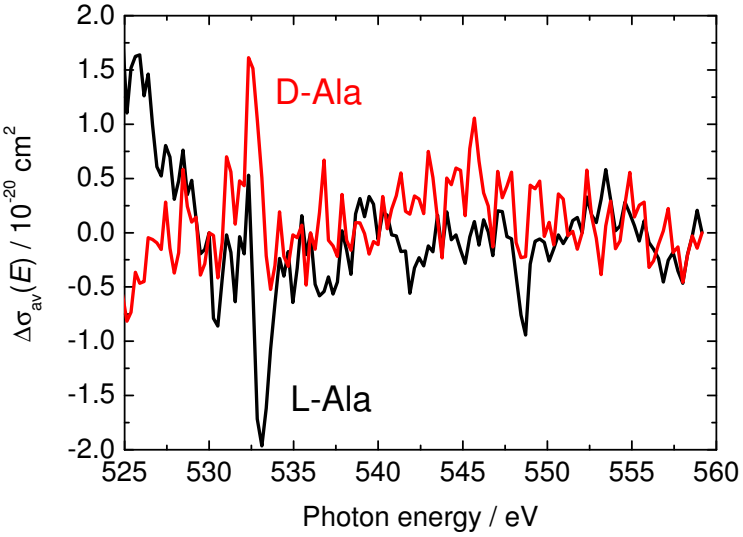

Figure 4.14: NCD component spectra $\Delta\sigma_{\mathrm{av}}(E)$ of L- and D-Ala

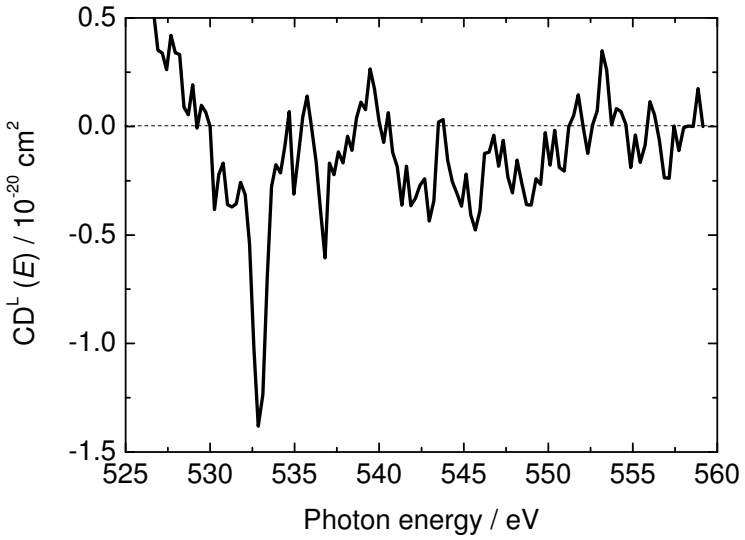

Figure 4.15: True NCD spectrum of L-Ala $CD^L(E)$

NCD spectrum was compared with theoretical calculation based on the electric-dipole-magnetic-dipole interaction mechanism (E1M1 mechanism) (Jiemchooroj *et al.*, 2007) with the focus at the oxygen of COO^- 1s $\rightarrow \pi^*$ transition since no theoretical calculation has been reported in the energy region $E > 540$ eV. Figure 4.16-(a) shows experimental and theoretical XANES spectra of L-Ala and figure 4.16-(b) shows true NCD spectrum of L-Ala CD^L and theoretical NCD spectrum of L-Ala. The photon energy of theoretical XANES spectrum was shifted by about 14.4 eV lower energy side in order to compare with experimental data at the XANES peak found around 532.8 eV. theoretical NCD spectrum was also shifted by about 14.4 eV. Although two XANES peaks were predicted around 532.6 and 533.0 eV, single XANES peak was observed at 532.8 eV. Probably the experimental resolution was not able to resolve the energy difference of 0.2 eV (figure 4.16-(a)). In figure 4.16-(b), two negative NCD peaks were predicted around 532.6 and 533.0 eV and a negative NCD peak was observed around 532.8 eV. The magnitude of theoretical NCD peaks was -0.93×10^{-20} cm^2 and -0.62×10^{-20} cm^2. The summation of magnitude of two theoretical NCD peaks was as large as the magnitude of experimental NCD signal. It was concluded that the intensity of experimental NCD of L-Ala was reproduced by this theoretical calculation within spectral resolution although large energy shift (about 14.4 eV) was required. Theoretical calculation about NCD assigned to be the oxygen of COO^- 1s $\rightarrow \sigma^*$ transition is expected.

4.3.4 Comparison of experimental NCD

Figure 4.17 shows true NCD spectrum CD^L of L-Asp, L-Ser and L-Ala. In this section, NCD spectra were compared with the focus at the NCD assigned to be the

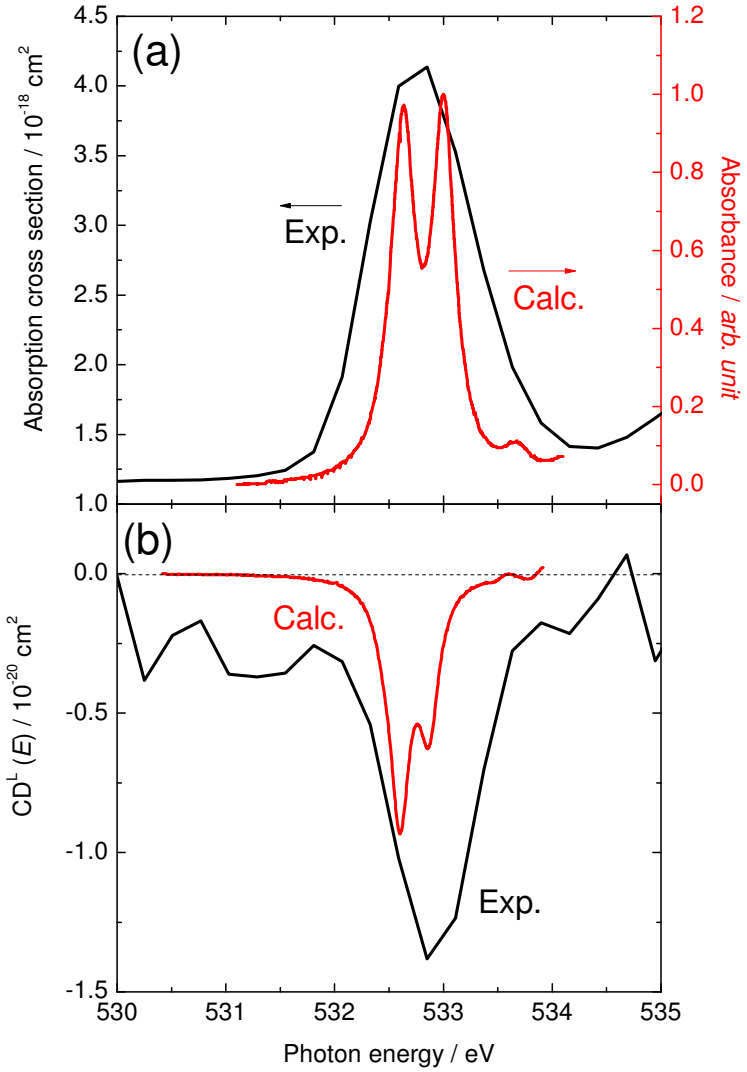

Figure 4.16: (a) Experimental XANES spectrum of L-Ala $\sigma(E)$ (black) and theoretical XANES spectrum of L-Ala (red; Jiemchooroj *et al.*, 2007) (b) True NCD spectrum of L-Ala $CD^{L}(E)$ (black) and theoretical NCD spectrum of L-Ala (red; Jiemchooroj *et al.*, 2007)

oxygen of COO^- 1s $\rightarrow \pi^*$ transition since other NCD was not partly correspond to theoretical calculations.

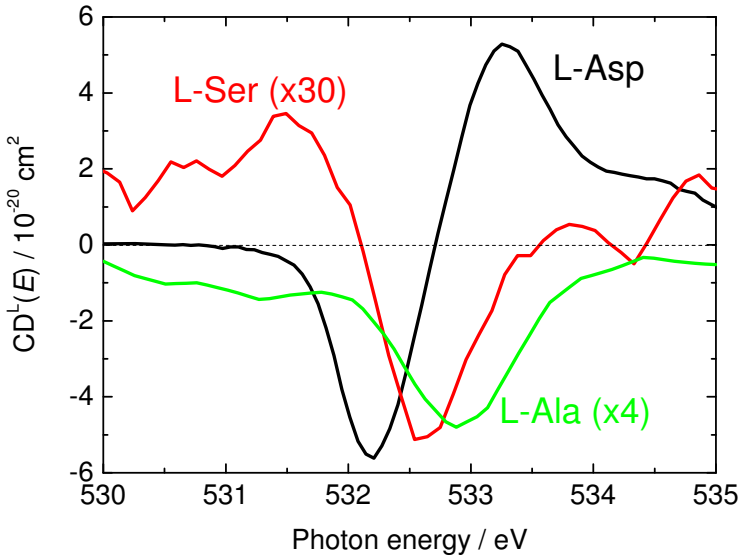

Figure 4.17: True NCD spectrum CD^L of L-Asp (black), L-Ser (red; multiplied by 30) and L-Ala (green; multiplied by 4)

The spectrum curve of L-Asp changed from negative to positive with the increase of photon energy. In contrast, the spectrum curve of L-Ser changed from positive to negative with the increase of photon energy. In the case of L-Ala, only one negative peak was observed. Difference among three amino acids reflects the difference of chiral environment of the core hole oxygen atom of COO^-. Since COO^- is common part of the biomolecular amino acids, side chain affects NCD of COO^-. It is interesting in view of application of NCD in soft X-ray region.

In order to compare the magnitude of NCD, the ratio g of NCD to absorption cross section ($\left|CD^L/\sigma\right|$) was obtained. Maximum g value of L-Asp was 1.4 %. In the case of L-Ser and L-Ala, Maximum g value was 0.055 % and 0.30 %, respectively. Maximum g value in soft X-ray region which have reported in the past (Turchini *et al.*, 2004; Tanaka *et al.*, 2005; Nakagawa *et al.*, 2005) besides L-Ser and L-Ala is 10^{-3} orders of magnitude. Thus 1.4 % is quite large value. The reason why L-Asp shows such a large NCD is open question at the present time. It is very interesting in view of both experimental and theoretical soft X-ray NCD studies.

Thus, magnitude of NCD among three kinds of amino acids were dramatically different. However, all amino acids satisfied Buchardt's required conditions (Buchardt, 1974). Therefore, it was concluded that asymmetric photolysis induced by circularly polarized soft X-ray would be occurred.

4.3.5 Estimation of enantiomeric excess induced by circularly polarized soft X-ray irradiation

In this section, enantiomeric excess (*ee*) induced by circularly polarized soft X-ray is discussed.

Figure 4.18 shows a schematic view of asymmetric photolysis of racemic molecules induced by circularly polarized light. It was assumed that the magnitude of NCD of red molecules and blue molecules were $+\alpha$ and $-\alpha$, respectively (figure 4.18-(a)). Positive NCD means that the molecules absorb LCPL rather than RCPL and negative NCD means that the molecules absorb RCPL rather than LCPL. Since the number of red molecules was equal to the number of blue molecules, namely racemic mixture, before irradiation, excess was 0 %. In the case of LCPL irradiation, red molecules were decomposed more than blue molecules since red and blue molecules had positive and negative NCD, respectively. In the example of figure 4.18-(b), two red molecules were decomposed and one blue molecules were decomposed. Thus, number of remains of blue molecules were larger than of red molecules after irradiation and excess was increased from 0 % to +14 %. In contrast, number of remains of red molecules were larger than of blue molecules after RCPL irradiation and the excess was −14 % (figure 4.18-(c)).

ee y induced by circularly polarized light is computable, called "Kagan's equation", under following assumptions (Balavoine *et al.*, 1974; Kagan *et al.*, 1974). The value of y is defined to be $([\mathrm{L}] - [\mathrm{D}]) \,/\, ([\mathrm{L}] + [\mathrm{D}])$, where [L] and [D] are number of L-type molecules and of D-type molecules, respectively.

- Racemic mixture of single-species molecules is irradiated with monochromatic LCPL or RCPL.
- Rate constant is linear-proportional to absorption cross section.
- Decomposition products are ignored.
- Production of reactant molecules from decomposition products are ignored.

Kagan's equation is derived from chemical kinetics and described as below.

$$x = 1 - \frac{1}{2}\left[\left(\frac{1+y}{1-y}\right)^{\frac{1}{g'}+\frac{1}{2}} + \left(\frac{1+y}{1-y}\right)^{\frac{1}{g'}-\frac{1}{2}}\right], \tag{4.10}$$

where x is extent of reaction, namely the ratio of the summation of decomposed enantiomers divided by the summation of initial amount of enantiomers and g' is the ratio of NCD to absorption cross section. Since L-Asp, L-Ser and L-Ala showed negative NCD, L-type excess would be observed after LCPL irradiation. Thus, L-type excess induced by left circularly polarized soft X-ray was calculated using Kagan's equation. The value of g' of L-Asp, L-Ser and L-Ala were −1.4 %, −0.055 % and −0.30 %, respectively. The results are shown in figure 4.19. The *ee* was increased with the increase of extent of reaction. Especially, *ee* was dramatically increased around $x = 0$ % and $x = 100$ %. For example, *ee* was 1.6 % at $x = 90$ %, 3.2 % at $x = 99$ % and 4.8 % at $x = 99.9$ % in the case of L-Asp.

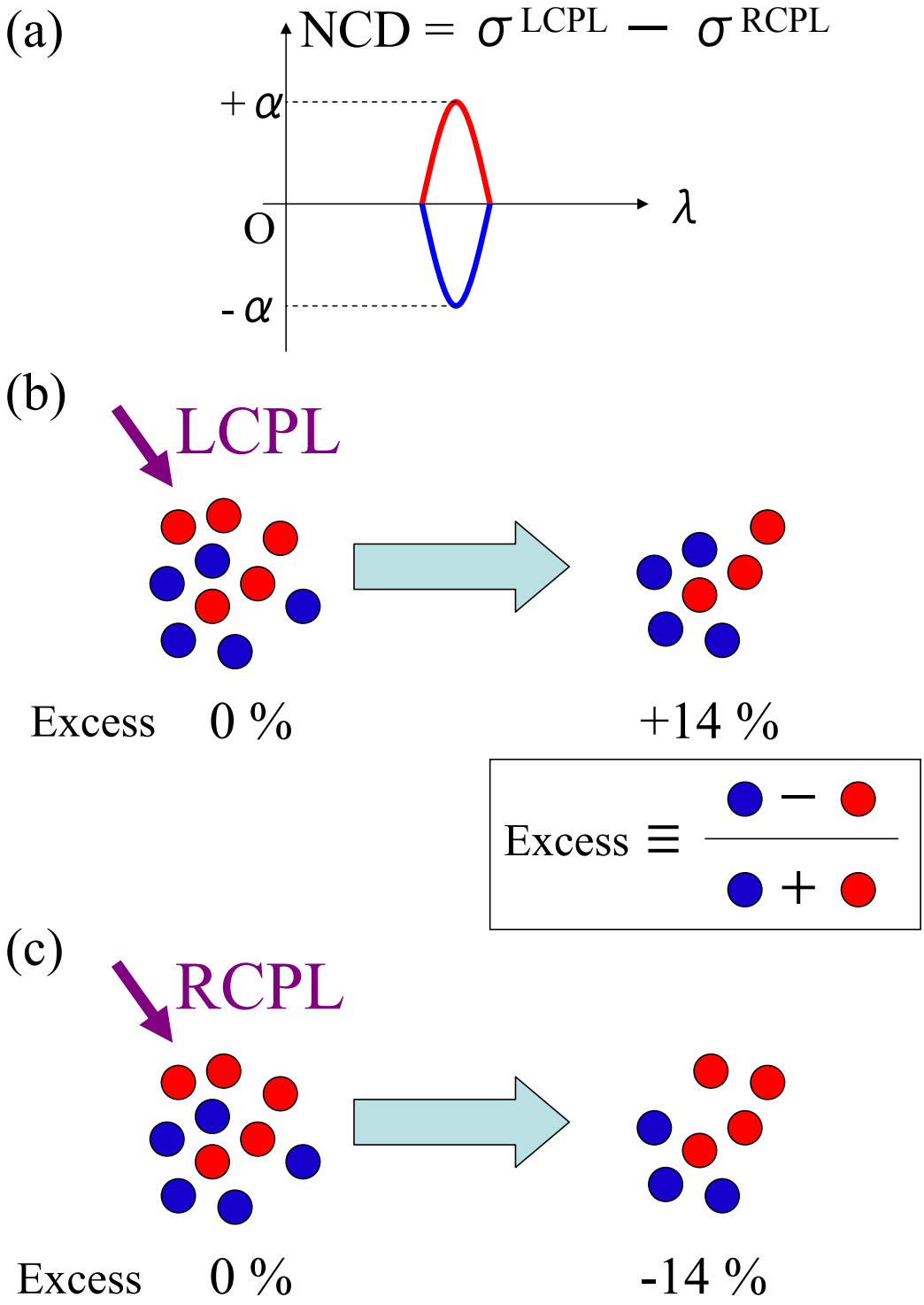

Figure 4.18: Schematic view of asymmetric photolysis of racemic molecules induced by circularly polarized light. (a) An example of NCD spectra, (b) asymmetric photolysis induced by left circularly polarized light (LCPL), (c) asymmetric photolysis induced by right circularly polarized light (RCPL).

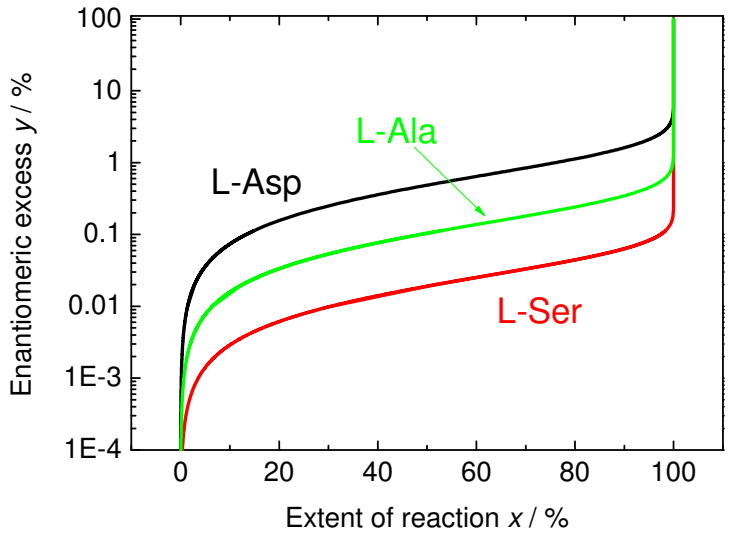

Figure 4.19: Enantiomeric excess induced by left circularly polarized soft X-ray calculated using Kagan's equation. Black; L-Asp ($g' = -1.4$ %), red; L-Ser ($g' = -0.055$ %) and green; L-Ala ($g' = -0.30$ %)

In order to discuss the numerical change of enantiomers, number of enantiomers were calculated. Using the definition of x,

$$x \equiv 1 - \frac{[\mathrm{L}] - [\mathrm{D}]}{[\mathrm{L}]_0 + [\mathrm{D}]_0} \tag{4.11}$$

$$\Leftrightarrow [\mathrm{L}] - [\mathrm{D}] = (1-x)([\mathrm{L}]_0 + [\mathrm{D}]_0) \tag{4.12}$$

is obtained, where $[\mathrm{L}]_0$ and $[\mathrm{D}]_0$ are initial amount of L-type and D-type. Using the definition of y,

$$\frac{[\mathrm{L}] - [\mathrm{D}]}{[\mathrm{L}] + [\mathrm{D}]} \equiv y \tag{4.13}$$

$$\Leftrightarrow (1-y)[\mathrm{L}] = (1+y)[\mathrm{D}] \tag{4.14}$$

is obtained. Solving equation (4.12) and (4.14), following equations are obtained.

$$[\mathrm{L}] = \frac{(1-x)\,(1+y)\,([\mathrm{L}]_0 + [\mathrm{D}]_0)}{2}. \tag{4.15}$$

$$[\mathrm{D}] = \frac{(1-x)\,(1-y)\,([\mathrm{L}]_0 + [\mathrm{D}]_0)}{2}. \tag{4.16}$$

The difference between number of L-type and D-type molecules ([L]−[D]) and the remains of molecules ([L]+[D]) are obtained as followings.

$$[\mathrm{L}] - [\mathrm{D}] = y\,(1-x)\,([\mathrm{L}]_0 + [\mathrm{D}]_0) \text{ and} \tag{4.17}$$

$$[\mathrm{L}] + [\mathrm{D}] = (1-x)\,([\mathrm{L}]_0 + [\mathrm{D}]_0)\,. \tag{4.18}$$

Assuming $[L]_0 = [D]_0 = 6.0 \times 10^{17}$ molecules, number of enantiomers were calculated. The difference between number of L-type and D-type ([L] − [D]) and the remains of molecules ([L]+[D]) are shown in figure 4.20-4.22 and detail values are are arranged in table 4.1-4.3 in the case of x =10 %, 60 %, 90 %, 99 %, 99.99999 % and 100 %.

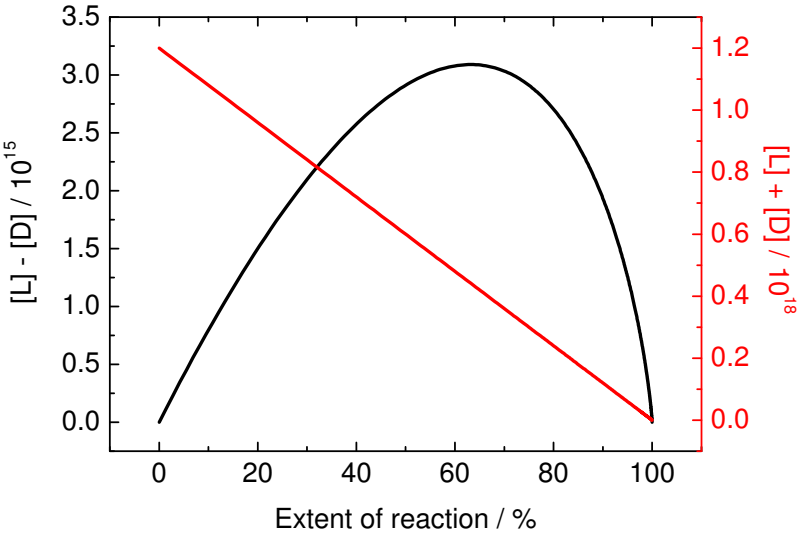

Figure 4.20: The difference between number of L-Asp and D-Asp ([L] − [D]; black) and the remains of molecules ([L] + [D]; red) in the case of $[L]_0 = [D]_0 = 6 \times 10^{17}$ molecules.

Table 4.1: Numerical change of L-Asp and D-Asp in the case of $[L]_0 = [D]_0 = 6 \times 10^{17}$ molecules. x and y show extent of reaction and enantiomeric excess, respectively.

x / %	y / %	[L]	[D]	[L] − [D]	[L] + [D]
0	0	6.0×10^{17}	6.0×10^{17}	0	1.2×10^{18}
10	0.074	5.404×10^{17}	5.396×10^{17}	8×10^{14}	1.08×10^{18}
60	0.65	2.4156×10^{17}	2.3844×10^{17}	3.12×10^{15}	4.8×10^{17}
90	1.6	6.096×10^{16}	5.904×10^{16}	1.92×10^{15}	1.2×10^{17}
99	3.2	6.192×10^{15}	5.808×10^{15}	3.84×10^{14}	1.2×10^{16}
99.99999	9.6	6.576×10^{10}	5.424×10^{10}	1.152×10^{10}	1.2×10^{11}
100	100	1	0	1	1

The *ee* was increased with the increase of extent of reaction (figure 4.19). However, remains of molecules are decreased with the increase of extent of reaction. For example, in the case of L-Asp at $x = 60$ % (table 4.1), the value of *ee* (y) is only 0.65 %, but the difference of number of molecules is almost maximum value. In contrast,

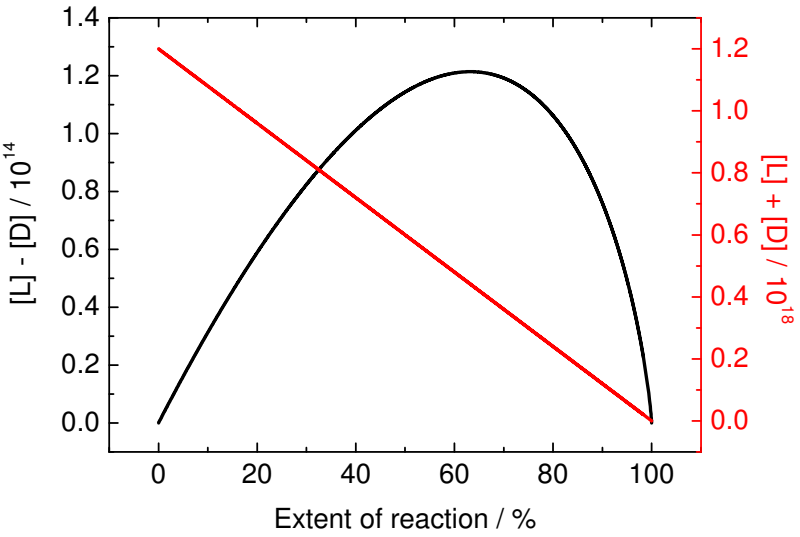

Figure 4.21: The difference between number of L-Ala and D-Ala ([L] − [D]; black) and the remains of molecules ([L] + [D]; red) in the case of $[L]_0 = [D]_0 = 6 \times 10^{17}$ molecules.

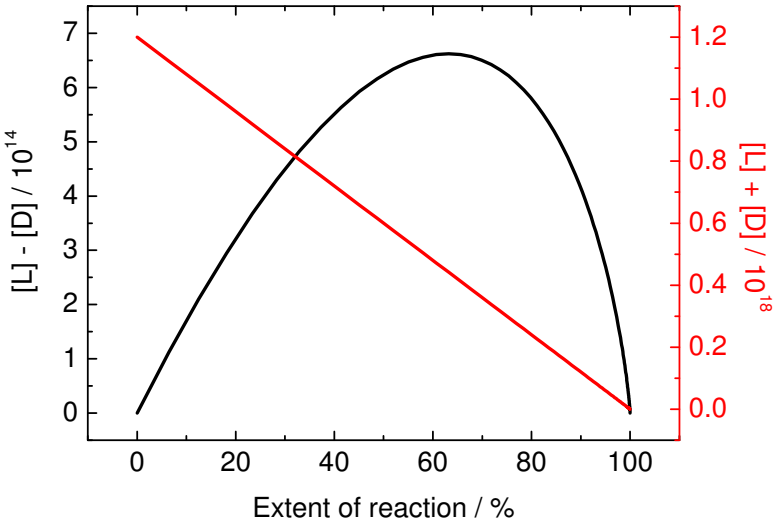

Figure 4.22: The difference between number of L-Asp and D-Asp ([L] − [D]; black) and the remains of molecules ([L] + [D]; red) in the case of $[L]_0 = [D]_0 = 6 \times 10^{17}$ molecules.

Table 4.2: Numerical change of L-Ser and D-Ser in the case of $[\mathrm{L}]_0 = [\mathrm{D}]_0 = 6 \times 10^{17}$ molecules. x and y show extent of reaction and enantiomeric excess, respectively.

x / %	y / %	[L]	[D]	[L] − [D]	[L] + [D]
0	0	6.0×10^{17}	6.0×10^{17}	0	1.2×10^{18}
10	0.0029	5.4001×10^{17}	5.3998×10^{17}	3×10^{13}	1.08×10^{18}
60	0.025	2.4006×10^{17}	2.3994×10^{17}	1.2×10^{14}	4.8×10^{17}
90	0.063	6.004×10^{16}	5.996×10^{16}	8×10^{13}	1.2×10^{17}
99	0.13	6.008×10^{15}	5.992×10^{15}	1.6×10^{13}	1.2^{16}
99.99999	0.44	6.026×10^{10}	5.974×10^{10}	5.2×10^{8}	1.2×10^{11}
100	100	1	0	1	1

Table 4.3: Numerical change of L-Ala and D-Ala in the case of $[\mathrm{L}]_0 = [\mathrm{D}]_0 = 6 \times 10^{17}$ molecules. x and y show extent of reaction and enantiomeric excess, respectively.

x / %	y / %	[L]	[D]	[L] − [D]	[L] + [D]
0	0	6.0×10^{17}	6.0×10^{17}	0	1.2×10^{18}
10	0.016	5.4009×10^{17}	5.3991×10^{17}	1.8×10^{14}	1.08×10^{18}
60	0.14	2.4034×10^{17}	2.3966×10^{17}	6.8×10^{14}	4.8×10^{17}
90	0.35	6.021×10^{16}	5.979×10^{16}	4.2×10^{14}	1.2×10^{17}
99	0.69	6.041×10^{15}	5.959×10^{15}	8.2×10^{13}	1.2×10^{16}
99.99999	2.4	6.144×10^{10}	5.856×10^{10}	2.88×10^{9}	1.2×10^{11}
100	100	1	0	1	1

finally, the value of *ee* achieves 100 %. However, remains of molecules are only one L-type molecule. Of course, this is an extreme case, but remains of molecules are very few in the case of high *ee*. High *ee* is required in view of achievement of homochirality, but small amount of molecules may be disadvantage in view of production of macromolecules. Therefore, it is necessary to examine the optimum value, which is most advantageous to achieve homochirality and produce macromolecules, experimentally and theoretically. In addition, in soft X-ray region, rate constant would not be linear-proportional to absorption cross section because of secondary electrons. Therefore, achieved *ee* would be different from the value shown in figure 4.19. It is necessary to carry out circularly polarized soft X-ray irradiation experiments.

4.4 Conclusion

The NCD spectrum curve of L-Asp changed from negative to positive with the increase of photon energy. In contrast, the NCD spectrum curve of L-Ser changed from positive to negative with the increase of photon energy. In the case of L-Ala, only one negative peak was observed. Difference among three amino acids reflects the difference of chiral environment of the core hole oxygen atom of COO^-. Since COO^- is common part of the biomolecular amino acids, side chain affects NCD of COO^-. It is interesting in view of application of NCD in soft X-ray region.

Magnitude of NCD of L-Asp is quite large value comparing with L-Ser, L-Ala and other molecules reported in the past (Turchini *et al.*, 2004; Tanaka *et al.*, 2005; Nakagawa *et al.*, 2005). The reason why L-Asp shows such a large NCD is open question at the present time. It is very interesting in view of both experimental and theoretical soft X-ray NCD studies.

Thus, spectrum shapes and magnitude of NCD among three kinds of amino acids were dramatically different. However, those amino acids satisfied Buchardt's required conditions (Buchardt, 1974). Therefore, it was concluded that asymmetric photolysis induced by circularly polarized soft X-ray would be occurred. In soft X-ray region, secondary electrons are important factor although it is "symmetric" reaction. Therefore, achieved *ee* would be affected by secondary electrons. It is necessary to carry out circularly polarized soft X-ray irradiation experiments.

Chapter 5

Summary

Following three experiments were carried out as the first step to examine the cosmic scenario.
1. Examination for racemization of aspartic acid during photolysis induced by non-polarized 8.5 eV vacuum ultraviolet (VUV) light irradiation.

In view of cosmic scenario, biomolecular must keep the enrichment induced by asymmetric reaction in space during space travel. However there are various racemization factors in space. In order to examine whether (1) Asp is racemized by VUV irradiation and (2) the decomposition products have same chirality as Asp, L- or D-Asp sublimated films were irradiated with non-polarized 8.5 eV VUV light.

Reactions expressed as "L-Asp + $h\nu \rightarrow$ L-Ala + β-Ala (+ other achiral molecules)" and "D-Asp + $h\nu \rightarrow$ D-Ala + β-Ala (+ other achiral molecules)" occurred for L- or D-Asp films irradiated with non-polarized 8.5 eV VUV light. It was concluded that chirality was preserved for photolysis of Asp to Ala. Decomposition quantum efficiency of solid Asp was smaller than that of aqueous solution. This result suggests that solid Asp is much stable than aqueous solution and supports cosmic scenario.

2. Examination for racemization and dimerization of alanine induced by non-polarized 7.2 eV VUV light irradiation

It is well known that "chiral defects" impede the formation of both double helix in nucleic acids and α-helixes and β-sheets in proteins. Therefore, amino acids and nucleosides must polymerize against racemization. In this experimetn, it was verified the decomposition, racemization and dimerization rate of solid L-Ala induced by non-polarized 7.2 eV VUV light.

L-Ala was stable with the probability of 11 % per 7.2 eV incident photon. The breakdown of 11 % was; 0.52 % racemization, namely production D-Ala, 0.13 % homo-dimerization, namely production of LL and 10.35 % the other production of other achiral molecules. The rate of racemization was 4 times as large as the rate of homo-dimerization. In view of chemical evolution in space and achievement of homochirality, this result may be critical problem. Therefore it is necessary to carry out similar experiments at ultra-cold temperature.

3. Verification of the possibility of asymmetric photolysis induced by circularly polarized soft X-ray

Asymmetric photolysis of amino acids induced by circularly polarized ultraviolet has been reported. If the circularly polarized light source is synchrotron radiation in space, circularly polarized soft X-ray may also act as an asymmetric energy source. In order to examine the possibility of asymmetric photolysis induced by circularly polarized soft X-ray, NCD spectra were measured in oxygen K-edge region.

Spectrum shapes and magnitude of NCD among three kinds of amino acids were dramatically different. Therefore, it was concluded that asymmetric photolysis induced by circularly polarized soft X-ray would be occurred in the case of those amino acids. However, in soft X-ray region, achieved enantiomeric excess would be affected by secondary electrons. It is necessary to carry out circularly polarized soft X-ray irradiation experiments.

Acknowledgment

NCD measurement was carried out at SPring-8 BL25SU under the approval of Japan Synchrotron Radiation Research Institute (JASRI) (proposal numbers; 2006A1474, 2007B1498, 2008A1307 and 2009A1491). The author would like to gratefully acknowledge to Dr. Takayuki Muro for his experimental supports.

The author would like to gratefully acknowledge to Drs. Masahito Tanaka (National Institute of Advanced Industrial Science and Technology) and Akane Agui (Japan Atomic Energy Agency) for their helpful discussions and assistance.

The author is grateful to Professors Shin-ichi Ueji, Kuniyoshi Ebina, Shigeki Aoki and Masayuki Itoh (Kobe University) for their advices and comments during the doctoral program.

The author would like to thank Drs. Jin Zhaohui, Fusae Kaneko and Hirofumi Ohyama, Messrs. Atsushi Kasahara, Tomo Kitada, Takahiro Matsui, Masafumi Tanaka, Kaveenga Rasika Koswattage, Katsuhiko Sugiki, Takahiro Kawabata, Takashi Miyamoto and Yohei Momoki and Mses. Yoshimi Ohta, Masumi Kamohara, Keiko Okamoto, Sayaka Fukuda, Akiko Imazu, Aki Mimoto, Risa Uchida and Maiko Tanabe (Kobe Univeristy) for their helpful discussions and experimental supports.

The author acknowledges financial support from the Japan Society for the Promotion of Science (JSPS): Grant-in-Aid for JSPS Fellows (21-3972).

Finally, the author would like to express the appreciation to Professor Kazumichi Nakagawa for his various instructions, supports and encouragement.

December 2009
Yudai Izumi

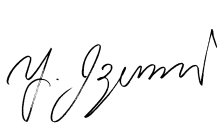

References

- Alagna, L. *et al.* (1998), "X-ray natural circular dichroism", *Physical Review Letters*, **80**, 4799-4802.
- Alargov, D. *et al.* (2002), "Reaction behaviors of glycine under super- and subcritical water conditions", *Origins of Life and Evolution of the Biosphere*, **32**, 1-12.
- Atoyan, A. M. and Aharonian, F. A. (1996), "On the mechanisms of gamma radiation in the Crab Nebula", *Monthly Notices of the Royal Astronomical Society*, **278**, 525-541.
- Bailey, J. *et al.* (1998), "Circular polarization in star-formation regions: Implications for biomolecular homochirality", *Science*, **281**, 672-674.
- Balavoine, G. *et al.* (1974), "Preparation of chiral compounds with high optical purity by irradiation with circularly polarized light, a model reaction for the prebiotic generation of optical activity", *Journal of the American Chemical Society*, **96**, 5152-5158.
- Barbier, B. *et al.* (2002), "Exposure of amino acids and derivatives in the Earth orbit", *Planetary and Space Sciences*, **50**, 353-359.
- Boillot, F. *et al.* (2002), "The Perseus Exobiology mission on MIR: Behaviour of amino acids and peptides in earth orbit", *Origins of Life and Evolution of the Biosphere*, **32**, 359-385.
- Bonner, W. A. (1991), "The origin and amplification of biomolecular chirality", *Origins of Life and Evolution of the Biosphere*, **21**, 59-111.
- Bonner, W. A. and Lemmon, R. M. (1978), "Radiolysis, racemization and the origin of molecular asymmetry in the biosphere", *Journal of Molecular Evolution*, **11**, 95-99.
- Bonner, W. A. *et al.* (1979), "Racemization of isovaline by γ-radiation. Cosmological implications", *Journal of the American Chemical Society*, **101**, 1049-1050.
- Bonner, W. A. *et al.* (1982), "The radiolysis and racemization of leucine on proton irradiation", *Origins of Life*, **12**, 51-54.

- Bonner, W. A. *et al.* (1985), "The radiolysis and radioracemization of amino acids on clays", *Origins of Life*, **15**, 103-114.
- Bonner, W. A. (1991), "The origin and amplification of biomolecular chirality", *Origins of Life and Evolution of the Biosphere*, **21**, 59-111.
- Buchardt, O. (1974), "Photochemistry with circularly polarized light", *Angewandte Chemie International Edition*, **13**, 179-185.
- Clark, D. T. *et al.* (1976), "An experimental and theoretical investigation of the core level spectra of a series of amino acids, dipeptides and polypeptides", *Biochimica et Biophysica Acta*, **453**, 533-546.
- Chyba, C. F. and Sagan, C. (1997) "Comets as a source of prebiotic organic molecules for the early Earth", in *Comets and the Origin and Evolution of Life*, edited by Thomas, P. J., Chyba, C. F. and McKay, C. P., pp. 147-173, Springer-Verlag, N.Y. USA.
- Corliss, J. B. *et al.* (1979), "Submarine thermal springs on the Galápagos rift", *Science*, **203**, 1073-1083.
- Cronin, J. R. and Pizzarello, S. (1997), "Enantiomeric excesses in meteoritic amino acids", *Science*, **275**, 951-955.
- Edmond, J. M. *et al.* (1982), "Chemistry of hot springs on the east pacific rise and their effluent dispersal", *Nature*, **297**, 187-191.
- Egawa, C. *et al.* (2003), "STM study of DL-alanine array structure on Cu(0 0 1)", *Surface Science*, **532-535**, 233-236.
- Flores, J. J. *et al.* (1977), "Asymmetric photolysis of (*RS*)-leucine with circularly polarized ultraviolet light", *Journal of the American Chemical Society*, **99**, 3622-3625.
- Fukue, T. *et al.* (2009), "Near-infrared circular polarimetry and correlation diagrams in the Orion Becklin-Neugebauer/Kleinman-Low region: Contribution of dichroic extinction", *The Astrophysical Journal*, **692**, L88-L91.
- Furuuchi, R. *et al.* (2005), "Evolving lipid vesicles in prebiotic hydrothermal environments", *Origins of Life and Evolution of Biospheres*, **35**, 333-343.
- Greenberg, J. M. *et al.* (1994), "Interstellar dust, chirality, comets and the origins of life: Life from dead stars?", *Journal of Biological Physics*, **20**, 61-70.
- Goldanskii, V. I. *et al.* (1986), "Chiral purity of nucleotides as a necessary condition of complementarity", *FEBS Letters*, **207**, 181-183.
- Goto, T. *et al.* (2005), "Condensation reactions of amino acids under hydrothermal conditions with adiabatic expansion cooling", *Journal of Chemical Engineering of Japan*, **38**, 295-299.

- Harada, K. and Fox, S. W. (1964), "Thermal synthesis of natural amino-acids from a postulated primitive terrestrial atmosphere", *Nature*, **201**, 335-336.

- Henke, B. L. *et al.* (1993), "X-ray interactions: Photoabsorption, scattering, transmission, and reflection at E = 50-30,000 eV, Z = 1-92", *Atomic Data and Nuclear Data Tables*, **54**, 181-342.

- Hirose, K. *et al.* (2000), "Basic performance of VUV exposure systems using head-on type Ar_2* and Kr_2* DBD excimer lamps", *Journal of the Illuminating Engineering Institute of Japan*, **84**, 290-295.

- Imai, E. *et al.* (2002), "Elongation of oligopeptides in a simulated submarine hydrothermal system", *Science*, **283**, 831-833.

- Inagaki, T. (1973), "Optical absorptions of aliphatic amino acids in the far ultraviolet", *Biopolymers*, **12, 1353-1362**

- Islam, M. N. *et al.* (2003), "Reaction of amino acids in a supercritical water-flow reactor simulating submarine hydrothermal systems", *Bulletin of the Chemical Society of Japan*, **76**, 1171-1178.

- Jiemchooroj, A. *et al.* (2007), "Near-edge x-ray absorption and natural circular dichroism spectra of L-alanine: A theoreteical study on the complex polarization propagator approach", *Journal of Chemical Physics*, **127**, 165104(1)-165104(8).

- Kagan, H. B. *et al.* (1974), "Can circularly polarized light be used to obtain chiral compounds of high optical purity?", *Jouranl of Molecular Evolution*, **4**, 41-48.

- Kamohara, M. *et al.* (2008), "Optical oscillator strength distribution of amino acids from 3 to 250 eV and examination of the Thomas-Reiche-Kuhn sum rule", *Radiation Physics and Chemistry*, **77**, 1153-1155.

- Kaneko, F. *et al.* (2005), "Chemical evolution of amino acid induced by soft X-ray with synchrotron radiation", *Journal of Electron Spectroscopy and Related Phenomena*, **144-147**, 291-294.

- Kawamura, K. and Yukioka, M. (2001), "Kinetics of the racemization of amino acids at 225-275 °C using a real-time monitoring method of hydrothermal reactions", *Thermochimica Acta*, **375**, 9-16.

- Kawamura, K. *et al.* (2005), "Consecutive elongation of alanine oligopeptides at the second time range under hydrothermal conditions using a microflow reactor system", *Journal of the American Chemical Society*, **127**, 522-523.

- Khoroshilova, E. V. *et al.* (1991), "Photosynthesis of peptides during irradiation of tyrosine with vacuum ultraviolet radiation", *Doklady Akademii Nauk SSSR*, **319**, 1244-1247.

- Kobayashi, K. *et al.* (2001), "Formation of bioorganic compounds in simulated planetary atmospheres by high energy particles or photons", *Advances in Space Research*, **27**, 207-215.

- Kuroda, S. and Miyagawa, I. (1982), "ENDOR study of an irradiated crystal of L-alanine: Environment of the stable $CH_3\dot{C}HCO_2^-$ radical", *Journal of Chemical Physics*, **76**, 3933-3944.

- Kuroda, R. *et al.* (2001), "A solid-state dedicated circular dichroism spectrophotometer: Development and application", *Review of Scientific Instruments*, **72**, 3802-3810.

- Love, S. G. and Brownlee, D. E. (1993), "A direct measurement of the terrestrial mass accretion rate of cosmic dust", *Science*, **262**, 550-553.

- MacDermott, A. J. *et al.* (2009a), "Electroweak parity-violating energy shifts of amino acids: The "conformation problem"", *Origins of Life and Evolution of Biospheres*, **39**, 407-437.

- MacDermott, A. J. *et al.* (2009b), "Evaluation of coupled perturbed and density functional methods of computing the parity-violating energy difference between enantiomers", *Origins of Life and Evolution of Biospheres*, **39**, 439-457.

- MacDermott, A. J. *et al.* (2009c), "Parity-violating energy shifts of Murchison L-amino acids are consistent with an electroweak origin of meteorite L-enantiomeric excesses", *Origins of Life and Evolution of Biospheres*, **39**, 459-478.

- Meierhenrich *et al.* (2005), "Asymmetric vacuum UV photolysis of the amino acid leucine in the solid state", *Angewandte Chemie International Edition*, **44**, 5630-5634.

- Miller, S. L. (1953), "A production of amino acids under possible primitive earth conditions", *Science*, **117**, 528-529.

- MOPAC (2000) Fujitsu Limited, Tokyo, Japan

- Muro, T. *et al.* (2007), "Status of the twin helical undulator soft X-ray beamline at SPring-8: Performance for circular dichroism measurements", *AIP Conference Proceedings*, **879**, 571-574.

- Muro, T. *et al.* (2004), "A measurement system for circular dichroism in soft X-ray absorption using helicity switching by twin helical undulators", *AIP Conference Proceedings*, **705**, 1051-1054.

- Nakagawa, K. *et al.* (2000), "Search for asymmetric reaction of amino acids by circularly polarized radiation using a polarizing undulator at the Electrotechnical Laboratory", in *The Role of Radiation in the Origin and Evolution of Life*, edited by Akaboshi, M., Fujii, N. and Navarro-González, pp. 352-362, Kyoto University Press, Japan.

- Nakagawa, K. *et al.* (2005), "Natural circular dichroism of amino acid films observed in soft X-ray and VUV region using polarizing undulator", *Journal of Electron Spectroscopy and Related Phenomena*, **144-147**, 271-273.

- Nakagawa, K. *et al.* (2009), "Radiation-inducedchemicalevolutionofbiomolecules", *Radiation Physics and Chemistry*, **78**, 1198-1201.

- Nemoto, A. *et al.* (2005), "Enantiomeric excess of amino acids in hydrothermal environments", *Origins of Life and Evolution of Biospheres*, **35**, 167-174.

- Neuberger, A. (1948), "Stereochemistry of amino acids", *Advances in Protein Chemistry*, **4**, 297-383.

- Nishino, H. *et al.* (2001), "Mechanism of pH-dependent photolysis of aliphatic amino acids and enantiomeric enrichment of racemic luecine by circularly polarized light", *Organic Letters*, **3**, 921-924.

- Nishino, H. *et al.* (2002), "Absolute asymmetric photoreactions of aliphatic amino acids by circularly polarized synchrotron radiation: Critically pH-dependent photobehavior", *Journal of the American Chemical Society*, **124**, 11618-11627.

- Ogata *et al.* (2000), "Hydrothermal circulation of seawater through hot vents and contribution of interface chemistry to prebiotic synthesis", *Origins of Life and Evolution of the Biosphere*, **30**, 527-537.

- Pizzarello, S. and Cronin, J. R. (2000), "Non-racemic amino acids in the Murray and Murchison meteorites", *Geochimica et Cosmochimica Acta*, **64**, 329-338.

- Pizzarello, S. *et al.* (2003), "Nonracemic isovaline in the Murchison meteorite: Chiral distribution and mineral association", *Geochimica et Cosmochimica Acta*, **67**, 1589-1595.

- Plashkevych, O. *et al.* (1998) "Theoretical study of X-ray circular dichroism of amino acids", *Chemical Physics*, **232**, 49-62.

- Ridley, J. and Zerner, M. (1973), "An intermediate neglect of differential overlap technique for spectroscopy: Pyrrole and the azines", *Theoretica Chimica Acta (Berlin)*, **32**, 111-134.

- Rosenbush, V. *et al.* (2007), "Circular polarization in comets: Observations of Comet C/1999 S4 (LINEAR) and tentative interpretation", *Icarus*, **186**, 317-330.

- Russell, M. J. *et al.* (1988), "Submarine hot springs and the origin of life", *Nature*, **336**, 117.

- Samson, J. A. R. (1967) *Technique of Vacuum Ultraviolet Spectroscopy*, pp. 212-217, John Wiley & Sons.

- Shirasawa, K. *et al.* (2004), "Fast helicity switching of circularly polarized light using twin helical undulators", *AIP Conference Proceedings*, **705**, 191-194.

- Shimoyama, A. *et al.* (1979), "Amino acids in the Yamato carbonaceous chondrite from Antarctica", *Nature*, **282**, 394-396.

- Shindo, Y. *et al.* (1990), "Problems of CD spectrometers (V): Can we measure CD and LD simultaneously? Comments on differential polarization microscopy (CD and linear dichroism)", *Biopolymers*, **30**, 405-413.

- Simakov, M. B. *et al.* (1996), "Abiogenic synthesis of oligopeptides in solid state under action of vacuum ultraviolet light (100-200nm)", *Advances in Space Research*, **18**, 61-64.

- Smith, G. G. and Sivakua, T. (1983), "Mechanism of the racemization of amino acids. Kinetics of racemization of arylglycines", *Journal of Organic Chemistry*, **48**, 627-634.

- Spach, G. and Brack, A. (1979), "β-structures of polypeptides with L- and D-residues. Part II. Statistical analysis and enrichment in enantiomer", *Journal of Molecular Evolution*, **13**, 47-56.

- Stewart, J. J. P. (1989a),"Optimization of parameters for semiempirical methods I. Method", *Journal of Computational Chemistry*, **10**, 209-220.

- Stewart, J. J. P. (1989b),"Optimization of parameters for semiempirical methods II. Applications", *Journal of Computational Chemistry*, **10**, 221-264.

- Stewart, B. *et al.* (1999), "Circular dichroism at the edge: Large X-ray natural CD in the 1s $\rightarrow$ 3d pre-edge feature of $2[Co(en)_3Cl_3]\cdot NaCl\cdot 6H_2O$", *Journal of the American Chemical Society*, **121**, 10233-10234.

- Takahashi, J. *et al.* (2009), "Chirality emergence in thin solid films of amino acids by polarized light from synchrotron radiation and free electron laser", *International Journal of Molecular Sciences*, **10**, 3044-3064.

- Takano, Y. *et al.* (2007), "Asymmetric synthesis of amino acid precursors in interstellar complex organics by circularly polarized light", *Earth and Planetary Science Letters*, **254**, 106-114.

- Tanaka, M. *et al.* (2001), "Oxygen K-edge X-ray absorption near edge structures (XANES) of sublimated films of amino acids", *Journal of Synchrotron Radiation*, **8**, 1009-1011.

- Tanaka, M. *et al.* (2005), "First observation of natural circular dichroism for biomolecules in soft X-ray region studied with a polarizing undulator", *Physica Scripta*, **T115**, 873-876.

- Tanaka, M. *et al.* (2008), "Fragmentation and dimerization of aliphatic amino acid films induced by vacuum ultraviolet irradiation", *Radiation Physics and Chemistry*, **77**, 1164-1168.

- Tanaka, M. *et al.* (2009), "First observation of natural circular dichroism spectra in extreme ultraviolet rgion using polarizing undulator-based optical system and its polarization characteristics", *Journal of Synchrotron Radiation*, **16**, 455-462.

- Turchini, S. *et al.* (2004), "Core electron transition as a probe for molecular chirality: Natural circular dichroism at the carbon K-edge of methloxirane", *Journal of the American Chemical Society*, **126**, 4532-4533.

- Yamagata, Y. (1966), "A hypothesis for the asymmetric appearance of biomolecules on earth", *Journal of Theoretical Biology*, **11**, 495-498.

- Yanagawa, H. and Kojima, K. (1985), "Thermophilic microspheres of peptide-like polymers and silicates formed at 250 °C", *Journalof Biochemistry*, **97**, 1521-1524.

- Zhao, X. *et al.* (1999), "Adsorption of alanine on Cu(0 0 1) studied by scanning tunneling microscopy", *Surface Science*, **442**, L995-L1000.

- Zubavichus, Y. *et al.* (2005), "Innershell absorption spectroscopy of amino acids at all relevant absorption edges", *Journal of Physical Chemistry A*, **109**, 6998-7000.